Sol Invictus: Holocene climate change and its impact in the Roman Mediterranean

The research in this thesis was funded by a Focus and Mass grant from Utrecht University awarded to Stefan Dekker, Marc Bierkens, Martin Wassen and Nanne Weber.

The cover artwork is composed of a reconstruction of solar irradiance during the Holocene by Steinhilber et al. (2009), a reconstruction of the surface temperature of the Western Pacific Warm Pool by Stott et al. (2004) and a map of the Mediterranean supplied by the National Oceanic and Atmospheric Administration. The network is an abstraction of Orbis: the Stanford geospatial network of the Roman World published by Scheidel and Meeks (2013).

Thesis printed at CPI Koninklijke Wöhrmann, Zutphen, the Netherlands

ISBN: 978-90-6266-378-1

Sol Invictus: Holocene climate change and its impact in the Roman Mediterranean

Sol Invictus: Klimaatverandering en de gevolgen hiervan in het Romeinse Middellandse Zeegebied

(met een samenvatting in het Nederlands)

Proefschrift

ter verkrijging van de graad van doctor aan de Universiteit Utrecht op gezag van de rector magnificus, prof.dr. G.J. van der Zwaan, ingevolge het besluit van het college voor promoties in het openbaar te verdedigen op woensdag 28 november 2014 des middags te 2.30 uur

door

Brian Dermody

geboren op 2 juni 1982 te Wicklow, Ierland

Promotoren: Prof.dr. M.J. Wassen

Prof.dr. M.F.P. Bierkens

Prof.dr. S.L. Weber †

Copromotor: Dr. S.C. Dekker

Contents

1 Introduction

1.1 Research context

As with all species on the planet, humans coevolved with the natural environment around them. Humanity's success at adapting to and exploiting the environment has progressed to a point where we are capable of changing the environment that supports us at a global scale (Rockström et al., 2009). Humans are not a unique life form in this respect (de Boer et al., 2012), however the rate at which we are changing the environment is likely unprecedented in the 3.6 billion year history of life on planet Earth (Young et al., 2006).

There is evidence that humans began to consciously engineer their environment as far back as the earliest homo sapiens through the use of fire (James et al., 1989). Fire is proposed to have been used to increase the carrying capacity of the environment for humans by supressing woody biomass thus increasing the abundance of large grazers. These large grazers provided ample meat whilst the openness of the landscape made them easier for humans to hunt (Stewart, 1951). However, it was with the innovation of agriculture about 10,000 years ago that humans began environmental engineering in more complex ways (Maisels, 1993). The emergence of agriculture coincided with a warming of global temperatures following the end of the last ice age (Mayewski et al., 2004). Agriculture was a watershed moment because it required a sedentary lifestyle which brought about congregations of people in small villages (Larsen, 2006). It also produced stable surpluses of food which allowed humans to focus on other pursuits, leading to an explosion in innovation (Boserup, 1981). Some of these early innovations drastically increased the carrying capacity of local environments for humans (Meyer and Ausubel, 1999). For example, the innovation of irrigation enabled early Southern Mesopotamian civilisations to grow edible plants in a region that had previously extremely low primary productivity, leading to a dramatic increase in the carrying capacity of the region.

However, higher carrying capacities also promoted population growth, which closed the gap between the carrying capacity and population demand over time. Thus, humans entered an innovation-growth cycle, whereby innovations promoted growth that required continued

innovation to maintain growth (Fig. 1.1a) (Brown and Kane, 1995). Environmental degradation accelerated the cycle by reducing the carrying capacity over time (Arrow et al., 1995). Taking the example of the early Mesopotamian civilisations again, the use of irrigation caused soil salinization leading to a reduced agricultural productivity over time (Helbaek, 1960). In addition to population and degradation pressure, early societies also had to contend with variability in their carrying capacities arising from the climate change (de Menocal, 2001). These changes were often unpredictable and varied in frequency and amplitude (Young et al., 2006). For example, a sudden shift to arid climate conditions in the Indus Valley 4,200 years ago (Staubwasser, 2003) is linked to the abandonment of lands belonging to the Harappan culture and a south-eastern migration of the civilisation (Possehl, 1997).

As more and more agricultural societies emerged, trade networks among different regions became established. Trade gave societies access to a greater range of resources than their local environment contained (Dixon et al., 1968). The advent of ship building technology was particularly important because it facilitated the trade in bulk goods such as food, which enabled populations to grow beyond the constraints of their local environmental carrying capacities (Rees and Wackernagel, 1996). In fact, access to shipping trade networks was likely the principal reason for the establishment of ancient cities next to water bodies because high food demands could be met through trade (Sherbinin et al., 2007). As a result the Mediterranean became one of the most urbanised regions in preindustrial times owing to a long and relatively easily navigated coastline (Leontidou, 1990). Trade in food as well as urbanisation reached its preindustrial peak with the emergence of Roman civilisation in the Mediterranean (Horden and Purcell, 2000; Scheidel, 2001). The Romans applied a range of technological innovations to maximise food production within their empire. A vast trade network in the Mediterranean and Black Sea regions enabled them exploit environmental conditions on one side of the Mediterranean to feed populations on the other (Erdkamp, 2005; Kessler and Temin, 2007). The scale and efficiency of the Roman system of food production and redistribution facilitated the growth of cities far beyond their local environmental carrying capacities. For example, the population of the city of Rome grew to an estimated 1 million inhabitants at the height of the Empire in the 2nd century AD with food imports coming from Sicily, North Africa and Egypt (Scheidel, 2001).

However, just as with earlier societies, the Romans were also impacted by population pressures and environmental degradation. The growth of cities produced high food demand which was satisfied by a switch to large-scale, monoculture farming (Horden and Purcell, 2000). These large-scale farms were worked by an influx of slaves from conquered territories and the farming methods practised led to massive soil degradation (Blaikie and Brookfield, 1987; Montgomery, 2008). Superimposed on pressures in carrying capacity arising from population growth and environmental degradation, climate also brought about changes in agricultural yields. However, it is important to realise that changes in climate were not always negative as illustrated by Columella (AD 70) in *De Re Rustica*:

For I have found that many authorities now worthy of remembrance were convinced that with the long wasting of the ages, weather and climate undergo a change; and that ….regions which formerly, because of the unremitting severity of winter, could not safeguard any shoot of the vine or the olive planted in them, now that the earlier coldness has abated and the weather is becoming more clement, produce olive harvests and the vintages of Bacchus in the greatest abundance

With the Age of Enlightenment in Europe a rapid acceleration in innovation occurred, culminating in the industrial and agricultural revolutions of the late 18th century. Innovations such as artificial fertilizers at this time brought about remarkable increases in food production accompanied by unprecedented global population growth (Ehrlich and Ehrlich, 1990). In addition, innovations in transport technology made it possible to transport food from one side of the globe to the other (Geels, 2002). Present day civilisations now engineer the environment on one side of the planet to feed populations on the other. Current food production and trade infrastructure are so efficient that whole regions of the world can grow beyond their local environmental carrying capacities. For example, more water resources are used in the production of food imported by the Middle East region than flows down the Nile River each year (Barnaby, 2009).

An unforeseen outcome of our innovations since the industrial revolution has been the release of greenhouse gases (GHG) into the atmosphere (Keeling, 1960). Elevated atmospheric greenhouse gas concentrations trap more of the suns radiation, leading to a rapid warming of the planets'

surface (IPCC, 2007; Tyndall, 1861). It is highly uncertain how the climate system will respond to these changes although the weight of evidence indicates that extreme climatic events will become more frequent (Fig. 1.1b) (IPCC, 2007). Given the unprecedented nature of these changes (Mann et al., 1998), it is also unclear whether we as a species have the ability to adapt to future climate change.

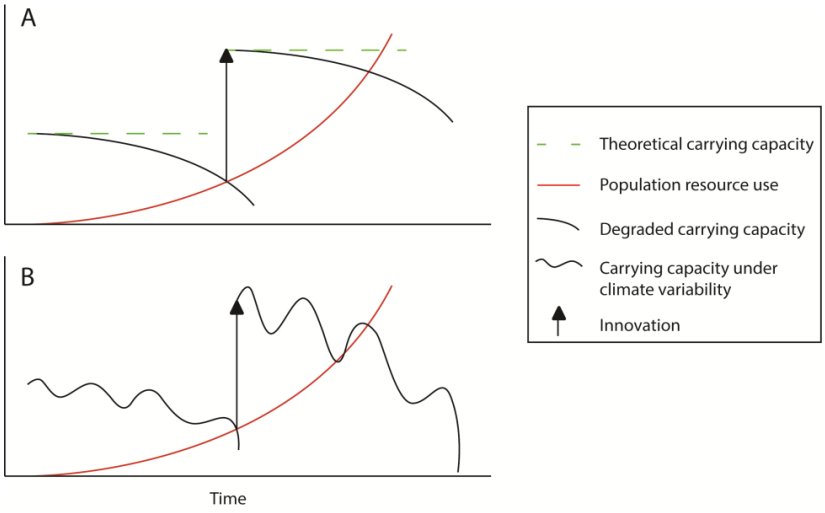

Figure 1.1 The relation between carrying capacity, innovation, degradation and climate (A) The carrying capacity of agricultural societies is often not constant as environmental degradation reduces productivity of the land over time. Innovations such as the plough may increase the carrying capacity of a region for humans, facilitating further population growth. **(B)** Carrying capacity is also variable over time owing to climate. An unforeseen outcome of the innovations associated with the agricultural and industrial revolutions was the emission of greenhouse gases to the atmosphere. Under global warming it is predicted that climate variability will increase in amplitude thus causing a higher variability in agricultural productivity.

In this thesis, I seek answers to these questions by investigating how climate has changed in the last 10,000 years and the impact that those changes had on the Roman civilisation. I begin at the largest scale relevant for our climate: the sun. My analyses concentrates on understanding how small variations in the radiation emitted from the sun can cause relatively large changes in the Earth's climate. I then focus on regional scale climate change with a reconstruction of precipitation in the Mediterranean during the period coinciding with the rise and fall of the

Roman Empire. The objective of my analyses in the Mediterranean is to inform about the causes of climate change during that period as well as the likely impacts those changes had on the Roman civilisation. Given the parallels between the Roman civilisation and our own, it is envisaged that the research undertaken in this thesis may illuminate how current civilisation can adapt to future climate change.

1.2 Why look to the past?

In order to predict the future state of a dynamic system it is first crucial to understand how that system operates. One of the central methods to understanding dynamic systems is to observe them over a timescale at which relevant mechanisms in the system change (Bacon, 1620). However, when those changes occur over long timescales, direct observations are not always possible. In that case, empirical data from the past can be invaluable. For example, Edmund Halley (1705) identified 3 comets that had identical orbital elements using historical records. This gave support to his theory that comets had an orbital trajectory and that the 3 comets observed were actually the same comet in orbit around the sun. He used these observations to refine his orbital calculations and accurately predicted the timing of the next fly pass of what became known as Halley's Comet. However, many of the relevant components of the climate system such as oceanic circulation, ice sheet dynamics etc. operate on timescales even longer than the historical observational record (de Menocal, 2001). Therefore, there is a need to extend our empirical data back before records began. Similarly, if we want to understand how society responds to climate perturbations the observational period only captures a fraction of the variability in climate since the birth of civilisation. Actually, there have been much larger changes in the climate in distant past more in line with the amplitude of climate change that will become more frequent in the future (Mayewski et al., 2004). Thus, to understand the range of climate variability and how this variability may impact society we can learn much from looking to the past.

1.3 Holocene climate anomalies

The Holocene began ~11,700 years ago with a rapid increase in global temperatures following the last glacial period (Fig. 1.2c) (Mayewski et al., 2004; Wanner et al., 2011). The Holocene is often described as a period of stable climate; however it was actually characterised by millennial-scale climatic trends superimposed with decadal-centennial scale climate anomalies (Mayewski et al., 2004). Millennial-scale climatic trends during the Holocene were caused by the precession of the angle of axial tilt of the Earth as well as precession of the perihelion (the time of year the earth is closest to the sun). During the Holocene, the angle of axial tilt decreased reducing the difference in insolation between the seasons (Fig. 1.2a) (Lorenz et al., 2006). In addition, the perihelion shifted from boreal summer in the early Holocene to boreal winter in the Late Holocene, thus further reducing seasonal differences in the Northern Hemisphere (Crucifix et al., 2002). These orbital trends led to a southward migration of the Inter Tropical Convergence Zone (ITCZ) (Haug et al., 2001), an increase in the frequency and amplitude of the El Niño Southern Oscillation (ENSO) (Fig. 1.2.d) (Conroy et al., 2008; Donders et al., 2008; Moy et al., 2002) and a weakening of the Northern Hemisphere Monsoons (Braconnot et al., 2007).

Superimposed on orbital forced climatic changes, variations in the radiation emitted from the sun impacted climate during the Holocene at shorter timescales (Fig. 1.2b) (Asmerom et al., 2007; Fleitmann et al., 2003; Steinhilber et al., 2012; Stuiver et al., 1995; Wang et al., 2005). Holocene climate reconstructions from around the globe exhibit correlations with reconstructed variability in solar irradiance. For example, the warm Medieval Climate Anomaly and cold Little Ice Age periods correspond with maxima and minima in solar irradiance respectively (Lamb, 1965). However, the mechanisms through which solar irradiance variations forced climate change remain unclear. In terms of radiative energy, reconstructed variations in total solar irradiance (TSI) are thought to have been too small (0.05-0.5% of TSI) to cause climate change of the magnitude recorded in the paleo record (Gray et al., 2010). Instead amplification mechanisms are thought to exist in the Earth Climate System that magnify these small changes in irradiance (Gray et al., 2010; Meehl et al., 2008; Shindell et al., 2001; Shindell et al., 1999).

Two of the principal amplification mechanisms for solar irradiance forcing are proposed to be top-down and bottom-up amplification of solar forcing (Gray et al., 2010). Top-down amplification of solar forcing is caused by increases in UV radiation during solar maxima that stimulate stratospheric ozone production (Shindell et al., 1999). Ozone absorbs radiation thus the increased absorption capacity of the stratosphere reinforces stratospheric warming during solar maxima (Shindell et al., 1999). The warming is greatest at lower latitudes leading to an increase in the latitudinal temperature gradient in the stratosphere. An associated acceleration of zonal stratospheric winds are communicated to the troposphere via wave propagation, leading to polar movement of the storm tracks during solar maxima (Haigh, 1996). Bottom-up amplification of solar forcing occurs in the Tropics whereby small changes in insolation arising from solar irradiance variations are reinforced by the coupled ocean-atmosphere system (Bjerknes, 1964; Meehl et al., 2008).

Although solar irradiance is correlated with a number of Holocene climate anomalies, there were also sudden and anomalous changes in climate during the Holocene that do not appear to exhibit any relation with solar variability (Mayewski et al., 2004; Wanner et al., 2011, 2008). It is thought that these changes arose from internal dynamics of climate system (Knudsen et al., 2011). At decadal and longer timescales, changes in ocean dynamics are of particular relevance. The ocean is by far the largest reservoir of heat in the climate system meaning that shorter term atmospheric changes are integrated by the ocean and re-communicated to the climate system at different regions of the ocean surface (IPCC, 2007). For example, slowing down in the speed of the overturning circulation and cooling of North Atlantic SST is implicated as the origin of anomalous cold events throughout the Holocene (Fig. 1.2e) (Bianchi and McCave, 1999; Bond et al. 2001). Although solar irradiance likely plays a role in these cooling events (Bond et al. 2001), changes in the thermohaline gradients in the ocean arising from processes internal to the climate system are also very important (Weber et al., 2004).

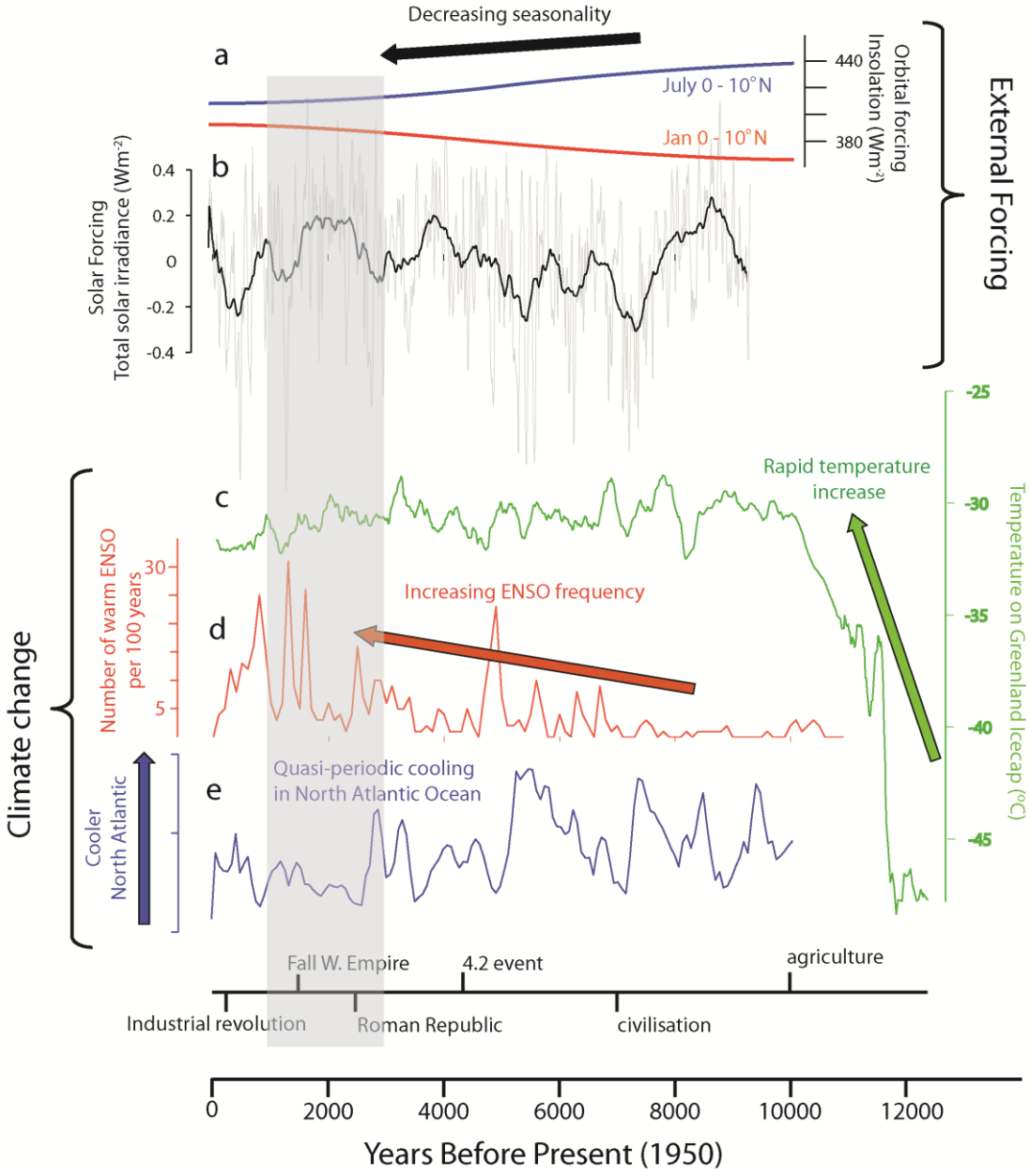

Figure 1.2 Holocene climate forcing and climate change (a) Orbitally forced changes in insolation in January and July averaged from 0 - 10°N (Berger and Loutre, 1991) **(b)** Total solar irradiance (TSI) variations reconstructed from ^{10}Be and ^{14}C isotopes (Steinhilber et al., 2012, 2009). A 500 year moving average is plotted over the original detrended reconstruction **(c)** Temperature on the Greenland Icecap (Alley, 2000) **(d)** Frequency of warm ENSO events from Laguna Pallcacocha in Ecuador (Moy et al., 2002) **(e)** Stacked record of percentages of ice rafted debris at core locations in the North Atlantic (Bond et al. 2001). Relevant historical events are presented on the timeline below. The grey shaded area shows the period of investigation in chapters 3 to 5.

1.4 Holocene climate and society

Undoubtedly the warmer conditions that were prevalent during the Holocene compared with the preceding glacial period facilitated the emergence and growth of human civilisation (Fig. 1.2c) (Rockström et al., 2009). It is proposed that warming in the Early Holocene and associated sea level rise flooded the Arabian Gulf pushing the inhabitants of the region into the marshlands of Southern Mesopotamia (Rose, 2010). It is theorised that the high population density in addition to a high water table and available surface water stimulated populations to develop irrigation technology and expand their habitable area thus increasing the carrying capacity of the region (Kennett and Kennett, 2006). The impact of sea level rise on human societies was gradual in most regions of the world providing them with time to adapt. However, there is evidence that more sudden climatic changes associated with Holocene climate anomalies may have had detrimental impacts on a number of past civilisations.

Archaeological excavations in present-day northern Syria indicate that ancient Amorite settlements which had developed over the previous 200 years, were suddenly abandoned 4,200 years ago (Weiss, 1982). Paleoclimatic evidence from the region (Arz et al., 2006; Cullen et al., 2000) implicates a sudden and extreme drought event as the cause of the abandonment of this prosperous urbanised society (Weiss, 1982). Amorite food production was based on rainfed grain, thus when the drought struck, the dry conditions are thought to have had a devastating impact on yields (Weiss et al., 1993). The drought caused an influx of climate refugees into Southern Mesopotamia and stimulated the construction of a 180km wall known as the "Repeller of the Amorites" to stem the flood of refugees (Weiss et al., 1993). Southern Mesopotamia is proposed to have been less vulnerable to drought conditions because their agriculture was based primarily on irrigation from the large Tigris and Euphrates river catchments (Fig. 1.3).

The dry climatic event at 4,200 yr BP was likely not restricted to the Fertile Crescent region with a short and dramatic aridification also indicated in Central Plains of North America (Booth et al., 2005) and the Indus Valley (Staubwasser, 2003). In contrast, evidence from Northern China indicates the period around 4,200 yr BP was typified by extreme flooding events (Huang et al.,

2011). The cause of sudden and extreme climate anomalies across the Northern Hemisphere at this time remain a matter of debate. A number of records indicate that a cooling of the North Atlantic caused by a slowing down in the overturning circulation led to these climatic changes (Bianchi and McCave, 1999; Bond et al. 2001; deMenocal et al., 2000). However, dating of the marine records remains too uncertain to isolate North Atlantic temperature changes as the cause (Booth et al., 2005).

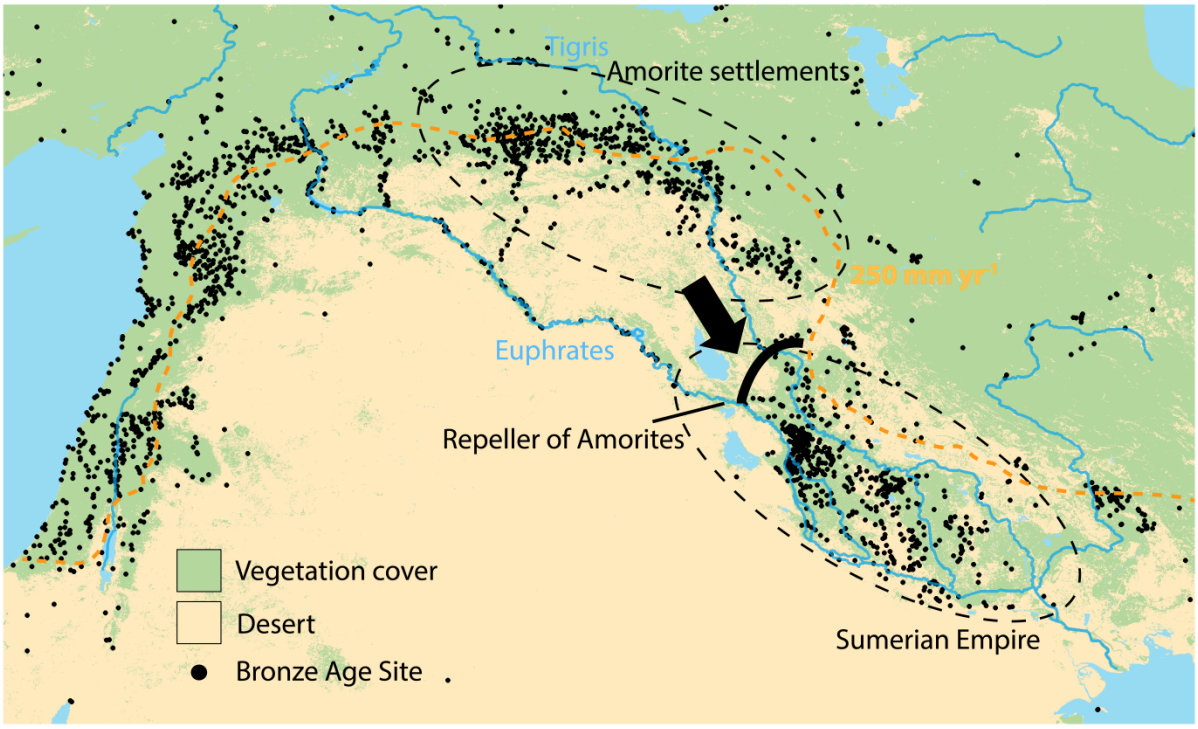

Figure 1.3 Distribution of Bronze Age settlements in the Fertile Crescent overlain with present day vegetation cover and the 250mm yr^{-1} rainfall isohyet. Vegetation cover and settlement distribution track the 250mm yr^{-1} rainfall isohyet in most of the Fertile Crescent region. However, along the Euphrates and Tigris rivers as well as in Southern Mesopotamia settlement was possible owing to an abundance of surface water and a high groundwater table that provided water for irrigation. During a climate change event 4,200 years ago, the rainfed agricultural plains of the Northern Fertile Crescent experienced dramatic aridification. Without alternative water sources wheat yields of the Amorite people were decimated. The Sumerian Empire on the other hand was less seriously affected owing to their use of surface and groundwater for agriculture. In order to stem the influx of climate refugees during this period, the Sumerians erected a 180 km wall known as the Repeller of Amorites.

Climate changes associated with solar variability have also been implicated in the fall of a number of past civilisations. For example, an accurately dated reconstruction of monsoon intensity from Wanxiang Cave in Northern China demonstrates that dynastic change in China in the last 1800 years coincided with periods of low solar irradiance and a weaker monsoon (Zhang et al., 2008). In contrast, the fall of the Mayan civilisation is attributed to dry climatic conditions associated with a peak in solar irradiance (Curtis et al., 1998; Hodell et al., 2001, 1995). A wealth of archaeological evidence indicates that the period leading up the dry climatic interval was typified by rapid population growth, extensive monument construction, and an intensification of deforestation for agriculture (Gill, 2001; Santley et al., 1986; Webster, 2002). The land use changes were particularly intense in the densely populated, low lying regions of the Yucatan Peninsula and are proposed to have caused high levels of soil erosion. During the period of climatic aridification, this low lying region exhibited far greater depopulation compared with mountainous and coastal regions of the Yucatan (Santley et al., 1986). This evidence has contributed to a growing understanding that socioecological developments in the period leading up the change in climate were crucial in determining the impact that climate change had on the Mayan society.

The importance of socioecological conditions for determining the impact of climate perturbations was dramatically illustrated by the Great Potato Famine in Ireland between 1845 and 1852. Anomalously warm and wet conditions in the mid-19th century created ideal conditions for the spread of a fungal pathogen called *Phytophthora infestans* or potato blight that destroyed successive potato crops (Anderson et al., 2004; Fraser, 2003). In total, 25% of the Irish population died of starvation or emigrated during this period (Donnelly Jr, 2012). Although the spread of potato blight was triggered by climate, the famine that caused the deaths of so many Irish was triggered by socioeconomic conditions in the period leading up to climatic perturbation (Fraser, 2003). The potato was introduced to Ireland from South America around 1600. The ability of the potato to grow in poor soils increased the carrying capacity of the island and caused a population explosion from 2 million to 8 million in approximately 200 years (Donnelly Jr, 2012). Most of the Irish population were rural tenant farmers under servitude to wealthy British landlords. With the end of the Napoleonic wars in 1815 wheat prices dropped in Britain whilst

the emerging industrial revolution created an affluent urban class who had an increased demand for meat. As Britain's principal agricultural exporter, demand for wheat dropped in Ireland whilst demand for livestock increased (Fraser, 2003). The change in agriculture led to large-scale evictions of Irish tenants as landlords switched to less labour intensive and more profitable livestock farming. These evicted tenants were pushed onto marginal land where they became wholly dependent on the potato for food owing to its ability to grow in poor soils. This dependence on a single food, made the Irish poor extremely vulnerable to the climatic changes that triggered the spread of potato blight. The ruling British elite, in contrast, had a much more varied diet as well as access to a global trade network which meant they were more or less unaffected by the potato blight.

1.5 Knowledge Gaps

1.5.1 Solar influence on climate

It is clear that solar irradiance variations are linked with many of the anomalous changes in climate that occurred during the Holocene. Climate model simulations have demonstrated mechanisms through which solar irradiance may be communicated to the climate system (Meehl et al., 2008; Shindell et al., 1999). However, attributing correlations in data to a particular solar forcing mechanism remains challenging. One reason for this difficulty is because models predict a coherent response of the climate system to solar forcing at large spatial scales. However at regional spatial scales internal dynamics of the climate are thought to dominate the external forcing signal (Goosse and Renssen, 2007; Goosse et al., 2005). Thus, in order to have confidence in attributing correlations in data to a particular solar forcing mechanism, it is necessary to determine if that correlation is consistent at a larger spatial scale than a single reconstruction allows. That requires comparing a number of climate reconstructions from different regions. Such comparisons are common for understanding orbital forcing of the climate system. However, solar variations operate on shorter timescales. Given that reconstructions vary in terms of resolution and dating uncertainty, comparisons among records are difficult. It has thus proven challenging to find evidence for a particular solar forcing mechanism of Holocene climate using data.

1.5.2 Mediterranean climate during the Roman Period

Despite a widespread interest in the Roman Period in the Mediterranean among a variety of scholars, a regional-scale reconstruction of the change in precipitation has never been done. Such a reconstruction is critical to understanding the impact that changes in climate had on the Roman civilisation in the water-limited environment of the Mediterranean. Some modelling studies have proposed that climate was wetter during the Early Roman Period because greater forest cover maintained a wetter climate through land-atmosphere feedbacks (Dümenil Gates and Ließ, 2001; Reale and Dirmeyer, 2000; Reale and Shukla, 2000). However, that theory has never been confronted with data. Regional reconstructions of precipitation in the Mediterranean also have the potential to illuminate changes in larger scale synoptic systems at the time because precipitation patterns in the Mediterranean are highly correlated with changes in winter storm tracks (Dünkeloh and Jacobeit, 2003; Xoplaki et al., 2004). An understanding of changes in the storm tracks would be an important step in understanding what caused climate change in the Mediterranean during the Late Holocene.

1.5.3 Climate and society

Climate change is implicated in having a detrimental impact on a number of past societies (de Menocal, 2001; Weiss et al., 1993). However, the impact of changes in climate on a society is not just dependent on the magnitude of change but also the socioeconomic conditions in that society at the time of the change (Fraser, 2003). Thus, in order to understand the impact of climate on societies it is necessary to understand the elements within that society that provide resilience or vulnerability. As I have mentioned, the factors within a society that are linked with resilience to climatic changes are varied but one of the key factors is a stable food supply. However, it is not instructive to simply infer an impact on food supply based on a change in climate, because the impact of the change will vary based on environmental conditions as well as food production and redistribution practices. Thus, in order to understand the heterogeneous impact of climate on societies in the context of food supply, a spatial, process modelling approach is desirable. In a past context reconstructions can provide constraints and validation for such models, whilst models can help with refining theories based on physical and environmental constraints.

1.6 Research aims and motivation

Significant gaps remain in our knowledge of the drivers of changes in climate during the Holocene. In addition, our understanding of how past civilisations were impacted by climate change is limited. In this thesis I undertake to close these knowledge gaps.

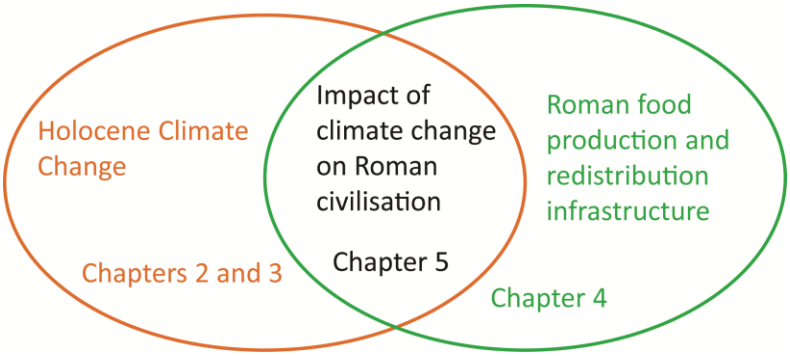

Figure 1.4 Thesis structure. The first part of the thesis is focused on understanding the causes of climate change during the Holocene. I begin in chapter 2 by investigating how small variations in solar irradiance led to relatively large climate changes during the Holocene. In chapter 3 I analyse climate change in the Mediterranean region during the Roman period. The second part of the thesis is concerned understanding how climate impacted the Roman civilisation. To that end, I develop a Virtual Water network of the Roman world in chapter 4 that simulates Roman food production and redistribution in response to interannual climate variability. Chapter 5 presents analysis of how resilient the Roman food supply infrastructure was to large scale and persistent climate change building on my findings in chapters 3 and 4.

I begin in chapter 2 with a global perspective by setting out to understand how solar irradiance variations impacted the climate system during the Holocene. It is clear that solar irradiance variations are linked with many of the anomalous changes in climate that occurred during the Holocene (Asmerom et al., 2007; Bond et al. 2001; Wang et al., 2005); however the mechanisms that enable small changes in solar radiation to cause relatively large climate changes are unclear (Gray et al., 2010; Wanner et al., 2008). One magnification mechanism is proposed to be the coupled ocean-atmosphere system of the Tropical Pacific, which is the largest source of heat and moisture to the atmosphere (Emile-Geay et al., 2007; Meehl et al., 2009, 2008). The dynamics of the Tropical Pacific changed during the Holocene owing to orbital forcing. I examine if there is evidence that the Tropical Pacific also responded to solar forcing during the Holocene. In

addition I investigate if orbital-forced changes in Tropical Pacific affected the communication of solar irradiance variations to the climate system. The methodology I apply to uncover solar forcing of the Tropical Pacific facilitates quantitative comparison among reconstructions whilst taking into account chronological uncertainties of the records used. **Research question 1: How are variations in solar irradiance communicated to the climate system?**

In chapter 3 I focus on the Mediterranean region during the period coinciding with the emergence of the Roman civilisation. The Mediterranean has a complex climate that is influenced by large-scale synoptic climatic systems as well more regional influences (Lionello, 2012). Precipitation patterns in the region have been shown to be highly correlated with synoptic scale changes in the position and intensity of the Jetstream in winter (Dünkeloh and Jacobeit, 2003; Xoplaki et al., 2004). In order to gain a better understanding of the changes in the Jetstream during this period I carry out a regionally comprehensive reconstruction of changes in climatic humidity. This reconstruction is also important as it demonstrates the dominant changes in precipitation during an important time in human civilisation. To understand the impact of local processes I use a combined modelling and data approach. In particular I investigate whether there is evidence for anthropogenic climate change during the Roman period owing to deforestation as has been theorised in previous studies. Given the interest of the Roman period in the Mediterranean to a wide variety of academics, it is envisaged that this regionally comprehensive reconstruction of changes in precipitation will provide a springboard for interdisciplinary studies on the interaction between climate and society during the Roman period. **Research Question 2: How did the climate change during the Roman Period in the Mediterranean and what were the drivers of these changes?**

In the second part of this thesis I set out to gain an understanding of the impact of climate on past societies. I maintain a focus on the Mediterranean and investigate the resilience of the Roman civilisation to interannual climate variability. I define resilience as ‘‘the capacity of a system to absorb and utilize or even benefit from perturbations and changes that attain it, and so to persist without a qualitative change in the system’s structure” (Holling, 1986). In chapter 4 I apply a process-based modelling approach to understand the impact climate change had on grain

production during the Roman Empire. Irrigation and trade are incorporated in the modelling approach used, as both are proposed to have been central to ensuring a stable food supply within the Empire (Erdkamp, 2005). The advantage of applying process-based models in an historical context is that process-based models provide constraints of what was physically possible given the environmental conditions. That allows theories to be refined based on physical constraints. However, historical and paleoclimatic information also provide constraints for models and allow us to compare modelled outcomes with what happened in reality (Cornell et al., 2010). Given the numerous parallels between the Romans and the present-day globalised society, it is envisaged that this analysis will illuminate how resilient our current water resource management strategies are to climatic variability. **Research Question 3: How did the Roman water resource management strategy impact their resilience to climate variability?**

Owing to the length of their reign it appears that the Romans developed mechanisms that made them highly resilient to the variable climate of the Mediterranean (Lionello, 2012). Nonetheless the Western Empire did eventually collapse whereas the Eastern Empire continued for almost another 1000 years in the guise of the Byzantine Empire (Gibbon, 1776). Thus, the Roman civilisation encapsulates a variety of responses to climate change. Building on the previous 2 chapters, in chapter 5 I set out to understand whether Roman water resource management provided resilience to large-scale and persistent climate change that occurred between the Roman Warm Period and the Dark Ages Cold Period. **Research Question 4: What was the impact of Holocene climate anomalies on Roman water resource management?**

In the chapter 6 I provide a synthesis and discussion of my results and provide recommendations for future research.

Chapter 2

The Tropical Pacific: A changeable communicator of Holocene solar forcing

Submitted as: Dermody, B.J., van der Velde, Y., de Boer, H.J., Donders, T.H., Wassen, M.J., Drijfhout, S.S., Bierkens, M.F.P., Dekker, S.C., 2014. The Tropical Pacific: A changeable communicator of Holocene solar forcing. Palaeogeography, Palaeoclimatology, Palaeoecology

Abstract

During the Holocene, small variations in radiation emitted from the sun were correlated with centennial-scale climate anomalies throughout the globe. Still, debate persists about how these small changes in solar irradiance were communicated to the climate system. Our multiproxy analysis indicates that the Tropical Pacific played a role in communicating solar forcing to the climate. We demonstrate that changes in SST in the Tropical Pacific were correlated with solar irradiance throughout the Holocene. Importantly, we demonstrate that the response of the Tropical Pacific to solar forcing likely changed in the Mid Holocene owing to the superposition of solar and orbital forcing. In the Early Holocene, the Tropical Pacific warmed (cooled) during solar maxima (minima). However, solar forcing of the thermostat response in the Late Holocene caused the Tropical Pacific to cool (warm) during solar maxima (minima).

2.1 Introduction

Holocene climate anomalies at sub-orbital timescales are linked to variations in radiation emitted from the surface of the sun as evidenced by numerous climate reconstructions throughout the globe that are correlated with reconstructed variations in solar irradiance (Asmerom et al., 2007; Bond et al. 2001; Marchitto et al., 2010; Steinhilber et al., 2012). However, our understanding of the mechanisms linking these variations in solar irradiance to climatic events remains unclear (Gray et al., 2010; Wanner et al., 2008). From a quantitative energetics perspective, the fluctuations in total solar irradiance (TSI) are thought to have been too small (0.05-0.5% of TSI) to cause climate change of the magnitude recorded in the paleo record (Emile-Geay et al., 2007; Gray et al., 2010). Instead numerous climate model studies reveal mechanisms within the Earth's climate system that may magnify the impact of these fluctuations in solar irradiance (Gray et al., 2010; Meehl et al., 2008; Shindell et al., 1999; Shindell et al., 2001). One of the principal amplification mechanisms is proposed to be solar forcing of the Coupled Ocean-Atmosphere System of the Tropical Pacific (COASTP) whereby small changes in radiation can be amplified by the system and communicated to the climate (Emile-Geay et al., 2007; Meehl et al., 2009, 2008).

2.1.1 The Tropical Pacific Ocean

The Tropical Pacific is of central importance to the global climate system being the largest reservoir of warm surface water on Earth and thus the main source of heat and moisture for the atmosphere (Pierrehumbert, 2000, 1995; Tierney et al., 2010). Changes in the spatial distribution of warm surface waters of the Tropical Pacific, particularly the waters comprising the Indo Pacific Warm Pool, modify the location and strength of convection in the rising limb of the Hadley and Walker circulations. As a result, variations in SST in the Pacific can have a considerable impact on atmospheric circulation and heat content globally (Pierrehumbert, 1995). Changes in the COASTP are integrated over time by the oceanic component of the system (Newman et al., 2003). Newman et al. (2003) demonstrated that decadal changes in the SST of the Pacific captured by the Pacific Decadal Oscillation (PDO) represent a low pass filtering of the El Niño Southern Oscillation (ENSO). This is particularly relevant in a paleoclimatic context

because it indicates that reconstructions of long-term changes in SST may illuminate past dynamics of the COASTP at shorter timescales (Newman et al., 2003).

The oceanic component of the COASTP comprises the Indo Pacific Warm Pool (IPWP) which is the largest source of heat and moisture for the atmosphere globally, the Eastern Pacific Cold Tongue (EPCT), which is the largest region of equatorial upwelling globally as well as the poleward currents such as the Kuroshio Current (KC), which is important for regulating wintertime temperatures in the Northern Pacific extra-tropics. All three of these components are linked by oceanic surface currents whose speed and direction are driven by a complex combination of atmospheric and oceanic gradients as well as the weak but persistent Coriolis force (Fig. 2.1) (Sun and Liu, 1996). Extended periods with more frequent El Niño events are characterised by a warming of the SST in the IPWP, EPCT and KC whilst periods with more frequent La Niña are characterised by cooling (Fig. 2.1b) (Mantua et al., 1997; Newman et al., 2003; Qiu, 2003).

2.1.2 Holocene Orbital Forcing of the Tropical Pacific

In order to understand how variations in solar irradiance may have impacted the Tropical Pacific during the Holocene, it is important to understand that orbital forcing was the 1st order forcing of the Tropical Pacific during the Holocene (Clement et al., 1999; Koutavas et al., 2006). Solar irradiance forcing was superimposed on a system that itself was responding to millennial-scale trends caused by changes in the orbit of the Earth around the sun (Donders et al., 2008; Haug et al., 2001). During the Holocene, the tilt of the Earth's axis decreased from a maximum of 24.2° in the Early Holocene to 23.4° in present day. In addition, the time when the Earth was closest to the sun (perihelion) shifted from boreal summer in the Early Holocene to boreal winter in the Late Holocene (Crucifix et al., 2002). The sum of these trends decreased the differences between the seasons from the Early to Late Holocene (Lorenz et al., 2006). It is simulated in models and demonstrated in data that these orbital trends led to a weakening of ocean-atmospheric coupling in the COASTP during the Holocene and an increase in the frequency and amplitude of the El Niño Southern Oscillation (ENSO) (Clement et al., 1999; Koutavas et al., 2006; Moy et al., 2002).

These trends were brought about by a mechanism known as the ocean dynamical thermostat (Clement et al., 1996).

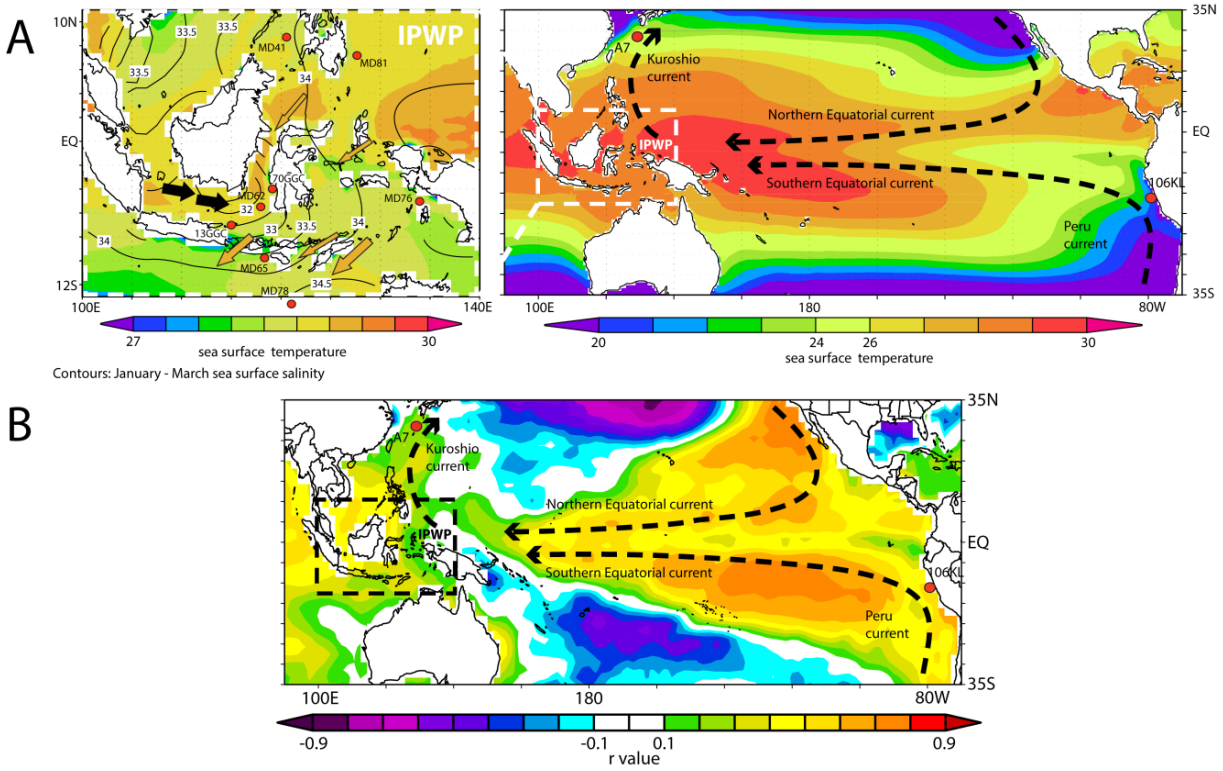

Figure 2.1 Tropical Pacific currents and proxy records used in analysis. (a) Coastal winds and trade winds cause upwelling of cool deep water to the ocean surface in the Eastern Pacific Cold Tongue. These waters are transported westwards by Equatorial surface currents, that are driven by the same trade winds that cause equatorial upwelling. On their passage westwards, these cool waters become progressively warmer owing to the suns radiation so that when they reach the land barriers in the Western Pacific there is a build-up and further warming of these warm waters, forming the Indo Pacific Warm Pool (IPWP). Along the coast of the Western Pacific, western boundary currents transport these waters poleward. The Kuroshio Current is the northern branch of these poleward surface water flows. Within the IPWP, SSTs are warmed by the flow of warm water from the Western Pacific via the Indonesian throughflow current (ITF) (Orange arrows). During the Asian Monsoon, freshwater anomalies in the South China Sea flow into the Makassar Straight blocking the ITF current (Black arrows), and cooling SSTs in the Makassar Straight. Our analysis is based on cores in the Eastern Pacific Cold Tongue, the IPWP and the Kuroshio Current. **(b)** Correlation between Pacific Decadal Oscillation index and SST. SSTs in core locations warm (cool) under a positive (negative) phase of the PDO (Mantua et al., 1997; Qiu, 2003). A positive (negative) phase of the PDO is associated with more frequent El Niño (La Niña) events (Newman et al., 2003).

The thermostat mechanism arises because radiation from the sun does not warm the surface waters of the Tropical Pacific evenly (Clement et al., 1996; Sun and Liu, 1996). Instead, upwelling and surface divergence in the Eastern Pacific Cold Tongue move some of sun's heat poleward meaning that equatorial SSTs in the Eastern Pacific warm less compared with the West (Clement et al., 1996; Seager et al., 1988). The increased equatorial east-west SST gradient strengthens easterly winds through associated changes in sea level pressure. A positive feedback exists whereby stronger Easterlies increase upwelling of cool waters in the East Pacific and push warmer waters towards the Indo Pacific Warm Pool (IPWP) in the west, strengthening the SST and pressure gradients further (Bjerknes, 1964; Zebiak and Cane, 1987). The thermostat mechanism was strongest during the Holocene Climatic Optimum (6,000 – 9,000 yr BP) when the difference in seasonality was greatest (Lorenz et al., 2006) as evidenced by a large SST gradient between the EPCT and IPWP at the time (Koutavas et al., 2006). Model simulations indicate orbital forcing of the thermostat mechanism was responsible for the persistence of La Niña-like conditions in the Early – Mid Holocene. In the Late Holocene, the perihelion shifted to the winter months and coupled with decreased seasonality the thermostat mechanism weakened as did the zonal gradient in SST (Clement et al., 2000, 1999; Koutavas and Joanides, 2012; Koutavas et al., 2006).

Weakening of the zonal SST gradient led to an intensification of ENSO with maximum frequency and amplitude recorded at approx. 1200 yr BP (Clement et al., 2000, 1999; Conroy et al., 2008; Koutavas and Joanides, 2012; Koutavas et al., 2006; Moy et al., 2002; Rein et al., 2005). Changes in ENSO in the Early – Mid Holocene are more controversial with some studies indicating almost no activity in the Early Holocene (Clement et al., 2000; Conroy et al., 2008; Moy et al., 2002). In contrast, other studies indicate that the Mid Holocene (4000 – 6000 yr BP) represented a minimum in ENSO activity with the Holocene Climatic Optimum exhibiting intermediate activity compared with the Mid and Late Holocene (Koutavas and Joanides, 2012; Rein et al., 2005). The discrepancy between model simulations which indicate a more or less linear trend of increasing ENSO frequency and amplitude during the Holocene (Clement et al., 2000; Emile-Geay et al., 2007) and proxy reconstructions, which demonstrate contrasting and often sudden changes in ENSO remains a source of uncertainty.

2.1.3 Holocene Solar Forcing of the Tropical Pacific

Superimposed on 1st order orbital forcing of the Tropical Pacific, solar irradiance variations provided a 2nd order forcing mechanism at shorter timescales (Emile-Geay et al., 2007; Mann et al., 2005; Marchitto et al., 2010). Orbitally forced reduction in the zonal SST and pressure gradients in the Tropical Pacific led to a weakening of the trade winds during the Holocene (Clement et al., 2000). The slackening of easterly winds increased the potential for warm waters of the IPWP to flow eastward thus enhancing the oscillation between La Niña and El Niño described by the ENSO index (Clement et al., 2000, 1999). Under an oscillating system, models simulate that small increases in insolation during solar maxima were able to force a thermostat response in the Tropical Pacific (Emile-Geay et al., 2007; Mann et al., 2005). Because the thermostat mechanism incorporates a positive feedback, these small changes in insolation were magnified by the COASTP making La Niña conditions more likely during solar maxima and El Niño conditions more likely during solar minima during the Late Holocene (Bjerknes, 1964; Emile-Geay et al., 2007; Meehl et al., 2008).

A number of data-based studies provide intermittent and contrasting evidence of solar forcing of the Tropical Pacific during the Holocene. For example Marchitto et al. (2010) show in-phase relations between solar irradiance and upwelling off the coast of Baja, California in the East Pacific for a 1500 year period in the Early Holocene, consistent with solar forcing of the thermostat mechanism but in a period earlier than predicted by models (Emile-Geay et al., 2007). SSTs in the Makassar Straight of the IPWP exhibited warming and cooling during Medieval Climate Anomaly and Little Ice Age, when irradiance was increased and decreased respectively (Newton et al., 2006; Oppo et al., 2009). In a study from the eastern IPWP, (Khider et al., 2014) conclude that there was no evidence for solar forcing based on analysis of a core which captures changes in SST as well as temperatures at intermediate depths. Hydrologic indicators from the East and West Tropical Pacific indicate a strengthening of Walker Circulation during the Little Ice Age (LIA) solar minima, whereas a weakening is indicated during the Medieval Climate Anomaly (MCA) solar maximum (Yan et al., 2011a, 2011b). Yan et al. (2011b) highlight that these results are inconsistent with reconstructions of the ocean component of the COASTP that

indicate El Niño-like conditions during the LIA and La Niña-like conditions during the MCA, consistent with solar forcing of the Tropical Pacific simulated in models (Emile-Geay et al., 2007; Mann et al., 2005).

The contrasting evidence for solar forcing of the Tropical Pacific at different locations and differing periods during the Holocene highlights the need for a study encompassing the important components of the COASTP throughout the Holocene as has been done in studies of orbital forcing (Koutavas and Joanides, 2012; Koutavas et al., 2006). Indeed, model simulations have demonstrated that the oceanic response to solar forcing is only detectable at larger spatial scales (Goosse and Renssen, 2007; Weber et al., 2004). However, a number of barriers exist that complicate the comparison of marine records from different locations at the centennial resolution relevant for solar forcing. Firstly, dating uncertainty is generally high among marine sedimentary records owing to variable accumulation rates, reworking of sediments as well as the dating method used (Andrews et al., 1999). In addition, individual records may be susceptible to local oceanic processes which influence the reservoir age of the record (Khider et al., 2014; Sun et al., 2005). Wiggle matching is sometimes used to overcome such chronological uncertainties, however that practice runs the risk of pulling unrelated anomalies among timeseries into one imaginary event (Blaauw et al., 2007). Aside from chronological uncertainties, external forcing may be overshadowed by internal oceanic dynamics at smaller spatial scales (Goosse and Renssen, 2007; Khider et al., 2014).

In this paper we set out to overcome these barriers and provide a picture of the impact of solar forcing on the Tropical Pacific throughout the Holocene. We do so by providing data-based evidence of the transient response of the COASTP to solar forcing throughout the Holocene from records from the Eastern Pacific Cold Tongue (EPCT), The Indo Pacific Warm Pool (IPWP) and the Kuroshio Current (KC). In order to confront the problem of chronological uncertainties among records we interrogate the relations we find taking into account the dating errors associated with each record (Blaauw et al., 2007). In addition, we use stacked records where available that smooth out anomalies associated with incorrect reservoir age estimation or the influence of local processes on measurements. Owing to the chronological uncertainties and varying resolution among records we focus our analysis on 500 – 1000 year timescales. We are

aware this timescale represents an upper limit relevant for Holocene climate anomalies; however when chronological uncertainty and temporal resolution among proxies is taken into account it also represents the lower limit at which the data can be interrogated. In addition, model simulations have indicated that a direct response of the ocean to solar forcing is likely only detectable at timescales longer than a few hundred years (Weber et al., 2004). Given that longer term changes in the SST of the regions analysed are indicative of the dominant behaviour of the coupled ocean atmosphere system at shorter timescales this timescale is nonetheless highly informative (Newman et al., 2003). Given the potential importance of the Tropical Pacific as a communicator of solar forcing, this study represents a preliminary but important step in understanding the mechanism behind Holocene climate anomalies.

2.2 Methods

We selected SST reconstructions from 3 regions of the Tropical Pacific where changes in the COASTP stimulate a response in ocean surface temperature: the region of upwelling in the Eastern Pacific Cold Tongue (EPCT) (Rein et al., 2005), the Indo Pacific Warm Pool (IPWP) (Levi et al., 2007; Linsley et al., 2010; Rosenthal et al., 2003; Steinke et al., 2008; Stott et al., 2007, 2004; Visser et al., 2003; Xu et al., 2008) and the Kuroshio Current (KC) (Sun et al., 2005) (see Table 2.1 and Fig. 2.1a for proxy locations). Given the importance of the IPWP for climate and the relative abundance of Holocene SST reconstructions from the region (Linsley et al., 2010), we carried out an in-depth analysis of the response of the IPWP to solar forcing, focussing on the Makassar Straight and Western Pacific Warm Pool (WPWP). All reconstructions are continuous from the Early to Late Holocene, which allows us to uncover the transient relation between solar irradiance forcing and orbital forced changes in Tropical Pacific.

Table 2.1. Sediment cores used in analysis. The cores highlighted in the green and orange comprise the stacked record of the Makassar Straight and Western Pacific Warm Pool respectively and the stacked record of the Indo Pacific Warm Pool combined.

Location	Core ID	Coordinates	Resolution (yr)	Reference
Makassar St.	13GGC	7° 24' S, 115°12'E	38	Linsley et al. 2010
S. Makassar St.	MD62	4° 41' S, 117° 54'E	418	Visser et al. 2003
Makassar St.	70GGC	3° 34' S, 119°23'E	126	Linsley et al. 2010
Sumba, Indonesia	MD65	9° 39' S, 118° 20'E	209	Levi et al. 2007
Banda Sea	MD76	5° 00.18'S, 133° 26'E	49	Stott et al. 2007
W. Pacific, Mindanao	MD81	6° 27'N, 125° 50'E	49	Stott et al. 2004
Sulu Sea	MD41	8° 47' N, 121° 17'E	90	Rosenthal et al. 2003
Okinawa Trough	A7	27° 49.2'N, 126° 58.7'E	90	Sun et al. 2005
Peruvian Shelf	106KL	12° 03' S, 77°39.8'W	20	Rein et al. 2005

2.2.1 Cross correlation and change point analysis

Cross correlation and change point analysis was used to quantitatively identify if correlations between SST reconstructions and solar irradiance were significant above red noise and if a change in the sign of the correlation occurred during the Holocene. Change point analysis provides a quantitative method of determining if a change in a time series has taken place. It is suited to identifying persistent behaviour in a time series and is not overly sensitive to anomalous events, which is important given the errors inherent in paleo timeseries. Further details of the methodology can be found in (Taylor, 2000). The statistical significance level of cross correlation and change points were estimated using Monte Carlo methods. Using an AutoRegressive Moving Average (ARMA) model (Box and Jenkins, 1976) we generated 1000 surrogate timeseries with

the same autocorrelation structure as the climate timeseries under investigation. Given that our analysis focused on 500 – 1000 timescale, 500 – 1000 year low pass filters were applied to all timeseries. For each timeseries we calculated the cross correlation with the equivalent low pass filter of solar irradiance. We then estimated the significance level for each at a 90 % confidence interval. We did this for a range of correlation window sizes, selecting at each time step the correlation window size with the most significant correlation. All timeseries were linearly detrended prior to performing the analysis to remove the influence of orbital trends and isolate the solar variability. Where a statistically significant change point was identified, the time series was split about the change point and the analysis repeated until no more change points were detected. Unlike, the popular cross wavelet transform technique, cross correlation analysis makes no *apriori* assumption of periodicity in the two time series under investigation (Grinsted et al., 2004).

2.2.2 Uncertainty analysis

For records with available age depth models and depth measurement data (Linsley et al., 2010; Rosenthal et al., 2003; Stott et al., 2007, 2004; Sun et al., 2005; Xu et al., 2008) we applied the method of Blaauw (2010) for estimating uncertainty in age depth calculations. In this method each measured ^{14}C age is assumed to have symmetrical error (normal distribution) whilst calibration results in widened, asymmetrical and multi-peaked calendar age distribution (Fig. 2.2). At each depth with a dated ^{14}C age we selected a calibrated age from the calibration distribution based on the probability density function of the date. We then carried out the age depth modelling, interpolating between dates employing the interpolation method used by the authors of the original papers. This process was repeated to provide us with 1000 candidate time series that varied based on the chronological uncertainty of the dated sediments. We then carried out cross correlation and switch point analysis between these 1000 candidate records and solar irradiance. The average cross-correlation between these 1000 candidate time series and solar irradiance was compared with the cross-correlation of a1000 random surrogate time series with solar irradiance to test for statistical significance above red noise. The cross-correlation was considered significant if the distributions of cross-correlations for the candidate and the surrogate time series

overlapped by less than 10%. A switch point between each of the 1000 candidate time series and solar irradiance was considered significant whenever this switch point could not be reproduced by more than 10% of the surrogate time series, potentially resulting in a distribution of a 1000 significant switch points (one for each candidate time series). In this way, the cross-correlation with between solar irradiance and each of the observed time series can be quantified taking the dating uncertainty fully into account.

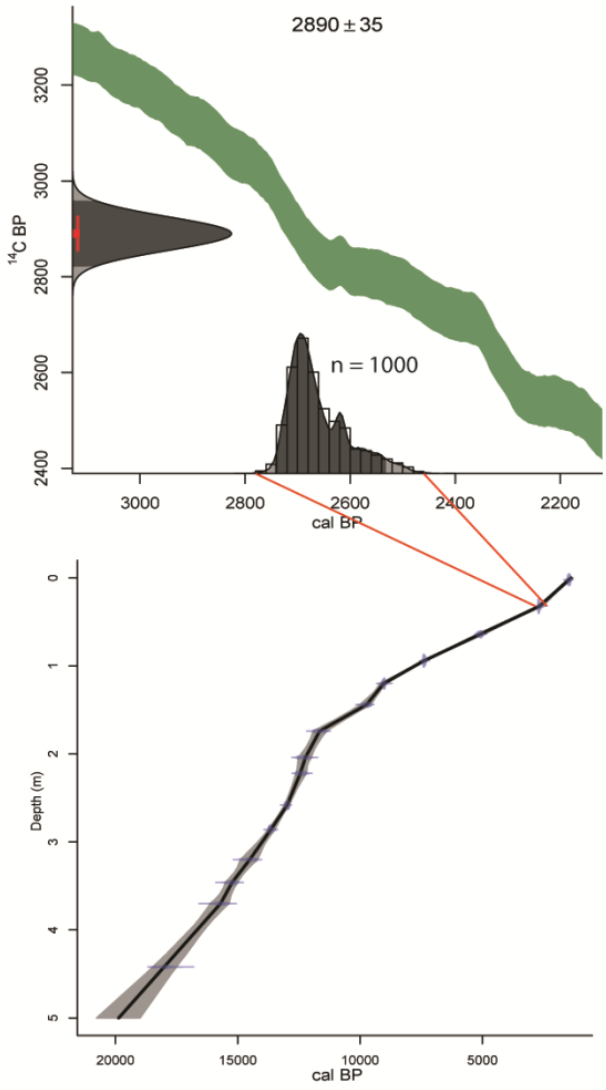

Figure 2.2 Generation of candidate time series (Kuroshio Current record of Sun et al. 2005) based on the chronological uncertainty of the dated sediments. At each depth with a dated ^{14}C age we selected a calibrated age from the calibration distribution based on the probability density function of the date. We then carried out the age depth modelling, interpolating between dates using the interpolation method used by the authors of the original papers. This was repeated to provide 1000 candidate time series that varied based on the chronological uncertainty of the dated depths.

2.3 Results

Cross correlation and change point analysis between solar irradiance and reconstructions of IPWP SST, KC SST and upwelling intensity in the EPCT is shown in Fig. 2.3. Statistically significant correlations between solar irradiance and stacked reconstruction of IPWP temperature are exhibited at centennial timescales (> 500 years) (Fig. 2.3). The sign of correlation between solar irradiance and IPWP temperature changes at the end of the Holocene Climate Optimum ~ 6000 yr BP. Before 6000 yr BP warmer IPWP temperatures were correlated with increased solar irradiance, after 6000 yr BP warmer IPWP temperatures were correlated with decreased irradiance. A similar pattern is shown for the KC with warmer temperatures of the current in the early Holocene during solar maxima whilst cooler temperatures are exhibited after 6000 yr BP during solar maxima. Statistically significant correlations are apparent at centennial timescales (> 300 years) of upwelling in the EPCT as well as a statistically significant change in sign. However, the change in sign of the correlation is delayed compared with the other two records occurring ~2000 years later at ~ 4000 yr BP. During solar maxima prior to 4000 yr BP, upwelling was subdued whilst after 4000 yr BP upwelling was increased during solar maxima. All time series are based on independent age models.

The cross correlation between solar irradiance and reconstructions of SST in the Western Pacific Warm Pool (WPWP) and Southern Makassar Straight are shown in Fig. 2.4 and 2.5 respectively. In each case the correlation between solar irradiance and the stacked reconstruction of SST from Linsley et al. (2010) is shown, with the correlations between solar irradiance and the individual records that comprise the stacked record shown below. The cross correlation between the stacked record of WPWP SST and the solar irradiance matches that of the entire IPWP. However, the stacked record from the Makassar Straight exhibits an opposite response to solar forcing, with cooler temperatures under increased irradiance during the Holocene Climate Optimum and warmer temperatures during solar maxima in the Late Holocene. The records that comprise the stacked reconstruction of WPWP SST are plotted based on their longitude with the most easterly record plotted on top (Fig. 2.4). The records that form the Makassar Straight stacked reconstruction are plotted along a gradient from low to high salinity (Fig. 2.5). The individual

records comprising the WPWP stacked reconstruction exhibit a lot of variation compared with the stacked record.

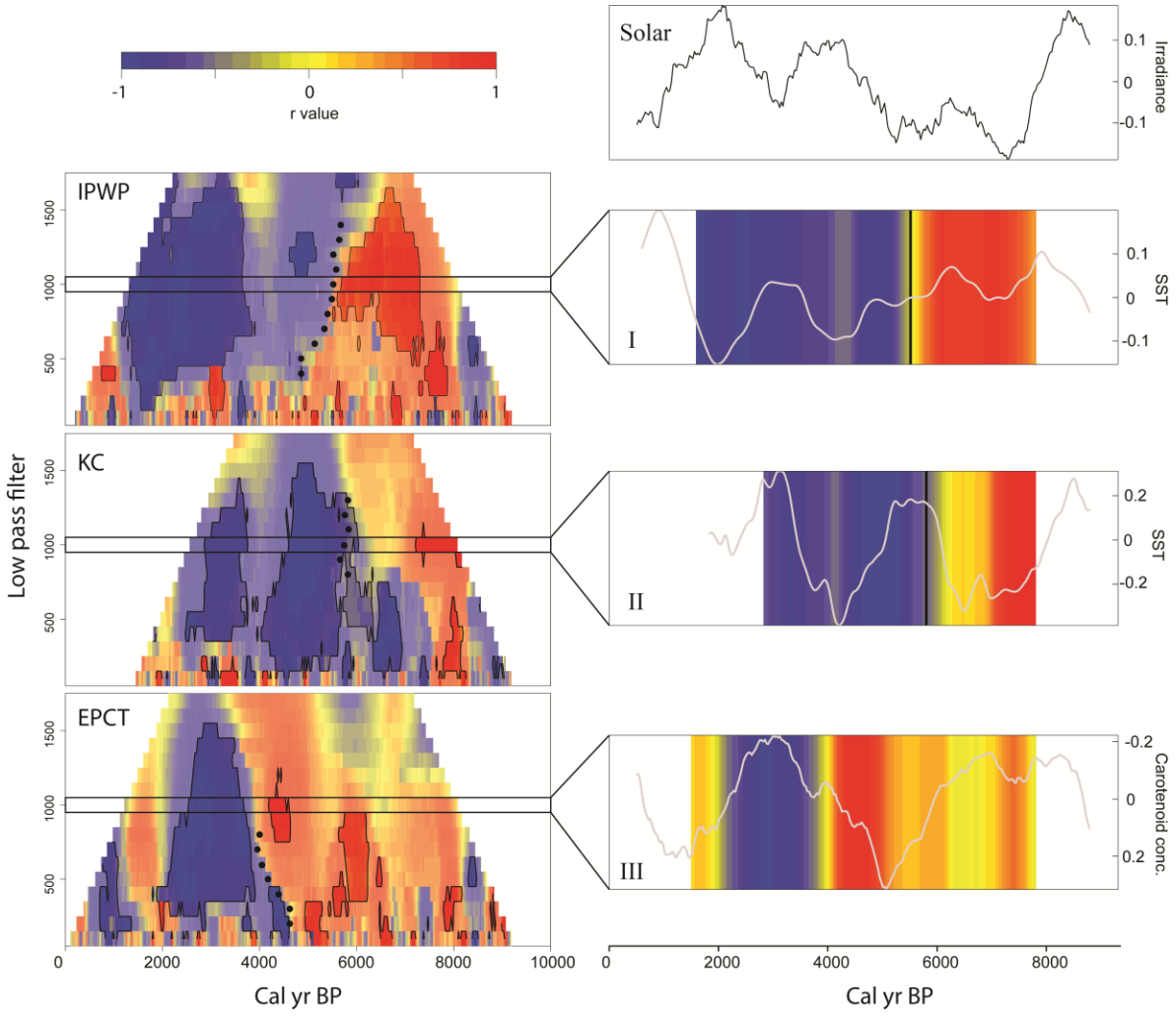

Figure 2.3 Cross correlation and change point analysis between reconstructions indicative of Tropical Pacific sea surface temperature and solar irradiance variations. The cross correlation between a stacked record of Indo Pacific Warm Pool SST (IPWP), SST of the Kuroshio Current (KC) and upwelling in the Eastern Pacific Cold Tongue (EPCT). The y-axis of the upwelling is inverted so that more positive values indicate less upwelling and warmer SST. All records exhibit a statistically significant shift in correlation with solar irradiance between 4000 – 6000 yr BP illustrated by black circles. In the Early Holocene, solar maxima are correlated with warmer SST in the IPWP, KC and decreased upwelling / warmer SST in EPCT. In the Late Holocene solar maxima are associated with cooler SSTs the IPWP, KC and increased upwelling / cooler SST in EPCT. Non-shaded regions exhibit statistically significant correlations.

The cross correlation, incorporating uncertainty analysis between the solar irradiance and the reconstruction of SST from the Okinawa trench are shown in Fig. 2.6. Sun et al. (2005) include two estimates of reservoir age, 700 hundred years, which they estimate is more accurate for the Holocene (A) and 400 years which they estimate is more accurate for the deglacial period (B). Both reconstructions exhibit the same pattern of a switch from positive correlation with solar irradiance prior to ~6000 yr BP to negative correlation after with a possible slight shift in correlation ~3000 yr BP. Unfortunately, we cannot test the uncertainties associated with the record of upwelling in the EPCT as the depth measurement data was lost (B. Rein pers. comm. 2014).

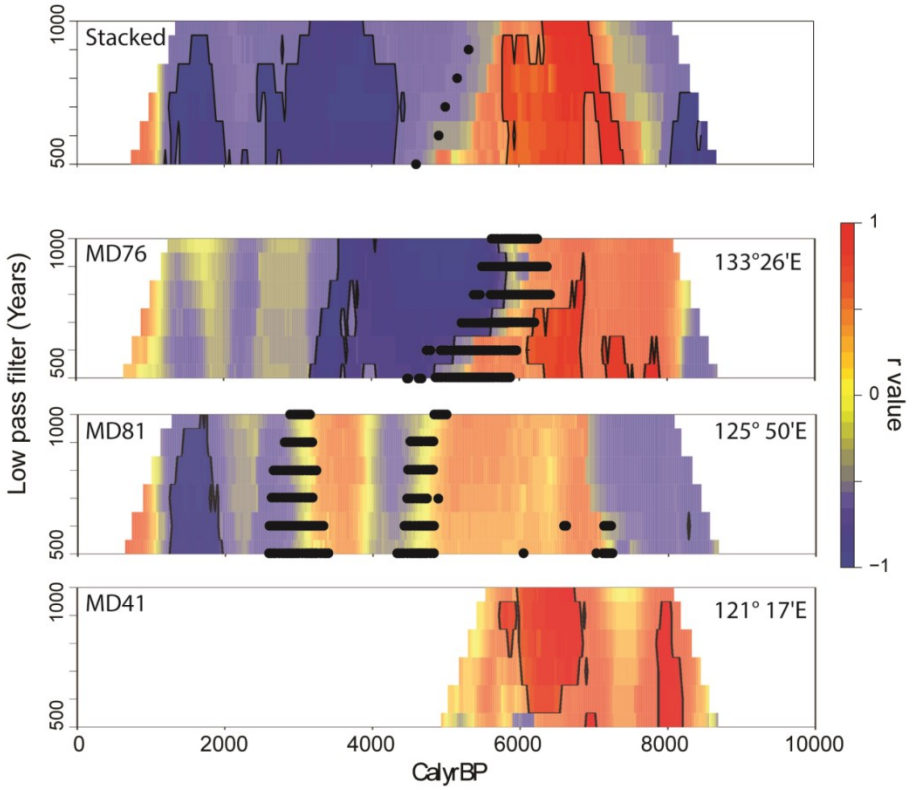

Figure 2.4 Cross correlation and change point analysis between solar irradiance and stacked reconstruction of SST in the Western Pacific Warm Pool SST. Below the stacked record the individual records comprising the stacked record including uncertainty analysis are shown. The individual records are arranged from east to west. MD76, furthest east in the WPWP exhibits the greatest coherence with the stacked record. For correlations incorporating uncertainty analysis, we have retained the range of switch points (black dots) arising from chronological error.

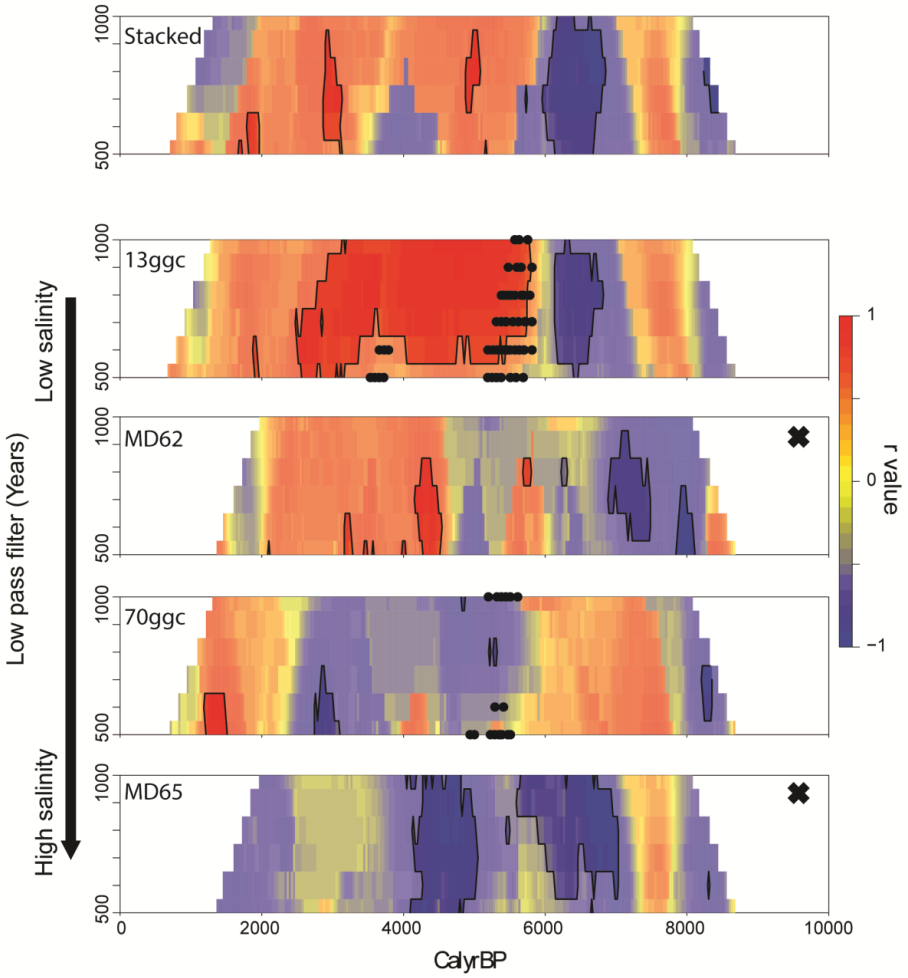

Figure 2.5 Cross correlation and change point analysis between solar irradiance and stacked reconstruction of SST in the Makassar Straight. Below the stacked record the individual records comprising the stacked record including uncertainty analysis are shown. The records from the Southern Makassar Straight are presented along a salinity gradient associated with fresh water influx during the Asian Monsoon. Those records impacted to the greatest extent by fresh water influx from the South China Sea during Monsoons exhibit the greatest coherence with the stacked record compared with those located at the boundary of freshwater intrusion into the Makassar Straight. Age model data was unavailable for the records marked with an 'X', thus correlations do not incorporate chronological uncertainty. For correlations incorporating uncertainty analysis, we have retained the range of switch points (black dots) arising from chronological error.

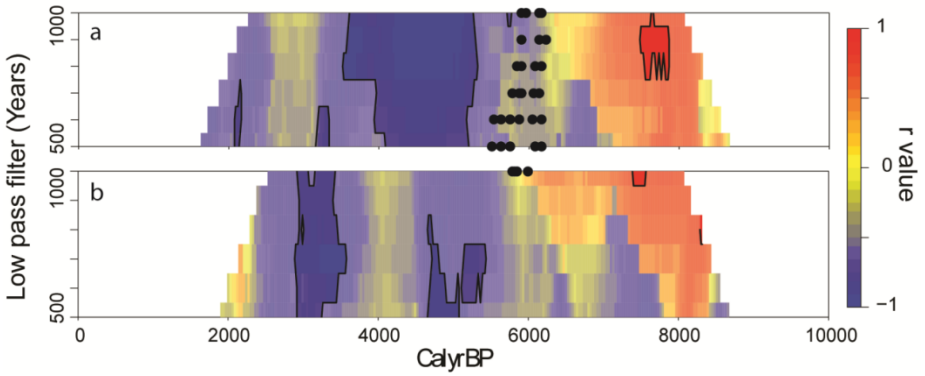

Figure 2.6 Cross correlation incorporating chronological uncertainty between Kuroshio Current SST and solar irradiance. Sun et al. (2005) include two estimates of reservoir age, 700 hundred years, which they estimate is more accurate for the Holocene **(a)** and 400 years which they estimate is more accurate for the deglacial period **(b)**. Both reconstructions exhibit the same pattern of a switch from positive correlation with solar irradiance prior to ~6000 yr BP to negative correlation after with a possible slight shift in correlation ~3000 yr BP. We have retained the range of switch points (black dots) arising from chronological error.

2.4 Discussion

Our analysis of reconstructions from the region of upwelling in the Eastern Pacific Cold Tongue (EPCT), Indo Pacific Warm Pool (IPWP) SST and SST of the Kuroshio Current (KC) indicates that solar irradiance variations forced changes in these components of the Tropical Pacific throughout the Holocene (Fig. 2.3). Importantly, our analysis demonstrates that the response of the Tropical Pacific to solar forcing likely changed after the Holocene Climatic Optimum. In the Early Holocene, it appears that SSTs throughout the Pacific warmed during solar maxima, whilst during the Late Holocene they cooled during solar maxima. There are discrepancies in the timing of changes among the records. In addition, the pattern varies strongly among individual records. Both of these non-trivial issues will be discussed in detail later in the discussion. However, given that the pattern of warming during solar maxima in the Early Holocene Climatic Optimum and cooling during solar maxima in the Late Holocene is exhibited in reconstructions with independent age models from three regions of the Pacific the signal shown is likely real and not an artefact of errors or uncertainties associated with a single record.

2.4.1 Solar forcing of the Tropical Pacific

Our analysis indicates that during the Early and Late Holocene, SSTs in the EPCT, IPWP and KC warmed and cooled coherently in response to solar forcing. However, the sign of the response switched from positive during the Holocene Climate optimum to negative in the Late Holocene (Fig. 2.3). Coherent warming and cooling of SST in the EPCT, IPWP and KC is consistent with decadal-scale changes in SST described by the Pacific Decadal Oscillation (PDO) index in current climate (Fig. 2.1b) (Mantua et al., 1997). Under a positive (negative) phase of the PDO SSTs warm (cool) in the EPCT, the IPWP and KC. In an analysis of observational data from 1900 – 2001, Newman et al. (2003) demonstrated that the PDO acts as a low pass filter of ENSO variability at all timescales studied. A positive PDO index (warm SSTs in the EPCT, IPWP, KS) is associated with periods of increased El Niño activity whilst negative PDO is associated with periods of increased La Niña activity. The coherence between the two indices is highest at longer timescales with significant cross wavelet correlation values of 0.98 at 40 year timescales (Newman et al., 2003).

Model studies simulate that during the Late Holocene solar forcing of a thermostat response meant that La Niña conditions were more likely to occur during solar maxima, whilst El Niño conditions were more likely to occur during solar minima (Clement et al., 2000; Emile-Geay et al., 2007; Mann et al., 2005). Our finding of cooler SST in the EPCT, IPWP and KC during Late Holocene solar maxima supports these model findings. During solar minima increased frequency of El Niño events were reflected by a warming of SST in the EPCT, IPWP and KC as we show (Newman et al., 2003; Sun and Liu, 1996) (Fig. 2.3). However, in the Early Holocene, our analysis indicates that the response of EPCT, IPWP, KS to solar forcing was opposite compared with the Late Holocene with warming during solar maxima and cooling during solar minima (Fig. 2.3). Models simulate that the greater seasonality in the Tropical Pacific during the Early Holocene supressed solar forcing of the thermostat mechanism (Emile-Geay et al., 2007). Therefore increased solar irradiance in the Holocene Climate Optimum elicited a direct warming response during solar maxima and a cooling during solar minima (Fig. 2.3).

It is notable that the switch in response of upwelling in the EPCT to solar forcing is delayed compared with records from the Western Pacific (Fig. 2.3). Given the reconstruction of upwelling is based on a single proxy record; we must consider that dating uncertainties could influence the timing of the correlations shown. However, a possible mechanistic explanation may relate to the location of the record at 12°S. Throughout the Holocene, as the angle of axial tilt diminished and the perihelion moved to boreal winter, the location of maximum insolation shifted southwards (Haug et al., 2001). As a result the Intertropical Convergence Zone also shifted southward and was tracked by the convergence of Easterly winds. The coastal winds that cause upwelling off Peru are intensified with the southward migration of the ITCZ (Montecino and Lange, 2009). Therefore, owing to the southerly displacement of the upwelling record, solar forced changes in the trade winds may not have impacted the region until later in the Holocene.

2.4.2 A focus on the Indo Pacific Warm Pool

Previous studies from the Makassar Straight of the IPWP have found that SSTs in the region warmed during solar maxima in the Late Holocene and cooled during solar minima which are contradictory to our findings in the Tropical Pacific (Newton et al., 2006; Oppo et al., 2009). In order to understand this discrepancy we carried out an analysis of stacked records from the Makassar Straight and the Western Pacific Warm Pool regions of the IPWP. The Makassar Straight and WPWP are influenced by different currents, with the WPWP region sensitive to changes in the Tropical Pacific whilst the Makassar Straight is influenced by currents flowing from the South China Sea as well as the Tropical Pacific via the Indo Pacific Throughflow Current (ITF) (Fig. 2.1a) (Linsley et al., 2010; Oppo et al., 2009; Stott et al., 2004).

In the case of the WPWP (Fig. 2.4), it can be seen that SSTs in the region exhibit correlations with solar irradiance consistent with solar forcing of the entire IPWP, EPCT and KC with warming during solar maxima in the Early Holocene and cooling during solar maxima in the Late Holocene. Because the WPWP is under a greater influence of the COASTP (Linsley et al., 2010; Stott et al., 2004), this finding is logical, notwithstanding the uncertainty among the individual records which comprise the stacked record (see section 2.4.3).

The Makassar Straight record (Fig. 2.5) on the other hand exhibits opposite response to solar forcing with cooler SSTs during solar maxima in the Early Holocene and warmer SSTs during Late Holocene solar maxima. SST in the Makassar Straight is impacted by freshwater intrusion from the South China Sea during the Asian Monsoon (Linsley et al., 2010; Oppo et al., 2009). The pulse of fresh water into the Makassar Straight forms a plug of freshwater that blocks the flow of the Indonesian throughflow (ITF) current which carries warm surface waters from the WPWP through the Makassar straight (Fig. 2.1a). Increases in fresh water intrusion caused by the Monsoon thus lead to cooler SSTs in the Makassar Straight (Linsley et al., 2010). It can be seen that the relation between the stacked record and solar irradiance is more closely represented by those records with lower salinities i.e. impacted more by freshwater intrusion during the Monsoon periods (Fig. 2.5).

Just as with the switch in response of the Tropical Pacific to solar forcing, we propose that the superposition of orbital trends and solar irradiance variations caused the opposite response of Makassar Straight and WPWP SSTs to solar irradiance forcing. Cooling of SST in the Makassar Straight during the Holocene was associated with increased fresh water influx from the South China Sea during Monsoons and blocking of the ITF current which transports warm water from the WPWP (Fig. 2.1b) (Linsley et al., 2010; Oppo et al., 2009). Monsoon strength was strongest during the Early Holocene climatic optimum (6000 – 9000 yr BP) when seasonality differences were greatest (Asmerom et al., 2007; Poore et al., 2005; Wang et al., 2005). Increases in the strength of the Southeast Asian Monsoon were associated with increases in solar irradiance (Dykoski et al., 2005; Fleitmann et al., 2003; Wang et al., 2005). Therefore strong monsoon events during Early Holocene solar maxima would have blocked the ITF, cooling SSTs in the Southern Makassar Straight (Fig. 2.1b and Fig. 2.5). As mentioned earlier, solar forcing of the COASTP was likely supressed in the Early Holocene leading to a direct warming response of SSTs during solar maxima in the WPWP (Fig. 2.4).

As seasonality reduced during the Holocene, the monsoon weakened (Asmerom et al., 2007; Poore et al., 2005; Wang et al., 2005) whilst solar forcing of the thermostat mechanism strengthened (Emile-Geay et al., 2007). Consistent with strengthening of solar forcing of the

thermostat mechanism, our analysis demonstrates a cooling of SSTs in the WPWP after the Holocene Climate Optimum (Fig. 2.4). Contrastingly, SSTs from the Makassar Straight warmed during solar maxima in the Late Holocene (Fig. 2.5), a finding also found for high resolution records spanning the last 2000 years (Newton et al., 2006; Oppo et al., 2009). The warming in the Makassar Straight during Late Holocene is inconsistent with solar forced changes in the Asian Monsoon, which was much weaker in the Late Holocene compared with the Holocene Climate Optimum (Linsley et al., 2010; Wang et al., 2005). Instead, warming of SST in the Southern Makassar Straight during the Late Holocene is alternatively attributed to a westward movement of the WPWP, an expansion of the WPWP (Linsley et al., 2010) or a decrease in the influx of cooler North Pacific surface waters through the South China Sea and Java Sea (Oppo et al., 2009). The explanation that is consistent with our findings elsewhere in the Pacific is that the WPWP moved westward during solar maxima in the Late Holocene owing to solar forcing of a La Niña-like state of the Tropical Pacific and a strengthening of Easterly winds (Emile-Geay et al., 2007; Newman et al., 2003). This westward movement of warm surface waters during solar maxima dominated over cooling brought about by freshwater intrusion.

2.4.3 Uncertainty Analysis

For the records that comprise the stacked record from the Makassar Straight, those most influenced by the influx of fresh water from the South China Sea during Monsoons (13GGC and MD62) are most representative of the response to solar irradiance demonstrated in the stacked record (Fig. 2.5). This gives us confidence that our interpretation of cooling of the Makassar straight in the Early Holocene was owing to an influx of fresh water caused by solar forced intensification of the Asian Monsoon (Linsley et al., 2010). However, the same signal is not demonstrated in cores 70GGC and MD65 which are located at the boundary of influence of freshwater influx (Fig. 2.1 and 2.5). This may be because these records are influenced to a greater extent by the WPWP compared with those records located further west in the Makassar Straight (Linsley et al., 2010). This is an important issue when interpreting individual proxy records as a lack of a signal may not be caused by lack of forcing but rather destructive interference arising from two forcing sources (Williams and Hanan, 2011). For example SSTs at core locations

70GGC and MD65 were likely cooled during solar maxima in the Early Holocene owing to solar forcing of the Monsoon whilst warming was caused by a direct response to increased insolation during solar maxima. In the case of the WPWP, the response among individual records to solar forcing is inconsistent with the stacked record (Fig. 2.4). Partly, the lack of a consistent signal is caused due to the chronological uncertainties among the records however, even without uncertainty analysis (not shown), the signal remains unclear. Khider et al. (2014) performed a detailed analysis of core MD81 which accounted for chronological errors as well ordinate errors. In line with our results they found no evidence of direct solar forcing of SST in the core MD81.

The discrepancy between the stacked reconstruction and individual records highlights the difficulty associated with estimating solar forcing in marine reconstructions. We cannot say categorically what causes the discrepancy between the stacked record and the individual records. However, it is likely that the stacked records smooth out anomalies associated with incorrect reservoir age estimation or the influence of local processes on measurements in the individual records (Linsley et al., 2010). Given the mechanistic and temporal consistency of the response of the stacked records from the IPWP, WPWP and Makassar Straight with reconstructions of changes in the Kuroshio Current and EPCT we have confidence that the stacked record accurately captures the response to solar forcing.

2.5 Summary and Conclusions

Our analysis indicates that solar irradiance variations forced changes in the coupled ocean-atmosphere system of the Tropical Pacific during the Holocene at 500 – 1000 year timescales. Importantly we show that orbital forcing likely modified how the coupled ocean-atmosphere system of the Tropical Pacific responded to solar forcing between the Early and Late Holocene. In the Early Holocene the Tropical Pacific warmed during solar maxima, whilst during the Late Holocene it cooled. The opposite response was caused by orbital trends bringing about a strengthening of solar forcing of the thermostat mechanism in the coupled ocean-atmosphere system of the Tropical Pacific after the Holocene Climate Optimum.

Given the importance of the Tropical Pacific for the global climate system, the switch in response to solar forcing after the Holocene Climatic Optimum has important implications for understanding Holocene climate anomalies. In regions teleconnected to the Tropical Pacific, changes in sign or phase angle of cross correlations with solar irradiance during the Holocene are often interpreted as arising from dating uncertainties or a lagged response owing to internal processes in the climate system. However, if our finding of a switch in response of the Tropical Pacific to solar forcing is correct, then phase changes between climate reconstructions and solar variations may result from changes in how solar forcing was communicated to the atmosphere via the Tropical Pacific.

Acknowledgements

Thanks to the ocean group at the Royal Meteorological Institute of the Netherlands (KNMI) for thought provoking feedback. Thanks to Maarten Eppinga for sharing the idea of using change point analysis. Thanks to the authors of previous studies that made their data freely, fully and transparently available to the wider scientific community.

Chapter 3

A seesaw in Mediterranean precipitation during the Roman Period linked to millennial-scale changes in the North Atlantic

Published as Dermody, B.J., de Boer, H.J., Bierkens, M.F.P., Weber, S.L., Wassen, M.J., Dekker, S.C., 2012. A seesaw in Mediterranean precipitation during the Roman Period linked to millennial-scale changes in the North Atlantic. Clim. Past 8, 637–651. doi:10.5194/cp-8-637-2012

Abstract

We present a reconstruction of the change in climatic humidity around the Mediterranean between 3000-1000 yr BP. Using a range of proxy archives and model simulations we demonstrate that climate during this period was typified by a millennial-scale seesaw in climatic humidity between Spain and Israel on one side and the Central Mediterranean and Turkey on the other, similar to precipitation anomalies associated with the East Atlantic/West Russia pattern in current climate. We find that changes in the position and intensity of the Jetstream indicated by our analysis correlate with millennial changes in North Atlantic sea surface temperature. A model simulation indicates the proxies of climatic humidity used in our analysis were unlikely to be influenced by climatic aridification caused by deforestation during the Roman Period. That finding is supported by an analysis of the distribution of archaeological sites in the Eastern Mediterranean which exhibits no evidence that human habitation distribution changed since ancient times as a result of climatic aridification. Therefore we conclude that changes in climatic humidity over the Mediterranean during the Roman Period were primarily caused by a modification of the Jetstream linked to sea surface temperature change in the North Atlantic. Based on our findings, we propose that ocean-atmosphere coupling may have contributed to regulating Atlantic Meridional Overturning Circulation intensity during the period of analysis.

3.1 Introduction

How human civilisation will adapt to future climate change caused by natural and anthropogenic forcings is an issue of extensive research and intense debate (IPCC, 2007). However, climate change is nothing new for human civilisation and much can be learned from understanding how past societies responded to changes in climate. One of the most advanced and enduring societies were the Romans who existed for almost 1000 years in the Central Mediterranean during a period when climate oscillated between relatively cool and warm phases (Bianchi and McCave, 1999; Desprat et al., 2003). The Roman economy was highly integrated throughout the Mediterranean (Erdkamp, 2005) and was based primarily on agricultural production (Horden and Purcell, 2000) that was adapted to the water-limited nature of the region (Zhang and Oweis, 1999). Thus, to understand how the Romans adapted to climate change it is also important to build a picture of the change in precipitation around the Mediterranean during the Roman Period (RP) (c. 2500-1500 yr BP). We focus our analysis on the period 3000-1000 yr BP to capture the change in climate leading up to and following the RP. Already a number of studies have provided evidence that changes in precipitation during the RP were influenced by changes in the pathway of the zonal storm tracks from the North Atlantic (Enzel et al., 2003; Jones et al., 2006; Rimbu et al., 2003). It is also proposed that large-scale deforestation beginning in the RP caused the climate around the Mediterranean to become drier as a result of a decrease in evaporative fluxes from the land to the atmosphere (Dümenil Gates and Ließ, 2001; Reale and Dirmeyer, 2000; Reale and Shukla, 2000). Using a range of proxy archives and model simulations we integrate these hypotheses to provide a complete regional picture of millennial-scale climate change during the RP and provide evidence of the probable forcing mechanisms responsible. It is hoped that our regional reconstruction provides a springboard for future multidisciplinary studies of the impacts of climate change on the Roman civilisation.

3.1.1 Variability in precipitation during the Roman Period

A number of proxy records provide evidence of a peak in climatic humidity in the Mediterranean during the RP. In Israel an increase in climatic humidity is apparent c.2000 yr BP in a speleothem record from the Soreq cave (Orland et al., 2009) and reconstructed levels of the Dead Sea

(Bookman et al., 2004; Migowski et al., 2006). An isotopic analysis of trees used to construct a Roman siege ramp against Jewish rebels at the Fortress of Masada above the Dead Sea also indicate a humid peak c. 2000 yr BP (Issar and Yakir, 1997). In Spain a reconstruction of riverine input to the Alboran Sea exhibits similar trends to lake levels from the south of the country that show a peak in climatic humidity c. 2000 yr BP preceded and followed by relatively arid periods (Martín-Puertas et al., 2010). However, there is contrasting evidence to suggest that the period centred on 2000 yr BP was anomalously arid in certain parts of the Mediterranean. For instance, a reconstruction of climatic humidity based on fossil ostracod taxonomy and isotope analysis indicates that c. 2000 yr BP was relatively dry around Lake Pamvotis in Greece (Frogley et al., 2001). Equally, a record of flood frequency based on pollen and charcoal analysis combined with physical indicators of floods demonstrate an anomalously dry period immediately after 2000 yr BP in Southeast Tunisia (Marquer et al., 2008). Based on $\delta^{18}O$ values of varved lake sequences from Central Turkey, Jones et al. (2006) show that the frequency of summer droughts was greater prior to 1500 yr BP after which winter rainfall increased and summer evaporation decreased. These changes are linked to changes in the winter storm tracks over the North Atlantic but also changes in summer evaporation linked to the intensity of the Indian Monsoon (Fleitmann et al., 2003). The contrasting signals in proxy archives from around the Mediterranean highlight that the pattern of climatic change between 3000-1000 yr BP was complex. Therefore, to form a clear spatiotemporal picture of the change in climatic humidity around the Mediterranean during the period of analysis we undertake an Empirical Orthogonal Function (EOF) analysis of available proxy records. The EOF statistics highlight the dominant variability among the set of proxies and thus the dominant pattern of change in climatic humidity around the Mediterranean during the period of analysis.

Under present-day conditions the dominant mode of variability in the Mediterranean is typified by a seesaw in precipitation anomalies between the Southeast of the Mediterranean and the remainder of the basin (Dünkeloh and Jacobeit, 2003; Xoplaki et al., 2004). This seesaw in climatic humidity has its greatest expression in winter and is correlated with the primary mode of sea level pressure (SLP) variability over the North Atlantic: The North Atlantic Oscillation (NAO) (Barnston and Livezey, 1987; Cullen and deMenocal, 2000). Under NAO+ (NAO-) a

strengthening (weakening) of the pressure gradient between a high pressure region over the Atlantic subtropics and a low near Iceland causes the track of westerly winds to move northwards (southwards) making Northern (Southern) European winters wetter and milder whilst Southern (Northern) Europe becomes drier and cooler (Barnston and Livezey, 1987; Hurrell, 1995). In the Mediterranean, NAO+ is associated with increased precipitation in the Southeast whilst the remainder of the Mediterranean becomes drier with the opposite case occurring under NAO- (Cullen and deMenocal, 2000). A number of other modes of variability have also been identified in Mediterranean precipitation fields (Dünkeloh and Jacobeit, 2003; Xoplaki et al., 2004). The 2nd mode of variability is typified by a correlation in precipitation anomalies between the Southeast Mediterranean and the Iberian Peninsula, which are anti-correlated with the Central Mediterranean and Turkey (Xoplaki et al., 2004; Dünkeloh and Jacobeit, 2003). Dünkeloh and Jacobeit (2003) illustrate that this pattern is linked to a pressure dipole between the North Atlantic and Europe similar in structure to the East Atlantic/Western Russia pattern (EA/WR) (Barnston and Livezey, 1987).

Longer term changes in the prominent modes of climatic variability over the Mediterranean are related to the intensity and position of the zonal Jetstreams (Thompson and Wallace, 1998; Wallace, 2000; Ziv et al., 2006). Variations in winter climate caused by the zonal Jetstreams are well captured by the annular indices of climatic variability such as the Arctic Oscillation (AO). Like the NAO, the high index of the Arctic Oscillation (AO) refers to northward movement of the zonal subpolar jet and intensification of the Polar Vortex (Namias, 1950; Thompson and Wallace, 1998). The index of the AO correlates with changes in surface air temperature (SAT) in the Northern Hemisphere, particularly over the North Atlantic where it is proposed that SAT is vertically coupled to the Polar Vortex at altitude (Baldwin and Dunkerton, 1999; Cohen and Jones, 2011; Thompson and Wallace, 1998). The correlation between SAT and the annular modes is expressed by the correlation of the high phase of the AO with anomalously warm Sea Surface Temperatures (SSTs) in the subpolar North Atlantic and cooler SSTs prevailing in the polar North Atlantic (Wallace, 2000).

In a paleo context, centennial-scale changes in the dominant modes of variability over Europe have been demonstrated in a number of studies (Büntgen et al., 2011; Cook et al., 2002; Enzel et al., 2003; Trouet et al., 2009). Trouet et al. (2009) link centennial changes in the NAO to SST variations in the North Atlantic between 900 yr BP to present. In fact SSTs in the North Atlantic are proposed to have oscillated with a periodicity of 1450 years known as Bond events throughout the Holocene (Bond et al., 1997; Bond et al., 2001). Warm intervals (cold events) of winter North Atlantic SST are inferred from a decrease (increase) in the percentage of ice rafted debris (IRD) in subpolar regions of the North Atlantic (Bond et al., 1997; Bond et al., 2001). Fluctuations in climate throughout the Northern Hemisphere coincident with Bond events have been indicated by a number of studies (Mayewski et al., 2004) for an overview). By comparing the dominant modes of variability identified in our EOF analysis with the periodicity of Bond events we can explore if a coupling between Bond events and the Jetstream existed that affected climate over the Mediterranean between 3000-1000 yr BP. To assist in the interpretation of land-based EOF statistics in the context of synoptic climate we have included proxies of winter precipitation from Central and Northwest Europe in our EOF analysis so that the primary mode of variability associated with the Jetstream can be identified. For example, wetter conditions in Northern Europe coincident drier conditions in the Central Mediterranean during a Bond interval would indicate a millennial coupling between North Atlantic SST and the position of the Jetstream consistent with present-day correlations.

3.1.2 Anthropogenic climate change during the Roman Period

In order to fully understand climate change between 3000-1000 yr BP and the responsible mechanisms we must also consider the impact that large-scale deforestation during the RP had on climate in the Mediterranean. It is proposed that a wetter climate was maintained in the Mediterranean during the RP by greater forest cover prior to the initiation of large scale deforestation coinciding with the expansion of Roman territory (Dümenil Gates and Ließ, 2001; Reale and Dirmeyer, 2000; Reale and Shukla, 2000). The decrease in evapotranspirative fluxes and increase in albedo coinciding with an intensification of deforestation is hypothesised to have initiated a positive feedback whereby the humid climate maintained by the biosphere became increasingly arid until it shifted to the present climate-vegetation equilibrium (Brovkin et al.,

1998; Charney et al., 1975; Dekker et al., 2010). The idea that the RP was more humid compared with present has been supported, and was likely inspired by cities such as Palmyra and Petra that were populous and prosperous during the RP but are now located in desert regions (Huntington, 1911; Reale and Dirmeyer, 2000). Should the basin-wide changes in sensible and latent heat fluxes of the magnitude proposed by previous studies have occurred it would have been imprinted on the proxy record as an aridification trend coincident with decreasing forest cover. However, such changes could be dampened by natural climate change or misinterpreted as such. Therefore we set out to isolate the potential contribution of past anthropogenic changes on climate using model simulations and the alternative proxy of archaeological and historical data. Therefore, we can have greater confidence that interpretations of conventional proxy records are based on the correct forcing agent.

We revisit previous studies that put forth the hypothesis that deforestation caused basin-wide climatic aridification during the RP in the Mediterranean motivated by a number of recently published palynological and charcoal-based reconstructions of mid to late Holocene forest cover. These studies indicate that large-scale deforestation took place prior to the RP. For example, Yasuda et al. (2000) present evidence of deforestation in Syria as early as 9000 yr BP. A new semi-quantitative method for determining land cover from pollen percentages known as REVEALS (Regional Estimates of VEgetation Abundance from Large Sites) has shown that the largest anthropogenic changes in land cover in the Czech Republic took place between 3200-2700 yr BP (Mazier et al., 2010). In addition to empirical reconstructions, a number of models of human induced land cover change (Gaillard et al., 2010) all indicate that extensive land clearance had occurred prior to the RP. Furthermore, we consider that the picture of the ancient Mediterranean landscape is open to misinterpretation. For instance, the city of Palmyra in modern Syria is presented as evidence of climatic aridification since the RP because this once flourishing city is now surrounded by desert (Huntington, 1911; Reale and Dirmeyer, 2000). However, Palmyra was established at an oasis (still present today) on an important trade route between the Western Levant and civilisations along the Tigris and Euphrates rivers. It was probably because of Palmyra's strategic location as a focal point of trade between kingdoms that it became such a large and prosperous city (Ortloff, 2005). In addition to the natural and historical archives, a

recent study using a regional climate model simulation has indicated that precipitation in the Mediterranean region is insensitive to changes in land cover between potential vegetation and current landcover (Anav et al., 2010).

In order to determine whether the timing and extent of deforestation during the Late Holocene could have caused basin-wide climatic aridification around the Mediterranean, we incorporate maps of simulated preindustrial deforestation based on population estimates and technological advances (Kaplan et al., 2009) into climate simulations using an Earth System model of Intermediate Complexity (EMIC). The outcomes of the simulations are interpreted in conjunction with a detailed analysis of the archaeological and historical record to understand if aridification trends between the RP and present existed and were great enough to have affected humans. Changes in climatic humidity are inferred based on the distribution of archaeological sites in the Fertile Crescent in relation to present-day precipitation and land use. The analysis of ancient habitation distribution as a proxy of climate change is a novel approach that potentially allows for local-scale changes in rainfall distribution to be resolved.

3.2 Methodology

To identify the regional pattern of change in climatic humidity during the RP in the Mediterranean we perform an EOF analysis on a selection of high quality proxies of climatic humidity. We use model simulations to determine whether large-scale deforestation during the RP could have caused basin-wide climatic aridification in the Mediterranean and imprinted on the signals of the proxies used in the EOF. An analysis of archaeological site distribution allows us to understand if aridification trends proposed to have occurred as a result of deforestation between the RP and present existed and were great enough to have affected humans.

3.2.1 Reconstruction of precipitation around the Mediterranean

3.2.1.1 Proxy records of climatic humidity

In total 12 proxy records of climatic humidity were used in our EOF analysis (Table 3.1). A search of the literature was carried out and each corresponding author contacted in order to access

proxy data for analysis. In instances where authors were not contactable we digitised figures from the original papers using GetData software. 9 records were used from around the Mediterranean while a further 3 proxies of winter precipitation were added from Central and NW Europe so that the signal in the Mediterranean proxies can be interpreted in the context of synoptic scale climate. The proxies in the Mediterranean are all records of annual changes in precipitation. However, because the Mediterranean receives the majority of its rainfall outside the summer months when precipitation is dominated by large-scale advection we can assume that the variability in the Mediterranean proxies is primarily associated with variability of the synoptic regimes (Heck et al., 2001; Peel et al., 2007; Xoplaki et al., 2004). The proxies were selected according to 3 criteria. Firstly, we chose records with a maximum dating uncertainty of ±500 years so that millennial-scale climate changes during the 3000 - 1000 yr BP window of investigation are resolved and temporal changes can be compared. To ensure that climatic signals rather than noise associated with a proxy was compared; we used records with a proxy uncertainty less than the amplitude of change recorded in each respective time series during the period of the analysis. An additional requirement to perform an EOF analysis is that each record must cover the entire period of analysis. Based on these 3 criteria a number of proxies of climatic humidity located around the Mediterranean were excluded from the analysis. 5 records that satisfy the first 2 criteria but did not cover the entire period of analysis are included in the general discussion (Frogley et al., 2001; Jones et al., 2006; Marquer et al., 2008; Martín-Puertas et al., 2009; Orland et al., 2009).

3.2.1.2 Empirical orthogonal function analysis of proxy records

An EOF analysis was used to identify the primary modes of variability among the 12 proxy records of climatic humidity. The EOF produces *n* modes of variability with the first *k* modes capturing most of the variability of the input dataset; *n* being the number of variables (i.e. proxy records used: n=12). The eigenvalue of each mode is a measure of the percentage of total variability explained by that mode. For those modes with high eigenvalues, the sign and magnitude of the loading values associated with each proxy illustrates the probable dominant patterns of change in climatic humidity between 3000 yr BP – 1000 yr BP recorded by the proxies used. Proxy time series with a large loading value in a certain mode have a larger

contribution to the variability explained by that mode compared with proxies with low loading values. If two proxy time series have opposing signs for their loading values it indicates that the time series of those proxies covary negatively in respect of the mode of variability under investigation. The principal component (PC), c_k of the *k'th* mode of the EOF is given by:

$$c_k(t) = \sum_{i=1}^{n} x'(t,i)a_k(i) \qquad \text{(eq. 3.1)}$$

Where *x'* is the detrended proxy time series, *t* is time, *i* is the proxy record, n are number of proxies, $a_k(i)$ is the loading value of proxy *i* in the *k'th* mode (Hannachi, 2004). Because we use only 12 input time series, it is important to test that the output statistics of the EOF are not affected by over-fitting due to an outlier in the input dataset. To test for over-fitting we applied a jack-knife resampling procedure. The jack-knife procedure was also used to determine which proxy records should be considered when interpreting the loading patterns in each mode of the EOF. Interpretation was confined to those records that decreased the average explained variability in each mode of the EOF when excluded from the jack-knife EOFs. The results of the jack-knife procedure and a more in-depth explanation of our statistical analyses is given in supplementary information.

Of the 12 proxy records used in the EOF each had differing sampling frequencies. In order that the comparison of variability in the EOF was based on equivalent frequencies of variation with noise reduced to a minimum, we derived a 1000 year running mean for each record following a linear interpolation of the original records to a consistent time interval. A 1000 year running mean was deemed appropriate to facilitate meaningful comparisons among heterogeneous proxy records, whilst capturing millennial climate change during the period of analysis. In each case, the running mean for the period 3000 – 1000 yr BP was extracted from the running mean of the complete proxy time series. The running mean within 1000 years of the beginning and end of the complete time series was scaled according to the number of years remaining. The running mean values were scaled to a common unit based on the amplitude of change in each record between 3000-1000 yr BP. These scaled running mean values were resampled into 200 time steps and used as input in the EOF.

Table 3.1 Proxy records of climatic humidity used as input in the empirical orthogonal function (EOF) analysis. The location of the proxy records is illustrated in Fig. 3.1.

ID	Location	Proxy type	Dating uncertainty (years)	Reference
a	Norwegian Coast	Reconstructed glacier dynamics	±50	Bakke et al. (2008)
b	Southwest Norway	Reconstructed glacier dynamics	±60	Nesje et al. (2000)
c	West Central Alps	Reconstructed glacier dynamics	±200	Holzhauser et al. (2005)
d	Northern Spain	Oxygen Isotope ratios in speleothem	±150	Dominguez-villar et al. (2008)
e	Northwest Italy	Oxygen Isotopes in speleothem	±70	Zanchetta et al. (2007)
f	Central Italy	Reconstructed lake levels	±50	Magny et al. (2007)
g	Southwest Turkey	Stable isoptope and pollen	±70	Eastwood et al. (2007)
h	Turkish Black Sea Coast	Uranium Isotopes in speleothem	±60	Göktürk et al. (2011)
i	Central Turkey	Stable isoptope and pollen	±250	Roberts et al. (2001)
j	Dead Sea Israel	Reconstructed lake levels	±50	Bookman et al. (2004)
k	Dead Sea Israel	Reconstructed lake levels	±40	Migowski et al. (2006)
L	Southeast Turkey	Stable isoptope and pollen	±500	Wick et al. (2003) *and* van Zeist and Woldring, (1978)

3.2.2 Isolation of anthropogenic signal

3.2.2.1 Deforestation simulation

Deforestation simulations were carried out at T42 spectral triangular resolution (~2.8 x 2.8 degrees latitude-longitude) with 10 vertical layers using the Planet Simulator (PS), an EMIC with dynamic vegetation, mixed layer ocean capabilities and an Atmospheric General Circulation Model (AGCM) (Fraedrich et al., 2005a, 2005b). Potential vegetation was derived by initialising

the PS with a map of modern day above ground biomass (AGB) (Olson, 1983) and simulating 300 years of dynamic vegetation growth until the biosphere had achieved equilibrium state (Dekker et al., 2010). Using model-derived AGB was deemed an appropriate method for an independent derivation of potential AGB for the Mediterranean because, although forest composition is known at different time periods at given sites, accurately estimating potential AGB for the entire Mediterranean from such records is difficult (Gaillard et al., 2010). Ancient deforestation was prescribed as a forested fraction of potential vegetation from 27.5N to 55N and 15W to 50E using maps of simulated deforestation based on population estimates and the contribution of technological advances (Kaplan et al., 2009).

Experiments were prescribed with climatologically derived, monthly SST averages for the period 1981 – 2002 (Reynolds et al., 2002). Each experiment lasted 30 years, with the final 20 years used in the analysis to ensure the system was at equilibrium with prescribed boundary conditions. We calculated the regional June-July-August (JJA) large-scale and convective precipitation (the contribution of vegetative evapotranspiration and other sources of precipitation) from the final 20 years of simulations and adjusted the averaging at each cell to account for change in cell size at different latitudes. The spatially weighted values were averaged over all land cells from 27.5N to 45N and 10W to 50E to provide the regional JJA average and standard deviation of precipitation for the Mediterranean region. To understand how deforestation affected climate we compared 5 simulations: one of potential vegetation and 4 prescribed with a forested fraction of potential vegetation for time slices of 2500, 2000, 1500 and 100 yr BP (Kaplan et al., 2009).

3.2.2.2 Archaeological site distribution as a proxy of aridification

The application of archaeological data as a proxy of climate change has precedent (Weiss et al., 1993), however rather than focusing on one site we aim to understand changes in water availability in a wider context with the analysis of the distribution of archaeological sites over the entire Fertile Crescent. The Fertile Crescent was chosen owing to the high density of archaeological sites and because previous studies indicate that precipitation reduced by half in the region owing to deforestation since the RP (Reale and Shukla, 2000). Additionally, there are a number of modern studies that indicate that climate in parts of the Fertile Crescent is highly

sensitive to changes in land cover (Alpert and Mandel, 1986; De Ridder and Gallée, 1998). Given that the region is in a marginal climatic zone with steep gradients in precipitation over relatively short distances, it represents an ecotone between arable land and desert. Therefore a trend towards aridification associated with deforestation will have caused the border of the ecotone to retreat leaving previously occupied archaeological sites now abandoned in desert regions. Such a retreat of the arable ecotone occurred during the aridification event at 4200 yr BP (Weiss et al., 1993). By analysing the spatial distribution of archaeological sites in relation to the present arable ecotone, we can identify specific regions where climate may have become more arid since ancient times. It is important to note that archaeological site distribution in relation to the arable-desert ecotone can only capture an aridification trend indicated by the retreat of the arable ecotone. Stratigraphic analysis is required to identify the waxing and waning of the ecotone as Weiss et al. (1993) demonstrated at Tell Leilan.

Archaeological site data was provided from a geo-referenced database of sites (Pedersen, 2010) dating from the Bronze Age until present. We used a gridded dataset of average yearly precipitation interpolated from rain gauge stations at 0.25 degree resolution for the period 1951-2007 (Yatagai et al., 2008) to determine present-day precipitation isohyets. Because this data is interpolated among rain gauges the potential errors at each grid point varies depending on the spatiotemporal variation in rain gauge density around a grid point (Yatagai et al., 2008). Using ArcGIS 9, a 2km buffer was placed around each site and a spatial analysis was done to determine whether a site coincided with agricultural or inhabited land (Tateishi et al., 2008). Visual inspection was carried out using Google Earth imagery and the Arc2Earth extension for ArcGIS.

3.3 Results

3.3.1 Dominant modes of variability in precipitation

The maps of the loading patterns of the 1st two modes of the EOF analysis, explaining a combined 91.4% of the variability in the 12 proxies used, are presented in Fig. 3.1. Plotted next to these maps are the running means of the scaled proxy time series. Only those time series that have the greatest contribution to the variability explained by EOF1 and EOF2 are plotted

according to the criterion set out in Section 3.2.1.2 (Fig. 3.1 I, II). A jack-knife resampling of the EOF procedure demonstrates that the EOF statistics are robust and not unduly influenced by an outlier proxy record (supplementary information).

The map of the loading pattern of EOF1 (Fig. 3.1), accounting for 62.7% of variability, displays positive correlation among 2 glacier records from Norway (a, b), 1 speleothem record from NW Spain (d) and 2 lake level records from the Dead Sea in Israel (j, k). These records are anti-correlated with 1 speleothem record (h) and 1 lake level record (L) from Turkey. The spatial pattern of the loadings from EOF1 indicates that the dominant change in climatic humidity during 3000-1000 yr BP was opposite between Turkey and the 3 other regions: Norway, NW Spain and Israel (NSI). Fig. 3.1 (I) of the proxy time series shows that NSI exhibited a coincident increasing trend in climatic humidity from c.3000 - 1800 yr BP followed by a decrease in climatic humidity of varying magnitude until 1000 yr BP. The Turkish proxies exhibit negative covariance with the time series of NSI and show an aridification trend from c.3000 - 2000 yr BP followed by an increase in climatic humidity of varying magnitude until 1000 yr BP.

The map of the loading pattern of EOF2 (Fig. 3.1), accounting for 28.7% of variability, displays positive correlation among a Glacier record from the West Central Alps (c), a speleothem record from NW Italy (e), 2 lake level records from Turkey (g, i) and 1 speleothem record from NW Turkey (h). Fig. 3.1 (II) illustrates that these proxies exhibit a general trend towards drier conditions between c.3000 - 1800 yr BP. After c.1800 yr BP all records exhibit a clear increase in climatic humidity. In general, the proxy records from The Alps, Italy and Turkey (AIT) exhibit negative covariance with NSI. In each mode the trends towards increased precipitation at the beginning and end of the period of analysis represent the lower and upper limits respectively of the scaled running mean time series. This indicates that there is an overall wetting trend during the period of analysis among most of the proxies used (Fig. 3.1 I, II). The EOF is performed on detrended time series so the seesaw in climate indicated in our EOF is superimposed on this longer term wetting trend. The patterns exhibited by the EOF are consistent with a number of high resolution proxy time series from Spain, Tunisia, Greece, Turkey and Israel (Frogley et al., 2001; Jones et al., 2006; Marquer et al., 2008; Martín-Puertas et al., 2010; Orland et al., 2009).

Although these proxies do not cover the entire period of analysis they demonstrate the same spatiotemporal signals as our EOF.

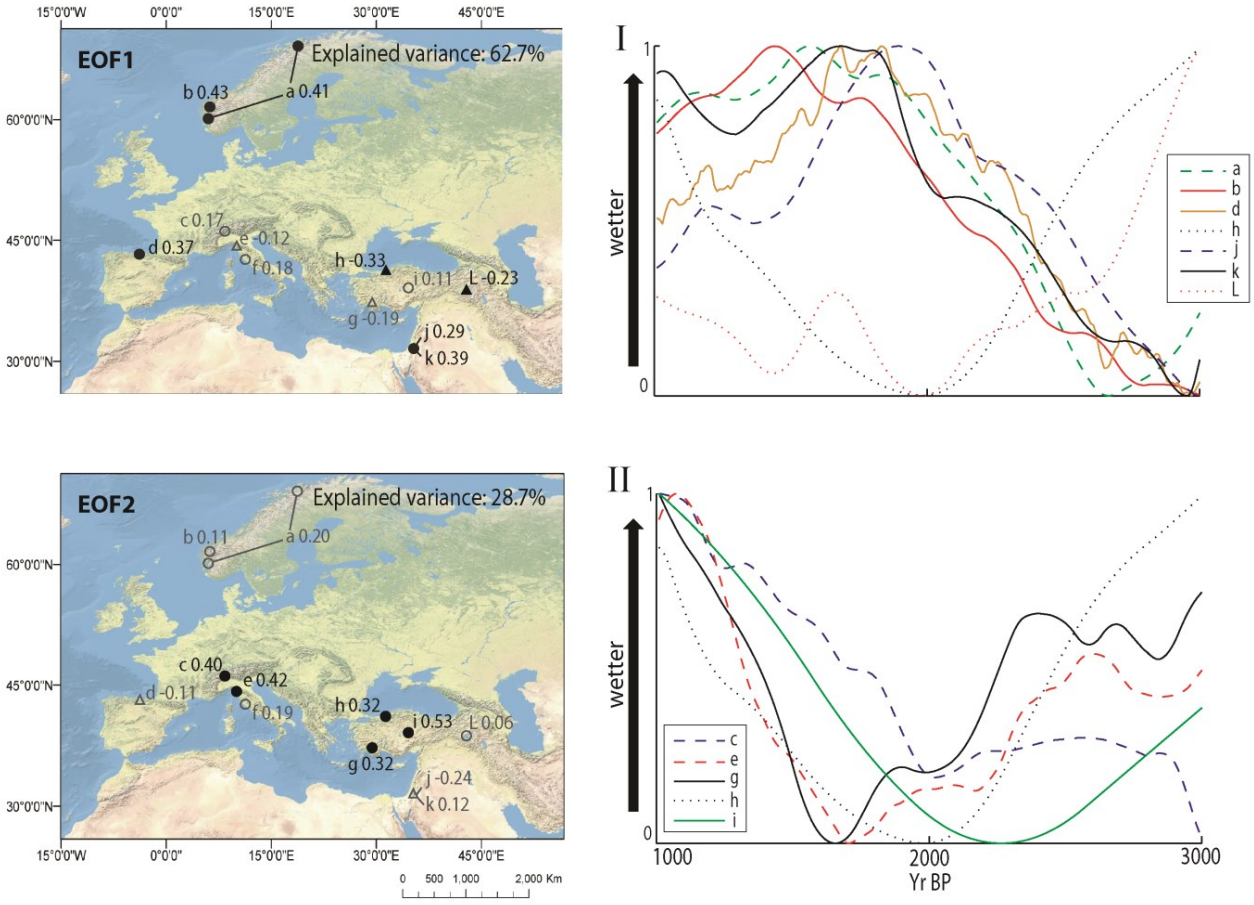

Figure 3.1 Empirical Orthogonal Function analysis of 12 proxy indicators of climatic humidity. The maps display the geographic location of each proxy record and the associated loading values from EOF1 and EOF2 respectively. Circles and triangles indicate proxies which are anti-correlated in each mode. Records with the highest loadings are selected according to the criterion set out in Sect. 3.2.1.2. These are indicated by filled symbols whilst records with loading values below the selection threshold are indicated by hollow symbols. Panels I and II show the scaled 1000 year running mean of the proxy time series with the highest loading values in each mode. Between 3000 – 1000 yr BP a wet-dry-wet fluctuation in climatic humidity is evident in the Central Mediterranean and Turkey while a dry-wet-dry fluctuation is indicated in Spain and Israel.

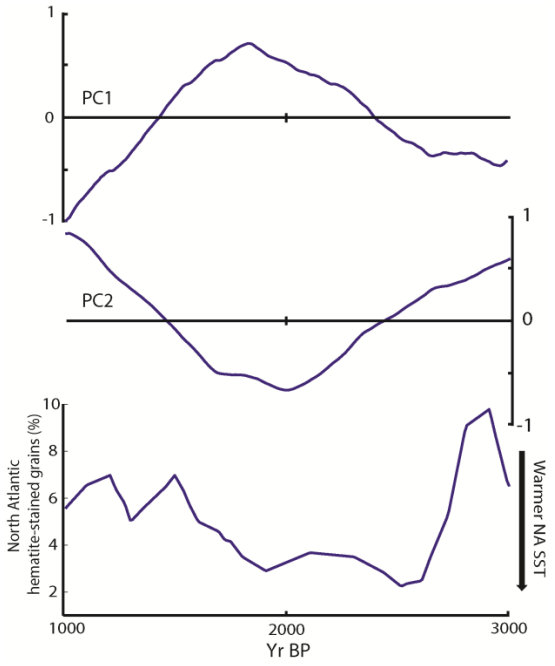

Figure 3.2 The first two principal components (PCs) of 12 proxy records of climatic humidity (explaining a combined 91.4% of variability) and a time series of ice rafted debris from the North Atlantic (Bond et al., 1997, 2001). The scale on the Y axis of the PC indices is dimensionless. Periods when the index of PC1 is highly positive coincide with wetter conditions in Norway, Spain and Israel. Periods when PC1 is highly negative coincide with wetter conditions in The Alps, Italy and Turkey.

The detrended principal component (PC) time series of EOF1 and EOF2 are displayed in Fig. 3.2 along with the time series of the percentage of hematite-stained grains found in North Atlantic (NA) sediments during the period 3000 - 1000 yr BP (Bond et al., 1997, 2001). A higher percentage of hematite-stained grains are indicative of cooler winter SSTs in the North Atlantic. During Bond intervals when the percentage of hematite-stained grains is less and SST is warmer, the index of PC1 exhibits an increasing trend whilst PC2 exhibits a decreasing trend. During Bond events North Atlantic SSTs become cooler and the index of PC1 shifts to a negative trend whilst the index of PC2 takes on a positive trend. Given that the timing of changes in the PC time series are almost coincident, given that the PCs explain the majority of variability and because they are orthogonal they are an index of the timing and magnitude of a seesaw in precipitation between AIT and NSI.

3.3.2 Impact of Deforestation on precipitation during the Roman Period

A map of the statistically significant ($t(38) = 2.024$, $p = 0.05$) anomaly in monthly mean JJA precipitation simulated by the PS between the situation of forest cover at 100 yr BP minus the situation with potential forest cover is presented in Fig. 3.3. It should be noted that the anomaly

in terms of biomass between potential vegetation and vegetation at 100 yr BP is considerably less in the Mediterranean compared with Northern and Central Europe. This is owing to the low potential biomass simulated for the Mediterranean by the PS compared with AGB at northern latitudes. In our simulations, Northern and Western Europe exhibit significant (see non-shaded areas in Fig. 3.3) reductions in precipitation caused by deforestation. The simulated anomalies in JJA precipitation for these regions with very high anomalies in AGB are of similar magnitude to the present-day total average precipitation (>0.1 m/month). The Mediterranean region exhibits significant reductions in precipitation only in the Northern Morocco and Northern Spain.

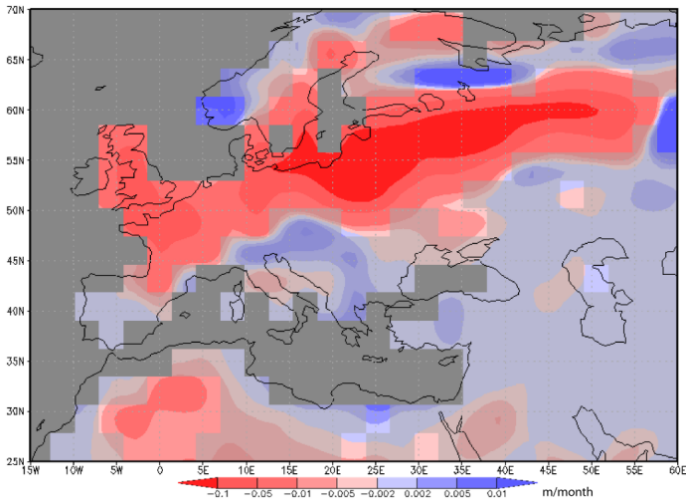

Figure 3.3 Summer (JJA) average anomaly in precipitation (m/month) for simulated forest cover at 100 yr BP minus potential forest cover. The largest changes in precipitation between potential forest cover and forest cover at 100 yr BP are in Northern Europe. The shaded areas are regions where the changes in precipitation are statistically insignificant ($t(38) = 2.024$, $p = 0.05$).

Mean monthly JJA precipitation averaged over land cells in the Mediterranean region (27.5N to 45N and 10W to 50E) for simulations prescribed with potential AGB and AGB arising from deforestation (from Kaplan et al., 2000) at 2500, 2000, 1500 and 100 yr BP is presented in Fig. 3.4. The averaging includes arid regions such as the North Coast of Africa, hence the low monthly averages. No trend in precipitation is simulated as a result of decreased AGB for the 5

time slices shown. The differences among simulations are less than the 'within simulation' standard deviation. Based on our simulations we conclude that deforestation in the Mediterranean was unlikely to have caused basin-wide aridification.

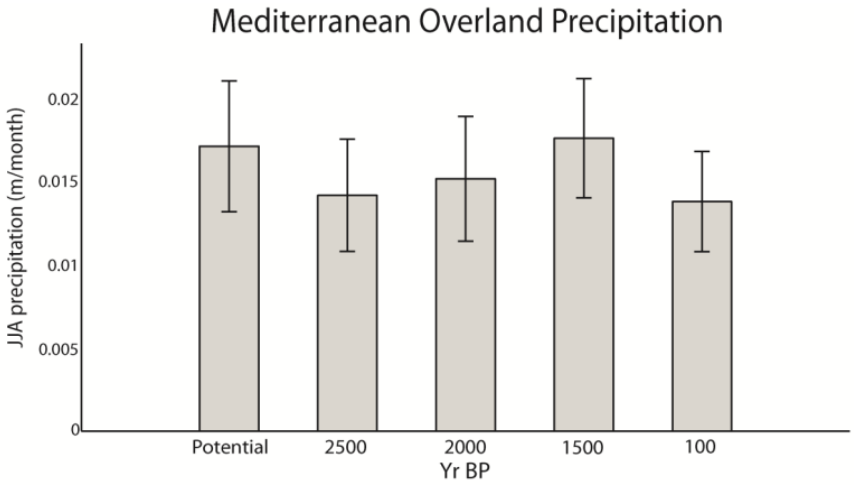

Figure 3.4 Mediterranean summer (JJA) average overland precipitation (m/month). The change in precipitation shown is in relation to land cover changes prescribed from Kaplan et al. (2009). Within simulation standard deviation is shown with error bars.

3.3.3 Archaeological site distribution in the Fertile Crescent

Archaeological site distribution in the Fertile Crescent in relation to present-day precipitation and arable land is presented in Fig. 3.5. The sites in green are those that coincide with currently inhabited or arable land. The sites in black are located neither on arable or inhabited land. In total 2345 sites were used in the analysis. Of these, 129 (5.5%) are now located in abandoned regions. The majority of abandoned sites are located along the north-east of the Jazira (A) and in lower Southern Mesopotamia (B). It can be seen that areas of arable land extend into regions that receive less than 250mm/y precipitation, which is considered the minimum requirement for dry-land farming (Bowden, 1979). In these regions, cultivation is possible owing to the supplementation of precipitation in dry periods with irrigation from rainwater harvesting, wadi's (ephemeral streams), rivers and groundwater extraction; practices that were employed in ancient times as they are today (Huntington, 1911).

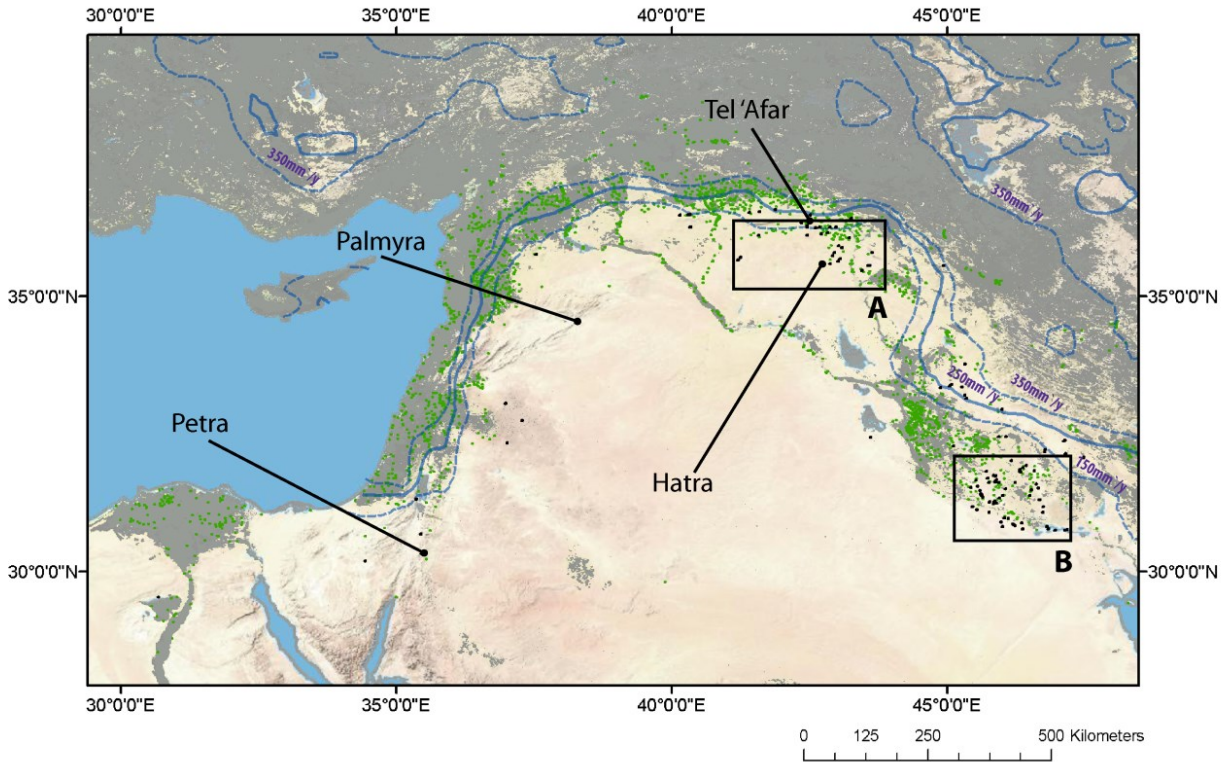

Figure 3.5 Archaeological site distribution (Pedersen, 2010) overlaid with present-day precipitation and land cover. Green points are sites coinciding with land currently under cultivation or habitation, black points are sites in presently abandoned regions. Present-day precipitation is represented in isohyets and the grey region is land that is currently arable or inhabited. The regions marked A and B, where most of the abandoned sites are located, are in the north-east of the Jazira and lower Southern Mesopotamia respectively.

3.4 Discussion

The dominant pattern of variability between 3000-1000 yr BP depicted in our EOF analysis indicates a seesaw in climatic humidity in Europe with Norway, Spain and Israel (NSI) on one side and the Central Mediterranean and Turkey on the other (Fig. 3.1). In the Mediterranean, the seesaw in climatic humidity is expressed by a dry-wet-dry cycle in Spain and Israel whilst a wet-dry-wet cycle occurred in the Central Mediterranean and Turkey. The timing of shifts in the seesaw is correlated with 1450 yr cycles in North Atlantic SST (Bond et al., 1997, 2001). The correlation between changes in climatic humidity and North Atlantic SST during the period of analysis is consistent with modern-day correlations between the position and intensity of the

zonal Jetstream and SST in the North Atlantic. Therefore we propose that changes in climatic humidity over the Mediterranean during the RP were primarily caused by changes in the zonal Jetstreams associated with 1450 yr cycles in North Atlantic SST.

3.4.1 Variability in Mediterranean precipitation during the Roman Period

The loading patterns of our EOF analysis illustrate an anti-correlation in climatic humidity between NSI and AIT during the period 3000-1000 yr BP (Fig. 3.1 I). NSI underwent a dry-wet-dry cycle between 3000-1000 yr BP whilst AIT exhibited an opposite wet-dry-wet signal during the same period (Fig. 3.1 I,II). A seesaw in climatic humidity between NSI and AIT is similar to the correlation in winter precipitation fields associated with the NAO index under present-day climate (Cullen and deMenocal, 2000; Hurrell, 1995). However, the positive correlation between Spain and Israel indicated in EOF1is inconsistent with the present-day precipitation anomalies associated with NAO. In the Mediterranean a seesaw in climatic humidity between the Central Mediterranean and Turkey on one side and Spain and Israel on the other is consistent with precipitation anomalies associated with the East Atlantic/Western Russia pattern (EA/WR) (Barnston and Livezey, 1987; Dünkeloh and Jacobeit, 2003; Xoplaki et al., 2004). Therefore, we propose that the pattern for the whole of Europe during the RP is indicative of a superposition EA/WR and NAO-like patterns.

Support that the loading pattern in our EOF reflects a superposition of the NAO and EA/WR patterns is indicated by record (a) from Norway which captures the gradient in winter precipitation between Northwest and Southwest Norway (Fig. 3.1 I). Periods when winter precipitation at both sites is at a maximum (minimum) indicate that the Jetstream is at its northernmost (southernmost) extent and strongest (weakest) intensity. When the precipitation gradient between sites increases it represents an intermediate state of the Jetstream (Bakke et al., 2008). The pattern indicated by the Norwegian Glacier records is consistent with present-day precipitation anomalies in Norway associated with coincident changes in the phases of the NAO and EA/WR (Krichak et al., 2002). Under coincident NAO+ and EA/WR+, a positive precipitation anomaly is seen along the entire west coast of Norway with the opposite case under

NAO- and EA/WR-. When the NAO and EA/WR phases are opposite the gradient in precipitation between North and South Norway is increased. In current climate the NAO is the dominant mode in this region, as positive precipitation anomalies in Norway only occur under NAO+ (Krichak et al., 2002). However, in the Mediterranean between 3000-1000 yr BP the EA/WR pattern appears to be the dominant mode as the loading patterns in our EOF in the Mediterranean are consistent with correlations in the modern precipitation fields associated with the EA/WR pattern (Dünkeloh and Jacobeit, 2003; Xoplaki et al., 2004). Following Thompson and Wallace (1998), we thus propose that our proxies illustrate millennial shifts in the Jetstream with NAO-like patterns illustrating the meridional expression of these changes whilst in the Mediterranean the EA/WR-like patterns illustrate the zonal expression of changes in the Jetstream (Enzel et al., 2003; Krichak et al., 2002; Thompson and Wallace, 1998). Therefore, we can conclude that the mechanism causing changes in precipitation over Europe during the RP are changes in the position and intensity of the Jetstream. These changes are captured in modern climate by the AO index (Thompson and Wallace, 1998).

Whilst the EOF loading patterns illustrate regions of teleconnection in climatic humidity during 3000-1000 yr BP, the Principal Components (PCs) are an index of the timing and intensity of changes in climatic humidity in these regions. For example, periods when the index of PC1 (PC2) is highly positive (negative) are generally consistent with precipitation patterns associated with AO+ when the zonal Jetstreams are pushed northwards and there is an increase in the intensity of the Polar Vortex (Thompson and Wallace, 1998). It can be seen in Fig. 3.2 that the timing of the shifts in the PC indices exhibit close correlation with the timing of cycles of ice-rafting events in the North Atlantic Ocean (Bond et al., 1997, 2001). During the Bond interval (c. 2700-1800 yr BP), when North Atlantic winter SSTs were relatively warm, there was a trend towards wetter conditions in NSI indicated by a positive trend in PC1. The initiation of a period of cooler North Atlantic SSTs (c. 1800 yr BP) coincided with a shift in the PC indices and a trend towards drier conditions in NSI. The correlation between North Atlantic SST and the position and intensity of the Jetstream indicated by our EOF is consistent with present-day correlations between the AO and North Atlantic SST. Therefore, we can tentatively conclude that changes in climatic humidity

over the Mediterranean during the RP were primarily caused by a modification of the Jetstream linked to SST change in the North Atlantic.

Changes in North Atlantic SST during Bond events have been linked to changes in the intensity of the Atlantic Meridional Overturning Circulation (AMOC) (Bond et al., 2001). Two important gradients relevant for AMOC intensity are the meridional gradient in SST between the equator and the poles and the vertical density gradient in regions of the North Atlantic where Deep Water Formation (DWF) takes place. A decrease in either of these gradients is proposed to inhibit overturning circulation and therefore cause a cooling in North Atlantic (Wunsch, 2002). Various mechanisms are proposed to cause changes in these gradients (Dima and Lohmann, 2007; Krebs and Timmermann, 2007; Timmermann et al., 2007; Wang, 2007) with changes in the flux of fresh water to regions of DWF cited by a number of authors (Dickson et al., 1988; Fairbanks, 1989; Hurrell, 1995; Karcher et al., 2005; Polyakov and Johnson, 2000; Thornalley et al., 2009). Following Dima and Lohmann (2007), we propose that our study provides evidence that ocean-atmosphere coupling was an important factor in regulating AMOC during the period of analysis by modifying fresh water fluxes to regions of DWF in the North Atlantic. An increase in the northward atmospheric transport of fresh water during warm Bond intervals is shown in proxies (a) and (b) which are located close to regions of DWF in the North Atlantic (Bakke et al., 2008; Nesje et al., 2000). The increased atmospheric transport of fresh water to DWF regions during the Bond interval would have contributed to inhibiting deep water formation and a slowing down the AMOC thus cooling the North Atlantic. The cooling of the North Atlantic initiated a low phase of the AO and reduced northward transport of atmospheric fresh water thus promoting deep water formation. Given that we only capture one full 1450 yr cycle of a warm Bond interval and cool Bond event during our period of analysis we must be cautious with extrapolating over longer periods. However, our study indicates that ocean-atmosphere coupling provided a negative feedback to AMOC intensity that reduced surface salinity in North Atlantic DWF regions under high AMOC intensity and increased it when AMOC intensity was low.

3.4.2 Anthropogenic climate change during the Roman Period

We simulated the impact of ancient deforestation on Mediterranean precipitation in order to determine whether anthropogenic aridification associated with deforestation could overprint the climatic signals in the proxies used in our EOF analysis. Our simulations indicated that precipitation in the Mediterranean at a basin-wide scale was probably insensitive to deforestation during the RP. Previous studies examining the basin-wide impact of deforestation on precipitation presented archaeological and historical evidence for large-scale aridification in the Eastern Mediterranean (Reale and Dirmeyer, 2000). However, our detailed analysis of the distribution of archaeological sites in the Fertile Crescent region in relation to present-day arable land showed no evidence of aridification since the RP.

3.4.2.1 Impact of Deforestation on Precipitation

The finding that precipitation at a basin-wide scale around the Mediterranean was insensitive to deforestation is consistent with a recent regional climate model (RCM) study that found that the change from potential vegetation to current landcover had no effect on precipitation around the Mediterranean (Anav et al., 2010). Like our study, Anav et al. (2010) found that climate in Central and Northern Europe was most sensitive to changes in forest cover (Fig. 3.3). In our case we ascribe the difference in sensitivity of the Mediterranean and North/Central Europe primarily to the fact that the anomaly in AGB between potential vegetation and deforestation scenarios was much less in the Mediterranean compared with North/Central Europe owing to the lower simulated potential vegetation particularly around the South Mediterranean. Lower biomass in these regions due to water stress is generally consistent with reality, however because the resolution of our model cannot simulate detailed orography some localised regions with higher elevations and thus higher annual rainfall are not captured by our simulations. It is possible therefore that individual proxy records in such regions may register feedbacks in climate owing to deforestation in the period of analysis. Thus the use of many records using various types of proxies in our EOF analysis is noteworthy. The identification of spatially and temporally consistent patterns across a variety of proxy reconstructions gives us confidence that our interpretations are based on large-scale, synoptic patterns rather than locally heterogeneous

feedbacks arising from anthropogenic activity.

3.4.2.2 Archaeological evidence for climatic aridification?

The analysis of archaeological site distribution in the Fertile Crescent region in relation to present-day arable land found that 5.5% of sites are in regions currently abandoned or too arid for viable habitation (Fig. 3.5). However, an understanding of the historical context of these sites is required before conclusions about climate based on their distribution can be made. Detailed historical descriptions of the North-Eastern Jazira region (Fig. 3.5A) exist from accounts of two Roman military campaigns in 177AD and 363AD. The site of Hatra, which is currently in a desert region, is described by Cassius Dion (177AD *in* Stein, 1941) as a city with *"neither water (save a small amount and that poor in quality) nor timber nor fodder. These very disadvantages, however, afford it protection, making impossible a siege by a large multitude"*. Hatra's location in an arid region was quite typical of fortified cities from this era but what such cities also had in common was that the groundwater table was high and could be exploited from wells within the city walls, thus making them almost impossible to besiege (Stein, 1941). A later account of the northward march of a Roman army from Hatra describes the crossing of an arid plain extending for 70 mille (110km) which was void of potable water or edible vegetation as far as Ur (present-day Tel 'Afar) (Ammianus Marcellinus, 363AD *in* Stein, 1941). Tel 'Afar today, as then, coincides with the northern border of the desert, indicating that the location of desert and arable ecotone has changed little since the RP in this region. The reason for a large number of abandoned sites between Hatra and Tel 'Afar is that this plain is thought to have been an important trade route between kingdoms in lower Mesopotamia and those in the Northern Jazira plains: the route along the Tigris being too rugged for rapid movement (Ammianus Marcellinus, 363AD *in* Stein, 1941). The abandoned sites along this route were located at springs (still present today) or where there was easy access to groundwater (Stein, 1941). Any site with even limited water supply in this arid plain could potentially profit as a focal point for trade on one of the busiest trade routes in the ancient world (Stein, 1941).

Lower Southern Mesopotamia (Fig. 3.5B) also exhibits a large number of abandoned sites. The extensive evidence for early irrigation in the Mesopotamian region suggests that in the past, as

now, Mesopotamia received limited precipitation. Regions of Southern Mesopotamia were probably abandoned because, over time irrigation canals became clogged with sediment owing to a breakdown in maintenance related to periods of political and social upheaval (Perry, 1986). Indeed many of the ancient, neglected irrigation canals in lower Mesopotamia are still visible from satellite imagery alongside abandoned archaeological sites in the dataset used. In fact, much of the region has only been brought back under irrigated cultivation in the latter half of the twentieth century (FAO, 2009). Therefore, the abandoned sites in lower Mesopotamia are not representative of change in climatic humidity; rather they demonstrate changes in land management over millennia. It could be argued therefore, that the sites in Southern Mesopotamia are not appropriate proxies of changing climatic humidity as agriculture in this region was always dependent on irrigation from the Tigris and Euphrates rivers. However, the establishment of early irrigation is indication in itself of persistent aridity in lower Mesopotamia from the beginnings of human civilisation in the mid Holocene.

Our archaeological analysis supports interpretations based on our simulations that no dramatic reductions in climatic humidity occurred in the Fertile Crescent since the RP as a result of deforestation. Of course, conditions in the Fertile Crescent cannot be indicative of the entire Mediterranean. However, the detailed analysis of the archaeological record in a region of distinct ecotones that exhibit high climatic sensitivity to land cover change is instructive of the upper level of climatic sensitivity to deforestation that can be expected for the entire Mediterranean region. Therefore, we can be reasonably satisfied when making interpretations based on the signals captured in the EOF that the records are uninfluenced by basin-wide aridification caused by preindustrial anthropogenic climate change.

3.4.3 The societal impact of climate change during the Roman Period

The climatic changes illustrated by our EOF analysis are indicative of the dominant millennial cycles in precipitation around the Mediterranean between 3000-1000 yr BP. However, as we have indicated these appear to overprint a longer term wetting trend among most of the proxies used. The cause of the wetting trend is not explored here; however it indicates that the shift from dry to wet conditions in NSI and AIT in the first and second half of the period of analysis respectfully

would have resulted in greater anomalies in precipitation than the shift from wet to dry in both regions. It is also important to realise that in many regions these shifts did not happen gradually as indicated by the smoothed time series used in our EOF but occurred quite suddenly. For instance the records of Jones et al. (2006) from Central Turkey and Bookman et al. (2004) from Israel illustrate sudden and dramatic shifts in climatic humidity of opposite directions between 1600 - 1400 yr BP.

Shifts in climate, whether gradual or sudden, undoubtedly had an impact on agricultural productivity during the Roman Period and therefore on Roman society itself. However, the impact of climatic shifts on a society is dependent on how that society responds during benign or harsh climatic regimes (Blaikie and Brookfield, 1987; Diamond, 2005). For example, increasing agricultural intensity in marginal regions is demonstrated in Syria during the RP which brought about population increases but also increased erosion and land degradation (Casana, 2008; Foss, 1997). The combination of population pressure and land degradation decreased societal resilience (Scheffer, 2009); nonetheless population continued to grow until c. 1400 yr BP, when a shift in climate appears to have been the trigger for widespread social upheaval in the region (Bookman et al., 2004; Jones et al., 2006). Whether the social upheaval in Syria c. 1400 yr BP would have occurred with a different climate forcing or different societal behaviour is worthy of further research particularly in the context of future climate change. Present societies are growing and degrading at unprecedented levels and risk eroding their resilience to deal with oscillations in climate such as those associated with Bond events. These risks are compounded by the fact that natural oscillations can alternatively dampen the effects of anthropogenic climate change or be magnified by it.

3.5 Summary

Climate around the Mediterranean during the RP was typified by a millennial-scale seesaw in climatic humidity between Spain and Israel on one side and the Central Mediterranean and Turkey on the other. The patterns in climatic humidity are similar to precipitation anomalies associated with the East Atlantic/West Russia pattern in current climate (Barnston and Livezey, 1987; Krichak et al., 2002). In the period 3000-1000 yr BP Spain and Israel underwent a dry-wet-

dry cycle whilst a wet-dry-wet cycle occurred in the Central Mediterranean and Turkey. A model simulation indicates that the cycles of climatic humidity were unlikely to be influenced by climatic aridification caused by deforestation during the RP. That finding is supported by an analysis of the distribution of archaeological sites in the Fertile Crescent which exhibits no evidence that human habitation distribution changed since ancient times as a result of climatic aridification.

The loading patterns of the first two modes of the EOF encompassing proxies from Northwest Europe and the Alps indicates that the climatic fluctuations in the Mediterranean were caused by millennial changes in the position of the Jetstream and intensity of the polar vortex. The correlation between changes in North Atlantic SST and changes in the position and intensity of the Jetstream indicated by our EOF is consistent with present-day correlations between the Arctic Oscillation and North Atlantic SST (Wallace, 2000). Therefore we conclude that changes in climatic humidity over the Mediterranean during the RP were primarily caused by a modification of the Jetstream linked to SST change in the North Atlantic (Bond et al., 1997, 2001). We tentatively propose that our findings indicate that ocean-atmosphere coupling may have contributed to a negative feedback in AMOC intensity during the period of analysis. Contextualizing long term climatic oscillations in terms of the Roman civilisation allows us to understand how such oscillations affect societal resilience. The interaction between climate oscillations and societal resilience is likely to become even more important in the future under unprecedented population growth and anthropogenic climate change (IPCC, 2007).

Acknowledgements

The authors wish to thank Kaplan et al. (2009) for providing the digital data from their reconstruction of ancient deforestation. Thanks also go to Olof Pedersen who maintains an open-access database of archaeological sites in the Near East that was used in this project. We would also like to thank all the people who provided their proxy data for use in the EOF analysis. Finally thank you to two anonymous reviewers whose detailed and considered comments greatly improved the revised manuscript.

Chapter 3 supplementary information

Details of Jack-knife procedure

Given that we had only 12 time series to use as input to the EOF in contrast with a gridded dataset consisting of many hundreds of 'time series', it was important to test that the output statistics from the EOF were not affected by over-fitting caused by an outlier in the input variable set. To test for over-fitting a jack-knife resampling test was carried out whereby the EOF was repeated 12 times, removing 1 proxy each time. The average loading values and standard deviation among the jack-knife EOFs are given as are the eigenvalues for each jack-knife EOF.

To assist in the interpretation of the loading patterns generated in each mode, it is desirable to apply a criterion that confines interpretation to proxy records that have the greatest contribution to each principal component. Based on jack-knife resampling of the EOF, those records that increased the average explained variability of EOF1 (EOF2) when removed were deemed to have low contribution to the variability explained by EOF1 (EOF2). Thus we confined our interpretations to the loading patterns of records that reduced the average explained variability of EOF1 (EOF2) when removed from the jack-knife test.

EOF 1

Record removed	a	b	c	d	e	f	g	h	i	j	k	l	Record removed	Explained Variance	Included in interpretation = 1
a		0.43	0.16	0.41	-0.16	0.19	-0.22	-0.38	0.08	0.34	0.42	-0.26	**a**	58.80	1
b	0.45		0.14	0.41	-0.17	0.17	-0.23	-0.38	0.06	0.34	0.41	-0.25	**b**	59.90	1
c	0.43	0.40		0.38	-0.14	0.17	-0.20	-0.35	0.08	0.31	0.39	-0.23	**c**	65.60	0
d	0.46	0.45	0.20		-0.11	0.20	-0.18	-0.33	0.14	0.30	0.42	-0.24	**d**	59.80	1
e	0.43	0.41	0.19	0.36		0.18	-0.17	-0.32	0.13	0.28	0.40	-0.23	**e**	66.60	0
f	0.43	0.41	0.16	0.38	-0.14		-0.20	-0.34	0.10	0.30	0.39	-0.23	**f**	63.50	0
g	0.44	0.42	0.19	0.37	-0.10	0.19		-0.32	0.13	0.28	0.40	-0.23	**g**	65.00	0
h	0.46	0.44	0.22	0.37	-0.09	0.20	-0.16		0.17	0.28	0.42	-0.23	**h**	62.90	1
i	0.42	0.40	0.16	0.37	-0.14	0.17	-0.20	-0.34		0.30	0.39	-0.23	**i**	68.60	0
j	0.45	0.44	0.20	0.37	-0.10	0.19	-0.18	-0.32	0.15		0.41	-0.23	**j**	62.60	1
k	0.46	0.43	0.16	0.40	-0.15	0.18	-0.22	-0.37	0.09	0.33		-0.25	**k**	59.50	1
l	0.44	0.42	0.18	0.38	-0.12	0.18	-0.19	-0.33	0.12	0.29	0.40		**l**	62.80	1
													Average explained variance =	62.97	
Average loading	0.44	0.42	0.18	0.38	-0.13	0.18	-0.20	-0.34	0.12	0.30	0.41	-0.24			
Std_dev loading	0.01	0.02	0.02	0.02	0.03	0.01	0.02	0.03	0.03	0.02	0.01	0.01			

EOF 2

Record removed	a	b	c	d	e	f	g	h	i	j	k	l	Record removed	Explained Variance	Included in interpretation = 1
a		0.25	0.43	-0.07	0.41	0.21	0.29	0.28	0.55	-0.20	0.17	0.02	**a**	32.20	0
b	0.20		0.45	-0.04	0.41	0.23	0.29	0.26	0.56	-0.18	0.20	0.01	**b**	30.80	0
c	0.18	0.27		-0.08	0.45	0.22	0.32	0.31	0.60	-0.22	0.18	0.04	**c**	25.60	1
d	0.07	0.16	0.39		0.44	0.17	0.34	0.35	0.52	-0.27	0.08	0.08	**d**	31.00	0
e	0.09	0.19	0.43	-0.16		0.17	0.34	0.39	0.58	-0.30	0.10	0.10	**e**	25.50	1
f	0.14	0.23	0.42	-0.09	0.42		0.30	0.31	0.55	-0.23	0.15	0.05	**f**	28.90	0
g	0.08	0.17	0.41	-0.16	0.44	0.17		0.38	0.56	-0.29	0.09	0.10	**g**	27.70	1
h	0.02	0.12	0.39	-0.20	0.48	0.17	0.38		0.53	-0.31	0.04	0.10	**h**	28.00	1
i	0.16	0.26	0.49	-0.09	0.50	0.26	0.38	0.33		-0.23	0.18	0.01	**i**	22.90	1
j	0.05	0.14	0.39	-0.17	0.46	0.17	0.36	0.37	0.52		0.07	0.08	**j**	29.10	0
k	0.16	0.25	0.43	-0.07	0.41	0.21	0.30	0.28	0.55	-0.20		0.03	**k**	31.40	0
l	0.10	0.19	0.40	-0.12	0.43	0.19	0.32	0.33	0.53	-0.24	0.11		**l**	30.20	0
													Average explained variance =	28.61	
Average loading	0.11	0.20	0.42	-0.11	0.44	0.20	0.33	0.32	0.55	-0.24	0.13	0.06			
Std_dev loading	0.06	0.05	0.03	0.05	0.03	0.03	0.03	0.04	0.02	0.04	0.05	0.04			

EOF1 + EOF2

Record removed	Exp_var EOF 1 + EOF2
a	91
b	90.7
c	91.2
d	90.8
e	92.1
f	92.4
g	92.7
h	90.9
i	91.5
j	91.7
k	90.9
l	93
Average explained variance =	91.58

Chapter 4

A virtual water network of the Roman world

Published as Dermody, B.J., van Beek, R.P.H., Meeks, E., Klein Goldewijk, K., Scheidel, W., van der Velde, Y., Bierkens, M.F.P., Wassen, M.J., Dekker, S.C., 2014. A virtual water network of the Roman world. Hydrol. Earth Syst. Sci. Discuss. 11, 6561–6597. doi:10.5194/hessd-11-6561-2014

Abstract

The Romans were perhaps the most impressive exponents of water resource management in preindustrial times with irrigation and virtual water trade facilitating unprecedented urbanisation and socioeconomic stability for hundreds of years in a region of highly variable climate. To understand Roman water resource management in response to urbanisation and climate variability, a Virtual Water Network of the Roman World was developed. Using this network we find that irrigation and virtual water trade increased Roman resilience to climate variability in the short term. However, urbanisation arising from virtual water trade likely pushed the Empire closer to the boundary of its water resources, led to an increase in import costs, and reduced its resilience to climate variability in the long-term. In addition to improving our understanding of Roman water resource management, our cost-distance based analysis illuminates how increases in import costs arising from climatic and population pressures are likely to be distributed in the future global virtual water network.

4.1 Introduction

Trade is central to safeguarding food security under the twin pressures of growing demand and intensified climate variability (Godfray et al., 2010; Schmidhuber and Tubiello, 2007). The redistribution of food through trade sustains populations where local food resources are insufficient to meet demand or where climatic variability causes low yields (Barnaby, 2009). Trade in food is intimately linked to the freshwater resources of trading regions with up to 90% of human freshwater use going to agricultural production (Hoekstra and Chapagain, 2011; Shiklomanov, 2000). The freshwater resources embodied in food production and traded among regions is known as virtual water (VW) (Allan, 1998) and by tracking VW flows it is possible to quantify how freshwater resources are redistributed around the globe (Hoekstra and Chapagain, 2011). Great strides have been made to empirically describe the global trade in VW (Carr et al., 2012; Konar et al., 2011; Suweis et al., 2011) and quantify the volume of VW flows among regions (D'Odorico et al., 2010; Hanasaki et al., 2010; Suweis et al., 2013). Studies have shown that VW predominantly flows from regions with a surplus in water resources (water rich) to those with insufficient resources to meet local demand (water poor) (Barnaby, 2009; Liu and Savenije, 2008; Suweis et al., 2013). However, Konar et al. (2011) found that while VW redistribution saves water on average globally, many bilateral VW trade links are irrational from a water savings perspective and exist instead for complex socioeconomic reasons such as trade agreements, wealth disparity, agricultural subsidies and so on (de Fraiture et al., 2004). As a result, isolating the impact of climate variability and population demand on VW flows is challenging because the imprint of complex socioeconomic forcings overprint and are intertwined with the response of the VW network to climate and population forcings (Dalin et al, 2012b; Suweis et al., 2011). Additionally, the complexity of socioeconomic forcings and crop response to climate change make future predictions on VW trade and VW content highly uncertain (Fader et al., 2010; Konar et al., 2013; Shi et al., 2014).

Sivapalan et al. (2012) recommend studying past society's relations with water, a term they refer to as historical socio-hydrology, to understand fundamental processes linking humans and water resources. They propose that water has played a role in the growth, evolution and eventual collapse of many past societies and thus studying past societies relation with water can help

answer questions such as how close we are to reaching the planetary boundaries of current fresh water resources (Bogardi et al., 2013; Rockström et al., 2009). The Roman Empire were likely the greatest exponents of virtual water trade in the preindustrial era as evidenced by the widespread trade in water resources, particularly grain, throughout the Mediterranean and Black Sea region (Erdkamp, 2005; Kessler and Temin, 2007; Rickman, 1980; Scheidel, 2010). Supplying the main cities of the Empire with sufficient grain was one of the principal preoccupations of the ruling elite throughout the lifetime of the Republic and Empire, to the extent that a stable supply of grain to the city of Rome became personified by the deity *Anonna* (Mazoyer and Roudart, 2006; Rickman, 1980). In a close parallel to current demographic trends (Chen, 2007; United Nations, 2012), an explosion in urban populations during the Late Republican era (Bowman and Wilson, 2011) led many cities to overshoot their local ecohydrological carrying capacities bringing about an increased reliance on imports of VW (Erdkamp, 2005). Similar trends are seen in present-day in countries such as China where rapid urbanisation, increased affluence and relaxing of trade restrictions have brought about a 20 fold increase in VW imports in less than a quarter of a century (Shi et al., 2014).

As with current society, the Romans sought to secure food security in two principal ways: through *in situ* water resource management using rainfed agriculture and irrigation (Torell et al., 1990) and through the redistribution of VW (Yang and Zehnder, 2001). Irrigation enabled the Romans to maximise exploitation of local water resources whilst VW trade allowed them to inhabit regions where local water resources were insufficient for the resident population (Barnaby, 2009). The Romans also made use of large municipal grain stores which were replenished after each harvest owing to spoilage. These municipal stores acted as a buffer for when imports became disrupted (Erdkamp, 2005). Temporal market speculation on grain through hoarding is thought to have been limited in the Roman Period, however. Market speculation was a high risk venture owing to the loss in value of grain as a result of storage and the high uncertainty associated with predicting surpluses or deficits in subsequent years (Erdkamp, 2005). As a result VW distribution predominantly responded directly to yield surpluses and deficits integrated over a short number of years rather than complex economic dynamics arising from speculation (Horden and Purcell, 2000).

In terms of *in situ* water resource management the Romans made use of a wealth irrigation technologies such as dams, aqueducts, canals, cisterns, water wheels and Qanats (Barker, 1996; Wilson, 1997). The maintenance and operation of irrigation infrastructure was tightly controlled with users taxed on the extent of land they irrigated in regions such as Egypt or on the magnitude of their harvest in Spain, Sicily and Sardinia (Beltrán Lloris, 2006; Erdkamp, 2005). The Romans were far from the first Mediterranean civilisation to use such water management technologies but the extent and organisation was unprecedented and enabled them to achieve high agricultural yields (Barker, 1996). Not only did irrigation increase grain production but it was a far more reliable source of agricultural water compared with precipitation, particularly in large river basins such as the Nile delta, the Po Valley and the Orontes, Ebro and Vera catchments in present-day Syria and Spain (Beltrán Lloris, 2006; Butzer et al., 1985; Leeuw, 1998).

VW redistribution during the Roman period was comparatively simple compared with present day global trade in water resources (Erdkamp, 2005; Konar et al., 2011). Within the Roman Empire few artificial trade barriers existed, instead the redistribution of VW was driven by satisfying demand of urban centres from regions with a surplus by means of tributary redistribution and free market exchange (Erdkamp, 2005; Scheidel, 2010; Temin, 2012). The principal barrier to VW redistribution was the 'struggle against distance' (Braudel, 1995). However, advanced shipping technology during the Roman Period combined with the relative safety of summer maritime travel within the Mediterranean facilitated unprecedented trade in bulk goods such as grain (Houston, 1988). As with present-day, trade costs of these bulk goods co-varied with distance (Hummels, 2007). However, transport by ship was significantly cheaper compared with overland transport owing to the difficultly in land-based transport of bulk goods by horse and cart (Scheidel, 2013); a feature of trade in bulk goods that remains despite modern advancements in transport technology (Limão and Venables, 2001).

In this paper we set out to understand how irrigation and VW trade contributed to Roman resilience against the twin pressures of urbanisation and climate variability. In order to examine this we have developed a Virtual Water Network of the Roman World. Our VW network contains two principal components: a hydrological model and a dynamic, agent-based redistribution network. We simulate yields under variable climate conditions using the hydrological model PC

Raster Global Water Balance Model (PCR-GLOBWB) (van Beek and Bierkens, 2009; van Beek et al., 2011). VW trade is simulated using Orbis, the Stanford Geospatial Network of the Roman World (Scheidel, 2013) as our network structure, with link weights reflecting transport costs at 200 AD associated with the 'struggle against distance' (Braudel, 1995). Our analysis of the Roman water resource management not only adds to our understanding of that civilisation but also helps us to understand the fundamental processes underpinning VW trade in present-day (Sivapalan et al., 2012).

4.2 Methods

The schematic of our Virtual Water Network of the Roman World is shown in Fig. 4.1. To summarise our methodology; we calculated yields using the global hydrological model PCR-GLOBWB based on estimates of the extent of Roman cropland cover in 200 AD from the History Database of the Global Environment (HYDE) (Klein Goldewijk et al., 2011). Land with a potential for irrigation was assigned within HYDE cropland regions based on the MIRCA dataset of Portmann et al. (2008). Natural landcover was assigned based on the Olson classification (Olson, 1994a, 1994b). The yield response to climate variability was calculated in PCR GLOBWB with climate prescribed using meteorological observations over the period 1949 – 2000 (Ngo-Duc et al., 2005). VW surpluses and deficits were calculated with VW demand based on HYDE gridded population estimates. Yearly VW surpluses and deficits were abstracted to Orbis and the redistribution of VW from VW rich to VW poor regions of the Roman Empire was simulated. A detailed description of our methodology follows.

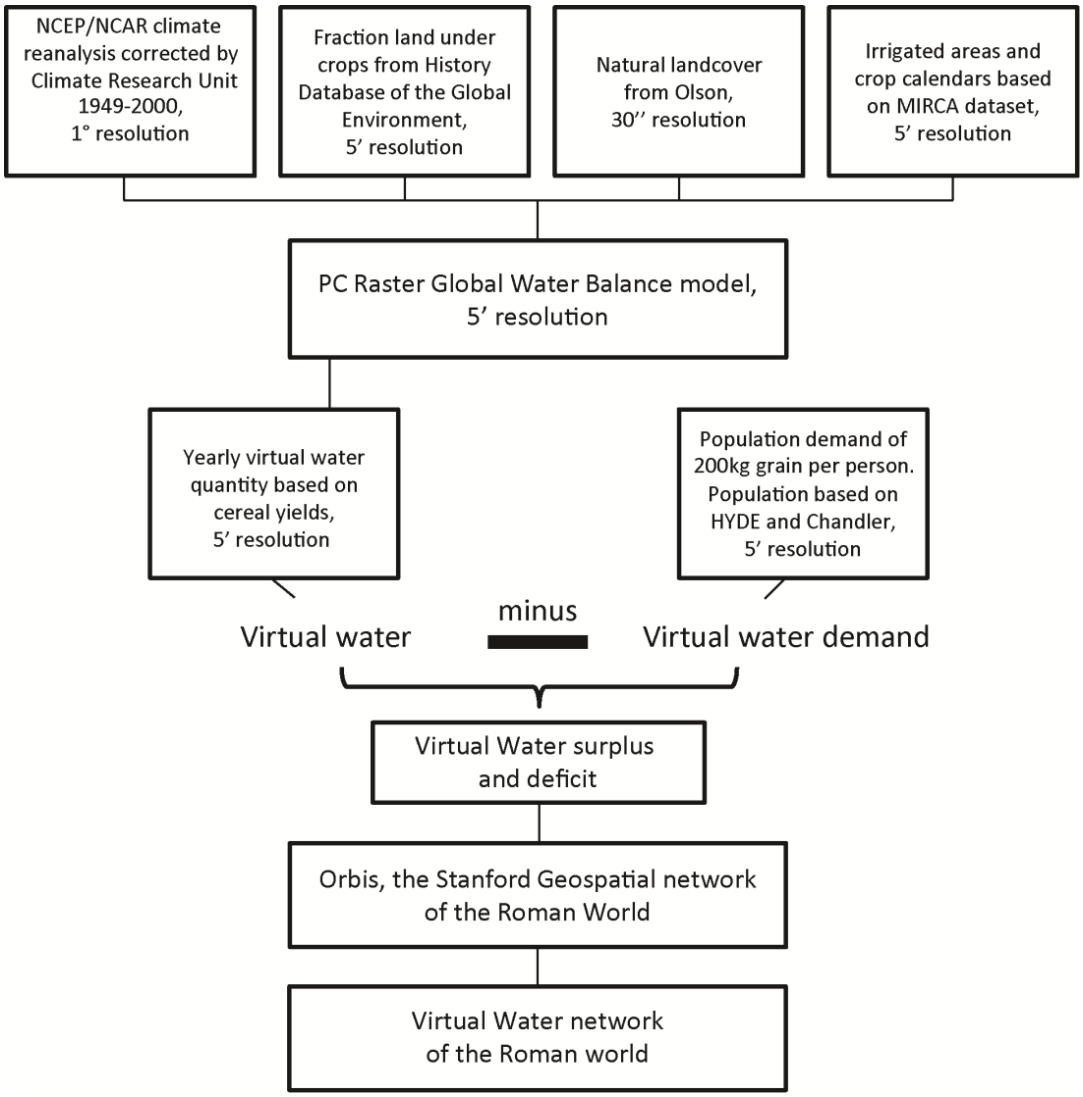

Figure 4.1 Schematic of the virtual water network of the Roman world. Roman landcover is reconstructed by combining HYDE cropland fractions and the global natural landcover database of Olson. For the cropland fractions, irrigated agriculture is assigned according to the MIRCA dataset of irrigated and rainfed crops. For these agricultural regions, cereal yields are calculated in PCR GLOBWB using NCEP/NCAR reanalysis data corrected by CRU for the period 1949-2000 as climate forcing. The surplus and deficits in VW are calculated based on the yield in each grid cell minus the yield demand, with demand based on gridded population estimates from HYDE and corrected by Chandler's estimates of Roman urban populations for the 20 largest cities in the Empire. The surplus and deficit VW values are abstracted to nodes in Orbis and imported into our Virtual Water network of the Roman world where VW redistribution is simulated.

4.2.1 Simulating cereal yields under variable climate

We computed cereal yields at 5' resolution under rainfed and irrigated cultivation using the Global Hydrological model PCR-GLOBWB (*see* van Beek et al. (2011) and van Beek and Bierkens (2009) for a detailed description of the model). PCR-GLOBWB is a spatially explicit hydrological model that computes the vertical water balance for different land cover types under prescribed meteorological conditions and routes the specific runoff to obtain discharge fields. One of the outputs of the vertical water balance is the actual transpiration (so-called *green water*) which was used here to estimate yield (Doorenbos and A.H. Kassam, 1979). When soil moisture is limiting, yield may be maximized for a healthy and fertilized crop if the crop water requirements are met by irrigation (*blue water*) and the crop transpires at the potential rate sustained by the atmospheric demand (Allen et al., 1998). Following this principle, yield can be taken to be proportional to the water use efficiency multiplied by transpiration (Zwart et al., 2010).The crop water requirements equal the difference between potential and actual evapotranspiration for the cropped area and correspond to the irrigation water demand when divided by the irrigation efficiency that accounts for conveyance and application losses. Using these principles, irrigation water demand and the realized yield were evaluated on a monthly scale with consideration of climate variability. To this end, the potential and actual evapotranspiration rates of cropped areas when fed by rainfall only were used to compute the irrigation water demand (see Wada et al., 2011 for details) and to ascertain what proportion of the irrigation water demand can be satisfied with the available discharge.

PCR-GLOBWB requires meteorological and land cover data as input. As meteorological forcing we used the National Center for Environmental Prediction/National Center for Atmospheric Research (NCEP/NCAR) corrected by the Climate Research Unit (CRU) climate reanalysis dataset over the period 1949-2000 (Ngo-Duc et al., 2005), which downscales NCEP/NCAR data to a regular 1-degree global grid with a daily resolution. Using current reanalysis data for the Roman period is deemed acceptable as the reconstructed Roman climate optimum was estimated to be comparable with the mean Northern Hemisphere temperature between 1961-1990 (Ljungqvist, 2010). In terms of precipitation, early modelling studies had suggested that greater forest cover in the Roman period maintained a wetter climate (Reale and Dirmeyer, 2000; Reale

and Shukla, 2000). However, historical, archaeological and paleoclimatological evidence indicates that the mean background climate in the Mediterranean during the Roman period was broadly similar to present day although there were likely centennial-millennial shifts in synoptic climate systems which would have made certain regions relatively drier or wetter on average at different times during the Roman Period (Büntgen et al., 2011; Dermody et al., 2012). The impacts of longer-term shifts in the synoptic climate systems on Roman water resource management will be assessed in a follow-up paper. The CRU TS 2.1 dataset only specifies variables for the global land mass and to ensure global coverage, the original NCEP/NCAR values were inserted if no values were specified. From this dataset, daily precipitation totals and the average temperature were used directly as model input. The model also requires reference potential evapotranspiration as direct input which was computed using the Hamon method (Allen et al., 1998), which only requires temperature as meteorological input compared to more complex equations. Monthly climatology's of wind speed and relative humidity were used indirectly to estimate the crop factors (see below).

To partition precipitation (rainfall, snow) into interception and throughfall and to prescribe the crop-specific potential evapotranspiration, PCR-GLOBWB requires the interception capacity, ground cover and the crop coefficient for each land cover type. The natural land cover parameterization is based on the Global LandCover Characterisation (GLCC) at 30" with the Olson classification (Olson, 1994a and 1994b) and the parameter set of (Hagemann, 1999). Irrigated areas were inserted using the MIRCA dataset of Portmann et al. (2008); (see Van Beek et al., 2011; Wada et al., 2011 for details). The fraction of each cell assigned as crop and pasture land was defined based on History Database of the Global Environment (HYDE) reconstructions for 200AD at 5' horizontal resolution (Klein Goldewijk et al., 2011) (Fig. S4.1). HYDE does not explicitly account for crop rotation and the issue of crop rotation in the Roman period remains controversial with some authors claiming that no rotation was practised in Roman times whereas others claim two-field rotation was practised with one half of fields laying fallow at any one time (Fox, 1986). Based on White (1970), we adopt an intermediate value of continual three field cropping with 2 years of a cereal crop and 1 year of fallow assigned as sparse grassland according

to GLCC. In irrigated regions we employ multi-season cereal cropping based on the crop calendars from the MIRCA dataset (Portmann et al., 2008).

The land cover parameterization is derived from the 30" distribution of the GLCC (Olson, 1994a, 1994b). In order to incorporate the information on cultivated area for the Roman period from the HYDE dataset, having a spatial resolution of 5', the distribution of cultivated and pasture areas was reconstructed at the resolution of 30". Within each 5' cell, all 30" cells were ranked on suitability; using the GLCC classification at 30", areas were delineated to represent respectively the presently cultivated areas and those under pasture. Within these areas, each cell was assigned a decreasing suitability with increasing slope. Outside the presently exploited areas, suitability was ranked using the slope parallel cumulative distance from the boundaries of these areas outwards. Suitability was then scaled between the minimum and maximum values to yield a range between 0 and 1. This suitability was then used to iteratively select the most suitable cells until the desired area was met. Precedence was first given to cultivated area, followed by pasture. The remaining area was filled with the reconstructed natural vegetation from the GLCC dataset. The resulting mosaic at 30" was consecutively used to compute the effective values of the land cover parameterization per land use type at 5'. Any remaining cells were assigned as semi-natural land cover types that were extrapolated spatially on the basis of the Holdridge Life Zones (Leemans, 1990, 1992). For the semi-natural vegetation, a subdivision between short and tall natural vegetation was made on the basis of forest fraction.

Cropland was subdivided proportionally into irrigated and rainfed land on the basis of the MIRCA dataset, giving, with pasture, a total of five land cover classes within each cell. Monthly characteristics were prescribed to account for seasonal growth changes in cereals and natural vegetation. For short-natural, tall-natural and pasture land cover types, these values were based on the original Olson classification and the corresponding parameterization of Hagemann et al. (1999). For the irrigated and rainfed cropland, the crop factors and calendars were taken directly from the MIRCA dataset (Portmann et al., 2008) for cereals under rainfed and irrigated conditions and weighted by area. Water use efficiency for all crops was assigned the value for winter wheat and crop yield taken to be equivalent to 25% of the total above-ground biomass compared to the 35% used by Zwart et al. (2010) for present-day crops, in line with estimates

from Roman and pre-agricultural revolution sources (Erdkamp, 2005; Goodchild, 2007). It is important to highlight that we only calculated yields based on cereal crops whereas large portions of land would have also been given over to viticulture, olives, market gardens etc. (Columella, 70AD; Erdkamp, 2005).

HYDE population values were used to calculate VW water demand as well as the workforce available for harvest. In addition to water availability, labour availability constrains the area that can be cultivated. The labouring population was calculated based on the grid-based population estimates from the HYDE dataset (Klein Goldewijk et al., 2011). We estimated a harvesting period of 1 month with an average harvest area per person per day of 0.2 ha which equates to 6 ha per person per year. We restricted harvesting to the able-bodied population aged between 12 and 55. Based on demographic life tables from Roman Egypt, this equated to 55% of the population that were capable of helping with the harvest (Frier, 1982). HYDE population values were also used to calculate VW demand based on a consumption of 200 kg of grain per person per year (Erdkamp, 2005). For the 20 most populous cities in the empire, the grid-based population values of HYDE were corrected using estimates of Roman urban population (Chandler, 1987). For each cell we subtracted the population demand from the realized yield providing yearly maps of surplus and deficit VW.

4.2.2 Simulating virtual water redistribution

Orbis, the Stanford Geospatial Network of the Roman World forms the basis for our VW redistribution network of the Roman World (Meeks, 2013; Scheidel, 2013). Orbis contains a database of 751 roman towns and cities that form the nodes within our network. These cities are linked by (1,371 x 2) directed edge segments that represent the cost to transport a kilogram of grain in *denarii* along Roman roads, rivers and over sea in each month of the year based on Diocletian's edict of Maximum Prices and physical cost distance calculations (Scheidel, 2013). The links between each node have a cost representing transport in each direction. For example, up-river transport is more costly compared with down-river transport. We used transport costs for the month of June because the majority of grain was transported during summer months when sea conditions were calm (Erdkamp, 2005; Horden and Purcell, 2000). We collapsed nodes

within 10km of each other into 1 node owing to the resolution of the underlying gridded data, leaving us with 649 nodes. To simplify calculations in our dynamic redistribution model, we converted the directed network of Orbis into an undirected network by taking the average cost of the directed links between nodes resulting in a total of 1,371 undirected links. As we are interested in Mediterranean climate variability, we restricted our analysis to the part of the network that extends from 10W and 45E and 25N 46N, however all simulations were carried out for the entire Empire. In order to convert grid-based surplus and deficit data to the Orbis network structure we assigned city regions using a Theissen polygon operation between our city nodes (see Fig. S4.2 for city regions). All gridded data within these regions were summed and applied to the relevant city or town node. Therefore certain nodes in the network were either VW rich or VW poor based on the (total grain yield – total grain demand) within that city region. The VW surplus and deficits in each node changed each year based on changes in yield owing to climate variability. We represent VW water imports and exports in terms of per person VW demand rather than cubic metres of water to make our findings more accessible to non-specialists in agronomy and hydrology.

Our VW redistribution network operates as a dynamical agent-based network (Wilensky, 1999). Using an agent-based dynamic VW redistribution network with the hydrological model PCR GLOBWB, allows us to explore complex emergent socio-hydrologic responses to climate variability and population growth (Bonabeau, 2002; Sivapalan et al., 2012). In line with our understanding of the Roman grain economy (Erdkamp, 2005; Scheidel, 2010), our network is demand driven with each VW poor node (nodes with a VW deficit) individually demanding VW from linked VW rich nodes. Similarly to D'Odorico et al. (2010), we do not simulate VW trade between VW rich nodes although this likely occurred. Since the links in our network are undirected, flow direction is dictated by the VW potential among VW rich and poor nodes. Thus, VW flow in our network responds directly to changes in yields arising from climate variability. Our network structure is consistent with the 'global water world' scenario described by D'Odorico et al. (2010). VW redistribution is simulated over 52 years of climate variability (Ngo-Duc et al., 2005), with a year ending when demand at all deficit nodes has been satisfied or

when all surplus nodes are depleted. We quantify the stress on the system in terms of the cost to import VW with costs measured at all VW poor nodes.

4.3 Results and discussion

4.3.1 Yield response to climate variability

The yearly average simulated yield for cereals per 5' cell is shown in Fig. 4.2a with the contribution to the total from rainfed (Fig. 4.2b) and irrigated (Fig. 4.2c) land shown separately. The yields in kg ha^{-1} are shown in Fig. S4.1, however since HYDE cropland fractions vary per cell, the yield per 5' cell give a clearer impression of spatial variability in total yield amount. Rather than reporting VW partitioned into its green and blue component sources we partitioned VW into VW derived from rainfed and irrigated land. Yields from rainfed land derive only from green water whereas yields from irrigated land incorporate blue water where there is a shortfall in green water to meet the evaporative demand (van Beek et al., 2011). Our simulations indicate that the most productive rainfed agricultural regions are located in present-day Spain, France, the Po valley, Western Turkey and the Fertile Crescent (present-day Syria, Iraq and Israel) (Fig. 4.2b). Irrigation agriculture is also widespread (Fig. 4.2c), with the largest areas of irrigated agriculture located in Egypt, the Po valley, south-eastern Turkey, the Fertile Crescent and Spain. Rainfed agriculture accounts for 71.5% of the total yields in the region with irrigation accounting for the remaining 28.5%. The kg ha^{-1} yields (Fig. S4.3) are consistent with yield estimates based on Roman sources and yields prior to the agricultural revolution in Europe (Erdkamp, 2005; Goodchild, 2007).

Lower than expected yields are calculated for Sicily and present-day Algeria and Tunisia related to what is known from historical sources about the productivity of these regions (Erdkamp, 2005). The low yields in these regions are due to a probable underestimation of cropland fractions in the HYDE dataset (Fig. S4.1). HYDE provides estimates of cropland fractions and population concentration at 5' spatial resolution globally for the entire Holocene using land suitability algorithms and back-calculating from current population and cropland distributions (Klein Goldewijk et al., 2011). Thus, it is not surprising that for certain regions cropland fractions are

inconsistent with historical accounts for the specific date of 200 AD (Fig. S4.1) (Klein Goldewijk and Verburg, 2013). For the purposes of this paper it was decided to use unadjusted HYDE grid-based estimates of cropland to transparently show our methodology.

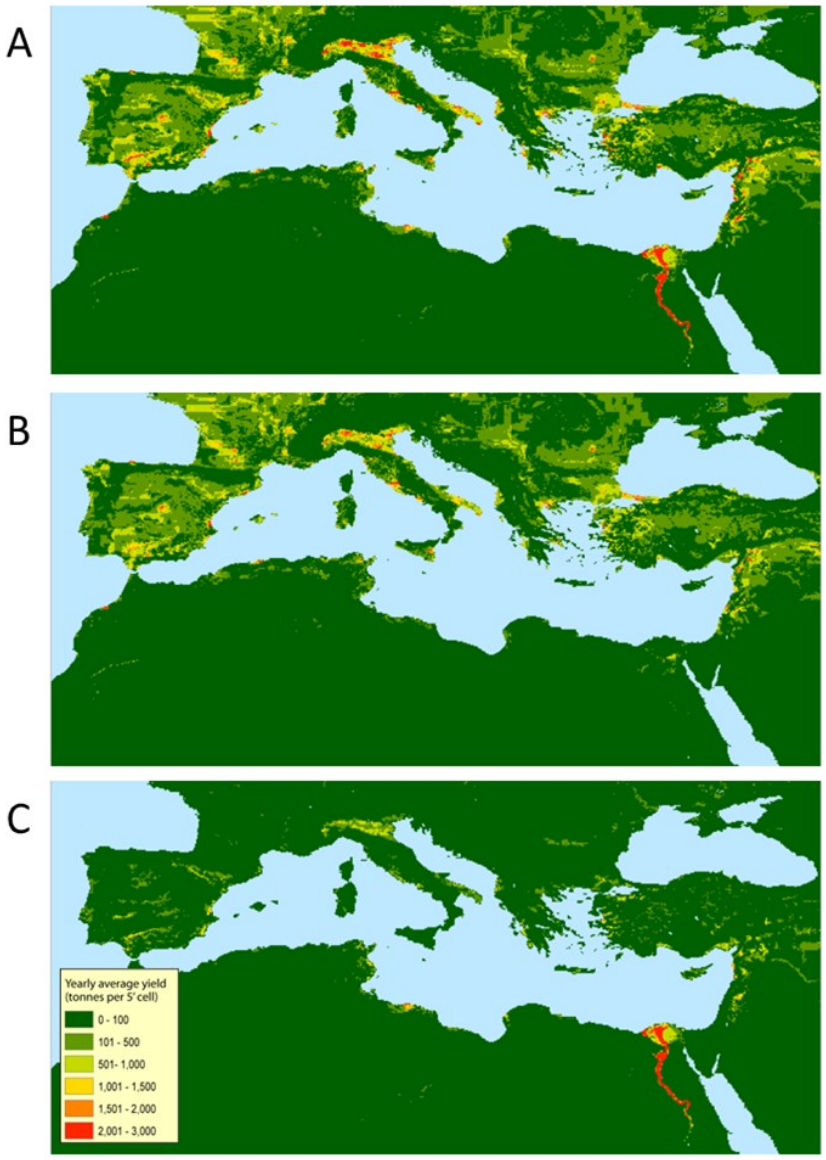

Figure 4.2 Average cereal yield (Ton per 5' cell). Average cereal yield calculated in PCR GLOBWB and based on 52 years of climate forcing **(A)**. The yields from rainfed **(B)** and irrigated **(C)** agriculture are shown separately. See Fig. S4.3 for yield in kg ha^{-1}. Yields are highest in irrigated regions where year-round supply of surface water allows for multi-cropping, which can take advantage of the seasons when temperatures for growth are optimal.

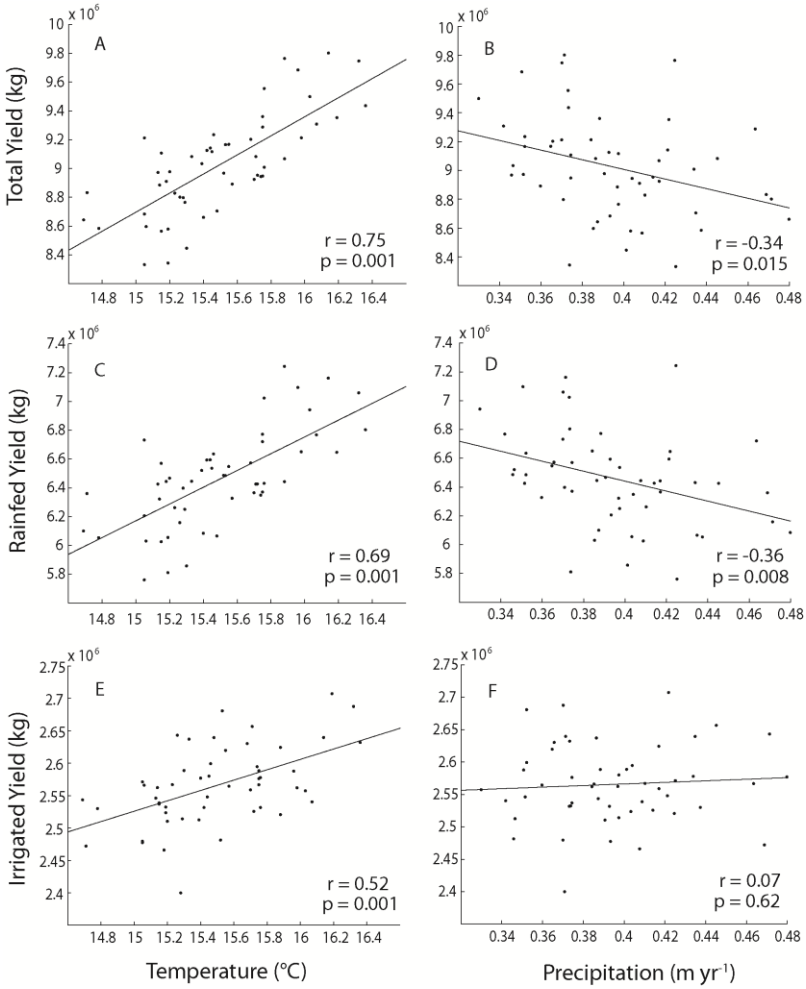

Figure 4.3 Yield plotted against temperature and precipitation. Total yield **(A and B)** in the Mediterranean increases with increasing temperature and decreases with increasing precipitation. The trend is strongest in regions where agriculture is rainfed **(C and D)**. Irrigated regions **(E and F)** also exhibit increased yields with increasing temperature whereas the impact of precipitation is negligible. The reduced yield under higher precipitation is likely related to decreased temperatures under increased precipitation in most of the Mediterranean and thus lower evapotranspiration (Fig. S4.4). This indicates that the majority of the Mediterranean is temperature-limited for cereals.

Proxy reconstructions indicate anomalously warm climate conditions during the Roman period owing to warm temperatures of the North Atlantic Ocean at the time (Bond et al. 2001; Desprat et al., 2003; McDermott et al., 2001). Fig. 4.3 shows the correlation between average annual temperature and precipitation over land cells in the Mediterranean region (25N 46N and 10W 45E) plotted against yield for each year of the reanalysis forcing. Under warmer temperatures, grain yield significantly increases in both rainfed (p=0.001) and irrigated (p=0.001) regions (Fig. 4.3 a, c, e). Somewhat counterintuitively, yield significantly decreases in rainfed regions under increased precipitation (p=0.008) (Fig. 4.3b). No significant relation was found between precipitation and yields in irrigated regions (p=0.62). Yield is calculated based on evapotranspiration, with warmer conditions bringing about higher evapotranspiration and thus higher yields where water is not limiting (van Beek et al., 2011).

Yield decreases under increased precipitation owing to the negative relation between temperature and precipitation in most of the Mediterranean for the predominantly winter-spring growing season (Fig. S4.3) (Portmann, 2008). Additionally, depending on soil type and average rainfall, transpiration can be limited in PCR-GLOBWB by oxygen stress in the soil caused by water logging (van Beek and Bierkens, 2009). In irrigated regions there is no relation with precipitation because much of the growing period in irrigated regions occurs during summer when rainfall in the Mediterranean region is very low. Added to this, many of the regions with large-scale irrigation have very dry climates (Lionello et al., 2006) with the vast proportion of water resources coming from surface water sources.

Increased yield under warmer temperatures and decreased precipitation indicate that in most of the Mediterranean, grain yields are temperature-limited and not water-limited. The spatial distribution of the correlation between climate during the growing season and yield indicates that water is limiting only in very dry regions such as the southern Fertile Crescent, parts of North Africa and coastal regions of the south-eastern Mediterranean (Fig. S4.5). Increased grain yields under higher temperatures were also found for Mediterranean climate conditions in Western Australia in simulations using the Agricultural Production Systems Simulator (APSIM)-N wheat model to predict the impact of changing temperature, precipitation and CO_2 on yield (Keating et al., 2003; Ludwig and Asseng, 2006; van Ittersum et al., 2003). In the Southern part of the study area (>500mm precipitation), wheat yields were predicted to increase with increasing temperature irrespective of predicted changes in rainfall, whilst in the drier north (<350mm precipitation) rainfall reduction was partially counteracted by increased temperatures (Ludwig and Asseng, 2006). It should be stressed that the response to climate is very heterogeneous throughout the Mediterranean (Fig. S4.5). Nonetheless, as we will show, Mediterranean-scale changes are highly relevant at the smaller city-region scale in an integrated network such as the Virtual Water network of the Roman world.

4.3.2 Virtual water redistribution

Rome is the largest importer of VW in our network with imports on average feeding ~460,000 citizens (Fig. 4.4a). Egypt is the largest exporter of virtual water, however much of this export is

local with large quantities flowing to the densely populated Egyptian cities of Alexandria and Memphis with a proportion also flowing towards Italy (Fig. 4.4b). The largest flows of VW occur between Eastern and Southern Spain and Rome. There are also large flows between south-eastern Italy and the densely populated region around the Bay of Naples. Other large flows occur along the Turkish Aegean Coast, within the Po Valley and locally in the region around Antioch in present-day southeast Turkey. Although only 28.5% of yield is from irrigated land, VW from irrigated agriculture accounts for 34% of VW flow among nodes. The disproportionately large exports from irrigated land are owing to the location of irrigated cropland close to the coast or along rivers where transport is less costly compared with transport over land. Indeed, all large VW flows originate in areas close to the coast or a large river. Rome has by far the biggest VW demand followed by other large coastal cities such as Alexandria, Ephesus and Antioch (Fig. 4.4a).

The node degree distribution of the VW redistribution network is shown in Fig. 4.5a. As with many real-world networks the node degree distribution of our network exhibits a power law distribution meaning that most nodes are connected to a few edges (low degree nodes) whilst there are a limited number of nodes that are highly connected (high degree nodes or hub nodes) (Lewis, 2011). The correspondence of the node degree distribution to a real-world network gives us confidence that Orbis faithfully captures the network structure of the principal roman trade routes (Scheidel, 2013). Fig. 4.5b shows the cost to import VW as a function of node degree. Our analysis indicates that low degree nodes incur the highest import costs in our network (Fig. 4.5b), consistent with finding that poor infrastructure increases import costs (Limão and Venables, 2001). However in Orbis, lower degree nodes are generally located inland where import costs are also higher owing to the difficulties in transporting large quantities of grain overland by horse and cart compared with ship (Braudel, 1995; Limão and Venables, 2001; Meeks, 2013; Scheidel, 2013). To isolate the effect of node degree from edge cost we simulated VW redistribution with the same network structure but reassigned edge costs and VW values at nodes randomly in each simulation year (Fig. S4.6a). This analysis demonstrates that import cost is closely related to node degree, independent of the transport costs of edges connected that node.

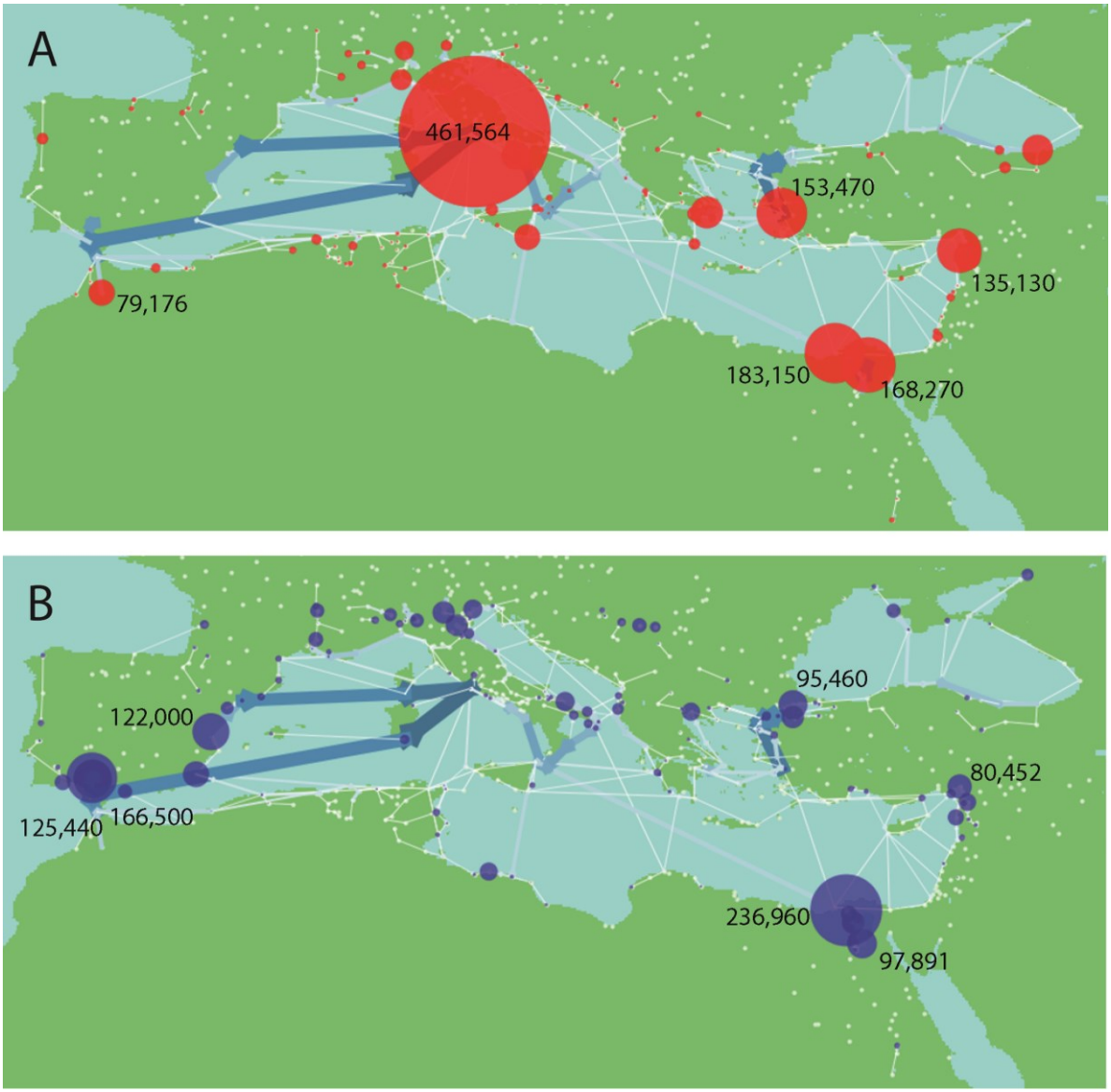

Figure 4.4 Virtual water imports and exports. The relative amount of VW imported **(A)** and exported **(B)** from each node is illustrated by the size of the nodes, whilst the associated numbers show amount of VW imported or exported in terms of per person population demand at a yearly consumption of 200 kg of grain. The edge colour and thickness indicates the relative volume of VW flow between nodes. The largest flows are between Eastern and Southern Spain and Italy, locally within Egypt, from south-eastern Italy to Western Italy and along the Aegean coast of Turkey. Rome is by far the largest importer of VW, followed by Alexandria and Memphis in Egypt, Ephesus on the West coast of Turkey, Antioch in south-eastern Turkey and Corinth in Greece.

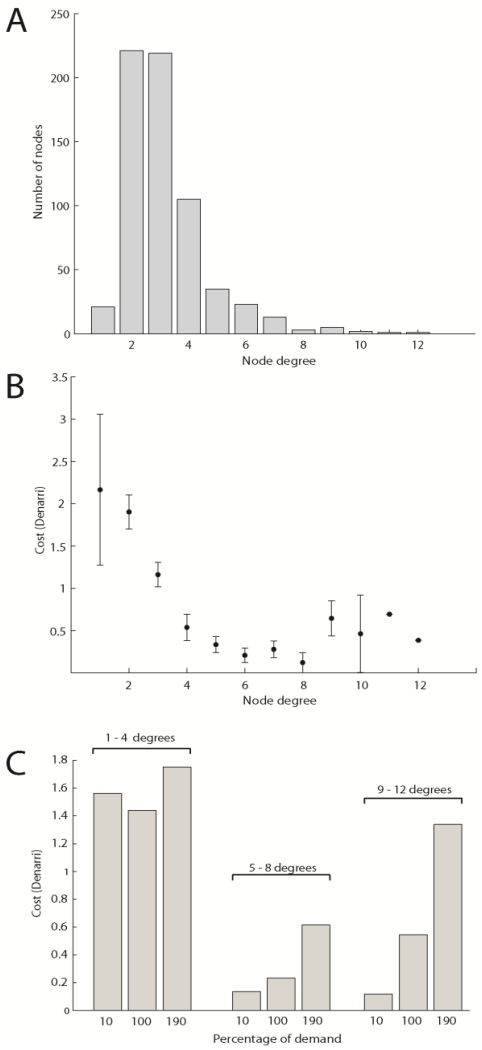

Figure 4.5 Cost to import VW in relation to node degree. (A) The node degree distribution of the virtual water redistribution network. **(B)** Lower degree nodes generally have higher costs to import VW compared with high degree nodes. For the highest degree nodes, the cost to import is higher than nodes with an intermediate number of links as many of the highly connected nodes in our network are also ports or urban centres with high demand. Therefore nearby nodes are often depleted leading the need to import from further away with an associated increase in cost. **(C)** For nodes with 1 – 4 links, import costs remain high irrespective of the level of demand. However, for nodes with 5 – 8 links and 9 -12 links, costs increase under increasing demand. 100 percent demand, represents the standard model simulations presented elsewhere in the paper.

In a network where costs covary with distance, higher import costs for low degree nodes arise because a node with few transport links has a higher chance of depleting neighbouring nodes compared with a high degree node, assuming equal demand. Once neighbouring nodes are depleted, a VW-poor node must import from further away, thus increasing cost. However, as node degree increases it is less likely that all neighbouring nodes become depleted, which on average will reduce import distance and costs. It is notable that for the highest degree nodes, import costs are higher on average (Fig. 4.5b). In network theory, highly connected nodes are known as hubs. Hub nodes are mostly located along the Mediterranean coast in our network (Scheidel, 2013). Konar et al. (2011) and Suweis et al. (2011) demonstrated that these hub nodes play a critical role in providing access for poorly connected nodes to the larger VW network. In

Orbis, hub nodes are usually ports (for example the port node at Ostia near Rome) or urban centres. Thus the demand of hub nodes is in reality the sum of demand from many inland nodes or large local populations. Owing to the high demand levels of these hub nodes they often deplete all their neighbouring VW-rich nodes and must import from further away, thus increasing import costs.

Changes in import costs indicate how stressed our VW network of the Roman World is. For example, if total network cost is 0, then all regions have sufficient local water resources to meet the demands of the local population. If total network cost > 0 then local water resources in at least one city region are insufficient to meet the local population demand, meaning that VW import is required. To investigate the impact of increased stress on our network, we simulated VW redistribution across a stress gradient based on increases or decreases in population at each VW poor node. We chose to only change populations at VW poor nodes as these are generally representative of urban regions and therefore reflect urban population growth during the late Republican and early Imperial era (Scheidel, 2001). Our analysis indicates that lower degree nodes exhibit a negligible increase in cost as a result of increased demand (Fig. 4.5c). However, high degree hub nodes exhibit an incremental increase in cost for increasing demand.

In all cases, as demand increases, a VW-poor node must import from further away in the network. For low degree nodes, most of which are inland, the largest costs are involved in bridging the gap to coastal hub nodes. Once a hub node is reached import costs increase relatively slowly owing to the increased number of coastal import routes that can be selected. For high degree nodes, the increased number of import routes that can be selected means that costs begin very low when demand is low and increase incrementally as demand increases and nearby nodes are depleted (Fig. 4.5c). The outcome of this is that although import costs in poorly connected, inland regions of the network are high, they do not increase substantially for increases in demand. However, for hub nodes that are adapted to low costs, increases in demand can cause substantial increases in import cost. This pattern is only applicable in a network such our VW network of the Roman World, where lower degree nodes tend to be located inland (Fig. S4.6b) (Scheidel, 2013), which is also typical of the present-day global trade network (Limão and Venables, 2001).

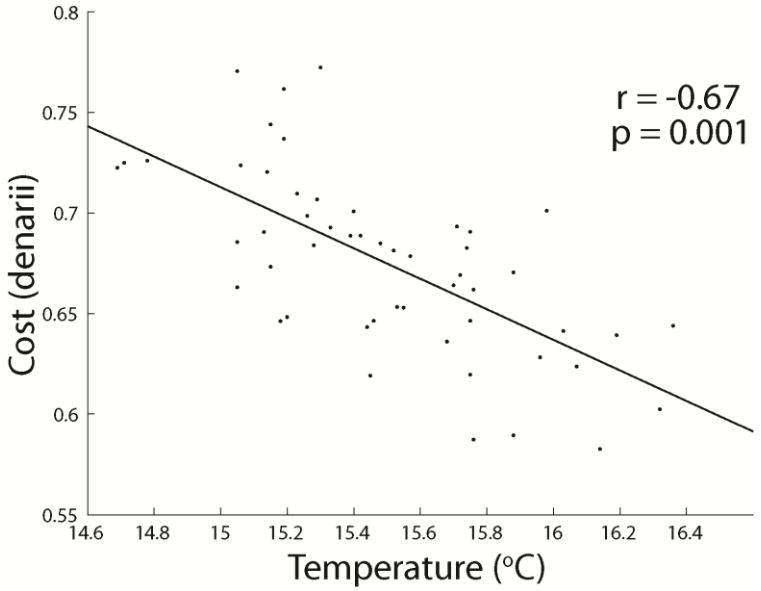

Figure 4.6 Cost of imports in relation to temperature. There is a negative relation between the cost to import VW and temperature because yields increase on average in the Mediterranean with increasing temperature. Therefore competition for VW resources reduces and as a result, import distances decrease.

We find that the total import cost of our water redistribution network is closely linked to climate, in particular temperature (Fig. 4.6). During warm years, increased yields (Fig. 4.4) mean that for many regions there is sufficient local VW to meet demand so imports are unnecessary. However, even in the case where import is required, total demand will drop with the result that a VW poor node competes with fewer VW poor nodes for increased VW resources. Consequently, nearby surplus nodes are less likely to become depleted and imports occur over shorter average distances. As stated, reconstructions of climate during the Roman period indicate that temperatures were anomalously warm (Chen et al., 2011; Ljungqvist, 2010; Martín-Puertas et al., 2009; Wang et al., 2012), creating optimal conditions for the growth of grain. Therefore, the average transport distance of VW in the Empire was likely reduced compared with the subsequent, cooler dark ages cold period beginning around 400 AD (Bond et al. 2001; Desprat et al., 2003; Martín-Puertas et al., 2009; McDermott et al., 2001).

4.3.3 Roman Water Resource Management

Taking Rome as an example, our simulations indicate the majority of its VW was imported from Spain with Sardinia, Southern France and Egypt also contributing substantial quantities (Fig. 4.4). However, historical sources indicate that Egypt, North Africa and Sicily were the dominant export regions of VW to Rome (Bransbourg, 2012; Erdkamp, 2005). As previously stated, grain yields are underestimated in HYDE for North Africa and Sicily thus Spain supplants these regions as the primary exporters of VW to Rome in the Western Mediterranean in our network. Additionally, our network solves VW transport along the most efficient routes with VW poor nodes having perfect knowledge of the VW status of the closest VW rich node. Thus import routes are constantly adapted to keep cost to a minimum. However, for the Roman period this is an unrealistic scenario as the efficiency of knowledge transfer varied based on distance, frequency of trade relations etc. (Kessler and Temin, 2007). In an era of inefficient information transfer, the most important factor was stability of VW imports as unpredictable failures in food supply could lead to famine and potential violent uprising among urban populations (Erdkamp, 2005).

Examining the year to year variability in yield we can see that much of the Eastern Empire likely had highly stable yields, in particular Egypt. In the Western Empire North Africa, Sicily and the Po valley exhibited the most stable grain production (Fig. 4.7). The stability of yields in irrigated regions such as Egypt and the Po Valley was borne out of a year round supply of surface water so that multi-cropping could take advantage of the seasons when temperatures for growth were optimal. Yields from rainfed agriculture were probably most stable in south-western Turkey, the Western Fertile Crescent, North Africa and Sicily. In these regions winter climate is relatively warm compared with Spain, Italy and France and the Adriatic coast (Lionello et al., 2006). In addition, winter climate was also quite stable owing to the reduced influence of Atlantic Storm tracks compared with the north-western Mediterranean (Lionello et al., 2006; Xoplaki et al., 2004). Although Spain and France could export large quantities of VW many years, the reliability of yields were much less compared with the aforementioned regions, a disadvantage that was unacceptable in an era of inefficient information transfer (Kessler and Temin, 2007). The high

productivity of Spain but low stability in yields is probably why its main exports during the Roman Period were non-staple foods such as olive oil (Blázquez, 1992; Woolf, 1992).

Although the redistribution of water resources practised by the Romans undoubtedly increased their resilience to climate variability, D'odorico et al. (2010) warn of the long term implications of a globalisation of water resources. Using a minimalist modelling framework of VW trade they propose that globalisation of water resources allows populations in VW poor regions to overshoot their local ecohydrological carrying capacities and at a global scale increased demand in VW-poor regions reduces the redundancy of water resources. In other words, population growth and

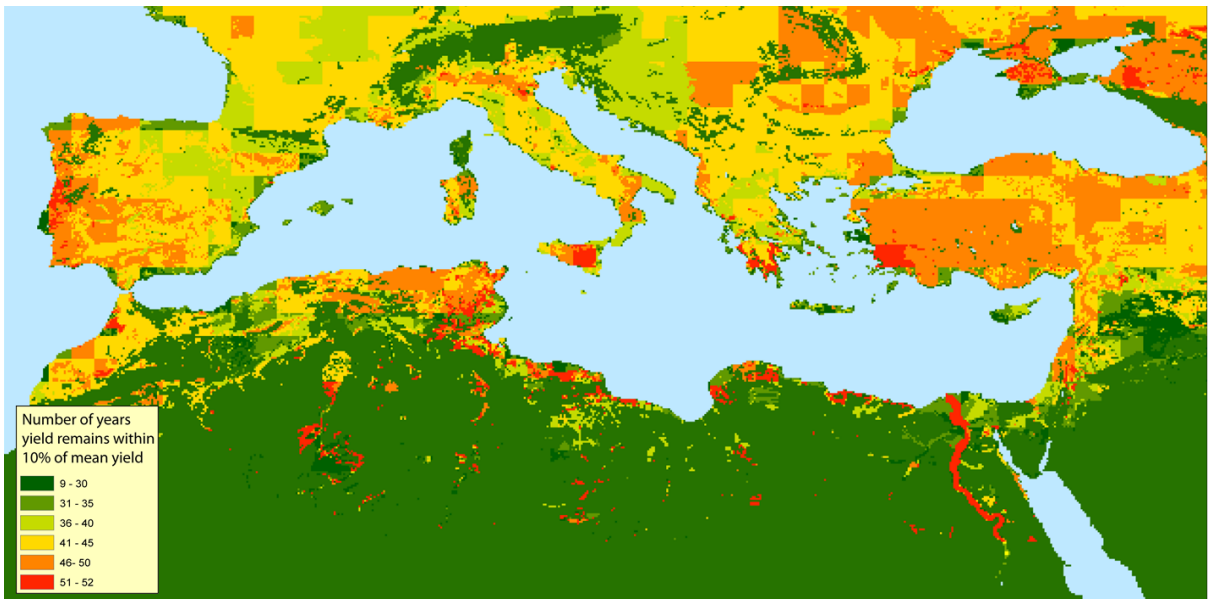

Figure 4.7 The stability of yields over time. The map shows in how many years the total annual yield in each cell remains within 10% of the average yield for the same cell calculated over 52 years of climate forcing. In the Nile Valley, yields remain within 10% of the average yield in all years, meaning that yields are exceptionally stable. Regions of Northern Spain and Northern France are relatively unstable with yields outside 10% of the average in at least 40 out of 52 years.

urbanisation pushes society closer to the planetary boundary of freshwater resources (Bogardi et al., 2013; Rockström et al., 2009) and reduces resilience to perturbations such as crop failures arising from climate variability (D'Odorico et al., 2010). Our simulations, which expand on those of D'odorico et al. (2010) by including climate-forced changes in VW using a hydrological

model, indicate that VW redistribution during the Roman Period certainly facilitated populations in VW poor regions, in particular urban areas, to overshoot their ecohydrological carrying capacities (Erdkamp, 2005; Garnsey, 1988; Rickman, 1980). The increased urbanisation during the Late Republican and Early Imperial periods (Scheidel, 2001) likely pushed the Empire closer to the limits of available fresh water resources and reduced resilience to climatic variability (D'Odorico et al., 2010; Garnsey, 1988). In addition, our simulations using a cost-distance based network show that increased urban demand arising from urbanisation caused an increase in average import distance and an associated increase in import costs. It is plausible therefore, that lower water resource redundancy and increased import costs may have been a contributing factor to the third century crisis which followed a period of peak urbanisation and trade in the 2nd century AD (Parker, 1992; Scheidel, 2010).

4.3.4 Present-day implications

In addition to informing our understanding of Roman water resource management, our cost-distance based network of VW trade in the Roman world uncovers general rules about VW trade that have relevance for present and future water resource management. Many studies of VW networks use socioeconomic trade relations to define the network structure. However, socioeconomic-based trade networks are highly changeable over time (Carr et al., 2012) with projections of future network structure based on economic trade models and expert assessment (Konar et al., 2013), although fitness-based models show promise by capturing changes in network properties based on the GDP, mean annual rainfall, agricultural area and population of trading nations (Dalin et al. 2012a). In contrast to socioeconomic trade relations, distance among trade regions is a variable that remains fixed. As with the Roman Period, present-day transport costs continue to co-vary with distance, particularly for bulk, staple foods such as grain (Hummels, 2007) with inland transport estimated to be 7 times more costly compared with sea-based transport (Limão and Venables, 2001). Indeed, it has been found that trade costs of bulk goods have become increasingly distance sensitive in the latter part of the 20th and early 21st century with approximately half of world trade occurring between trade partners less than 3000 kilometres apart (Berthelon and Freund, 2008). The reasons for a stronger relation between cost and distance in recent decades are not straightforward (Berthelon and Freund, 2008), but it is

likely that future increases in fuel costs will strengthen the trend further (Curtis, 2009). Therefore, the 'struggle against distance' (Braudel, 1995) which was a characteristic of preindustrial trade remains a central constraint for present-day VW redistribution.

As increasing urbanisation (United Nations, 2012) reduces water resource redundancy (D'Odorico et al., 2010) our analysis demonstrates that an associated increase in import distance will be unevenly distributed throughout the global VW network, with hub nodes experiencing the greatest increases in import distance and thus cost. How such costs will manifest in reality is complicated by the fact that exports are often controlled at hub nodes and therefore protectionism is likely to occur (Messerlin, 2011). As a result, research on VW trade should continue to use socioeconomic network structures because socioeconomic forcings are perhaps the primary force driving VW trade (Hoekstra and Chapagain, 2011). However, cost-distance based networks provide an additional avenue for understanding the underlying processes influencing VW trade. In addition, the high stability of cost-distance network structure and edge weight contributes to improving future projections as well as identifying the most economical VW trade routes, not just in terms of saving water but also in terms of fossil fuel use.

4.4 Conclusions

The question of what brought about the fall of the Roman Empire is one that has occupied Roman scholars for centuries (Gibbon, 1776). However, an equally relevant question is what enabled the Roman Empire to persist for so long in a region of highly variable climate (Lionello et al., 2006) and associated high variability in agricultural yields on which their economy and survival depended (Erdkamp, 2005; Garnsey, 1988; Rickman, 1980). Our findings show that the majority of the Mediterranean is temperature-limited for the growth of grain. Given that climate during the Roman Period in the Mediterranean was anomalously warm (Bond et al. 2001; Desprat et al., 2003; Ljungqvist, 2010) conditions for the growth of Rome's staple food were likely optimal. However, higher frequency climate variability has been demonstrated to have catastrophic impacts for other past civilisations where water resource management was not spatially integrated to the extent of the Roman Empire (de Menocal, 2001; Weiss et al., 1993). Our findings indicate that the combination of an increase in yield stability brought about by

irrigation in combination with VW redistribution in the relatively easily navigated Mediterranean Sea provided the Romans with high resilience to climate variability in an era of inefficient information transfer (Kessler and Temin, 2007) and undoubtedly contributed to the longevity of their reign over the Mediterranean region (Gibbon, 1776). The importance of VW redistribution in the Mediterranean as a buffer to climate variability is illustrated in the writings of Pliny the Younger (98 AD – 117 AD) *in* Erdkamp (2005) *'Even the heavens can never prove so kind as to enrich and favour every land alike. But he [the emperor] can so join East and West by convoys that those people who offer and those who need supplies . . . appreciate . . . having one master to serve'*.

However, although VW redistribution increased resilience to shorter term climate variability, it was also central to facilitating the growing urbanisation which occurred during the Late Republican and Early Imperial Period because it enabled urban regions to overshoot their local ecohydrological carrying capacities (Barnaby, 2009; D'Odorico et al., 2010). The associated increase in water resource exploitation pushed the Empire closer to the boundary of its freshwater resources and reduced its long term resilience to crop failures arising from climatic variability. In addition, growing urban demand led to an increase in average import distances of VW and an associated increase in import costs. The combination of reduced resilience to crop failures and increased import costs may have contributed to the 3rd century crisis following a peak in urbanisation in the 2nd century AD. Our cost-distance based network analysis demonstrates that increases in VW import costs arising from increased demand are unevenly distributed among all nodes in a VW network with hub nodes experiencing the greatest increase in import cost. Given that present-day trade costs in bulk, staple foods continue to covary with distance, the 'struggle against distance' will continue to be critical constraint on future VW trade.

Chapter 4 Supplementary information

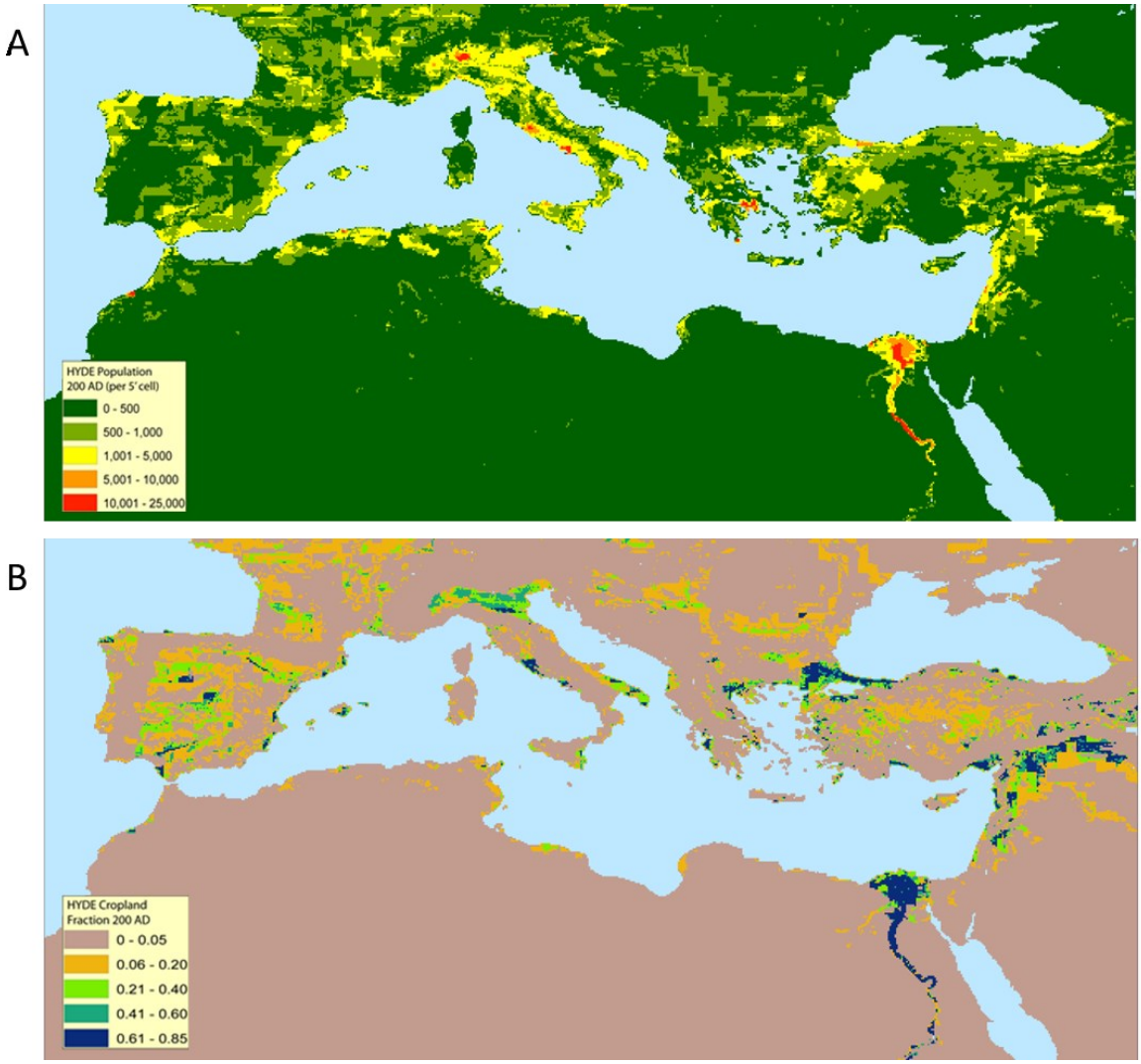

Figure S4.1 HYDE reconstructions of population and cropland at 200 AD. (A) Population values are per 5' cell. **(B)** Cropland fractions indicate the fraction of each 5' designated as cropland.

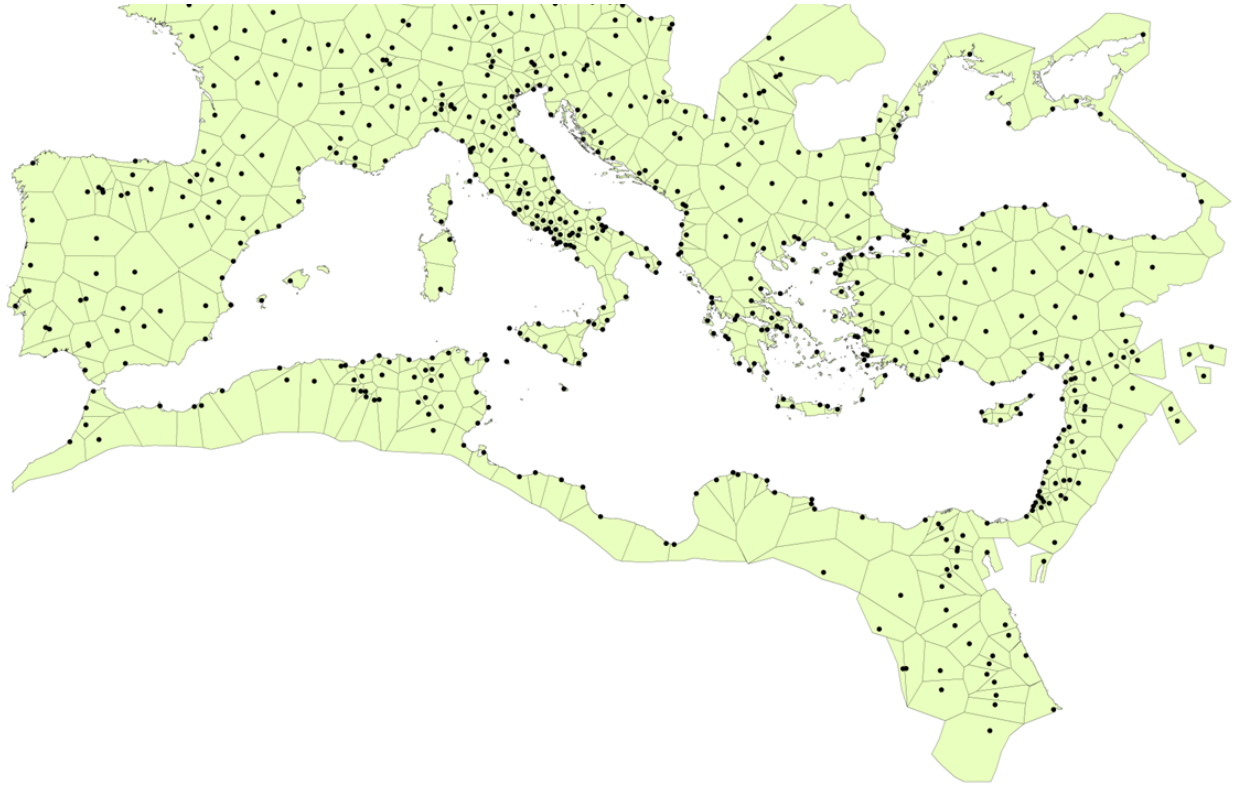

Figure S4.2 City regions. A Theissen polygon operation was carried out between nodes to define each city region. The polygons were cut with a land-sea mask at the coast and with the estimated maximum extent of the Roman Empire along the south, east and northern borders.

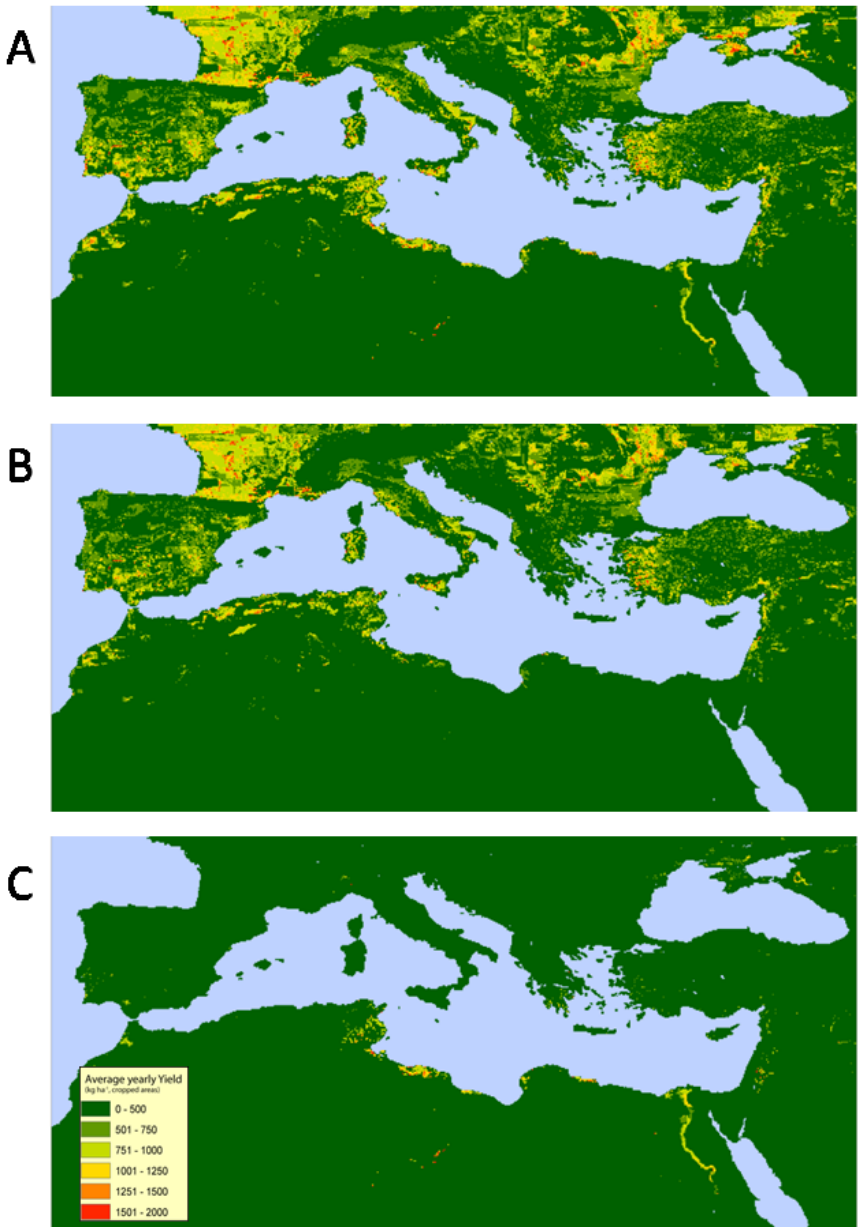

Figure S4.3 Average cereal yield (kg ha^{-1}). Average cereal yield calculated in PCR GLOBWB and based on 52 years of climate forcing **(A)**. The yields from rainfed **(B)** and irrigated **(C)** agriculture are shown separately.

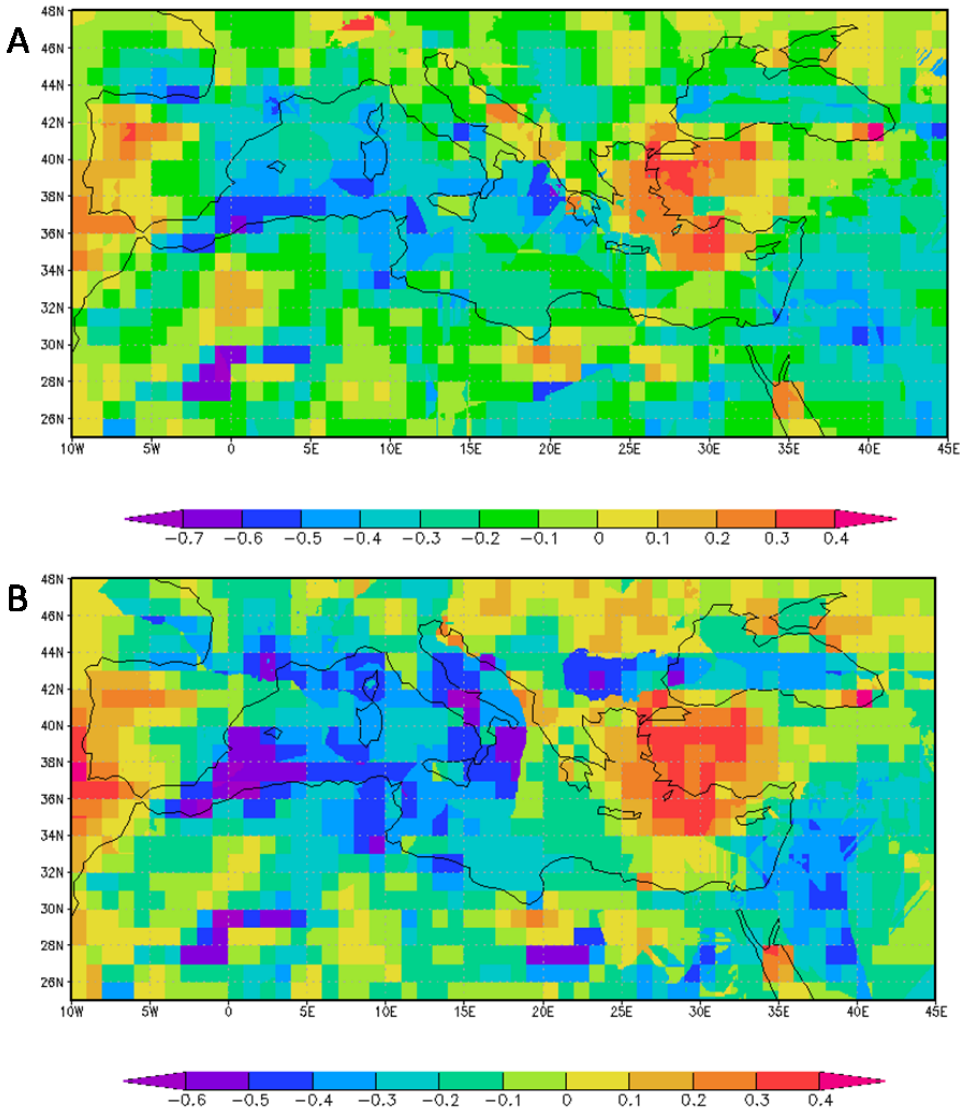

Figure S4.4 Correlation between temperature and precipitation over the growing season for rainfed (A) and irrigated **(B)** cereals. There is a negative correlation between temperature and precipitation in most of the Mediterranean apart from Western Turkey, the Western Balkans and Portugal.

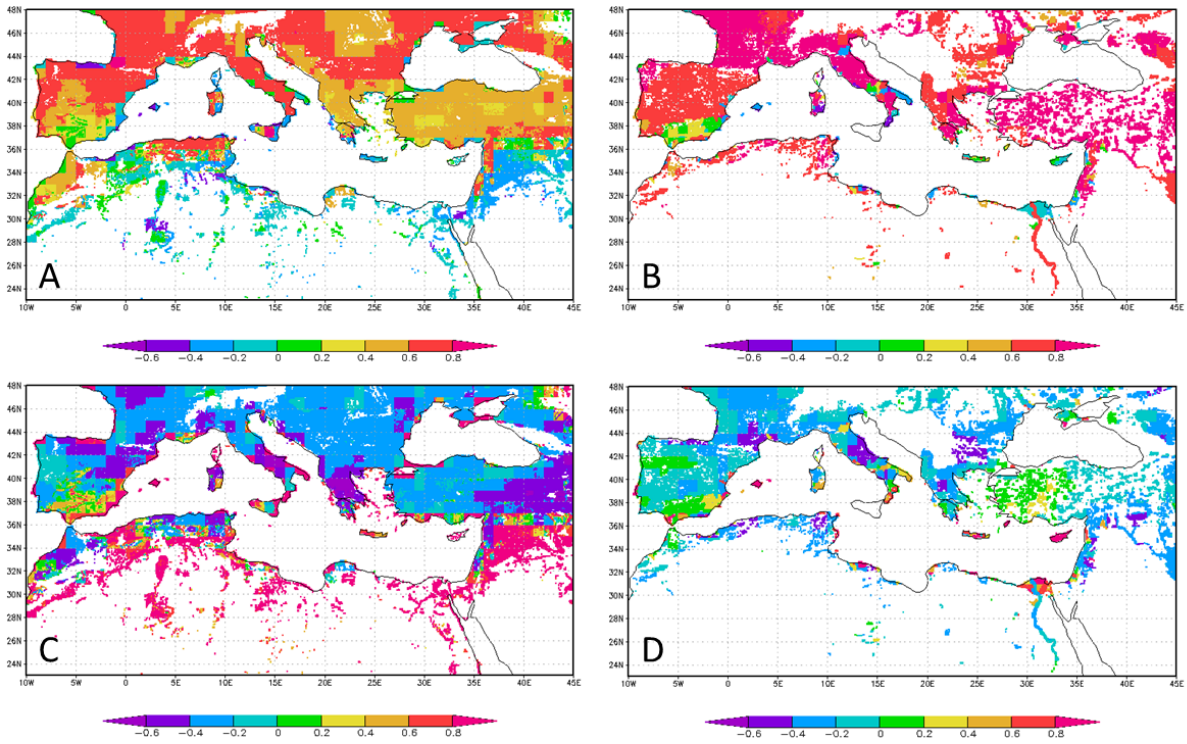

Figure S4.5 Correlation between temperature and precipitation over growing season with yields in rainfed and irrigated land. The correlation between temperature and yield in rainfed **(A)** and irrigated **(B)** land. The correlation between precipitation and yield in rainfed **(C)** and irrigated **(D)** land. White regions have no agricultural vegetation cover.

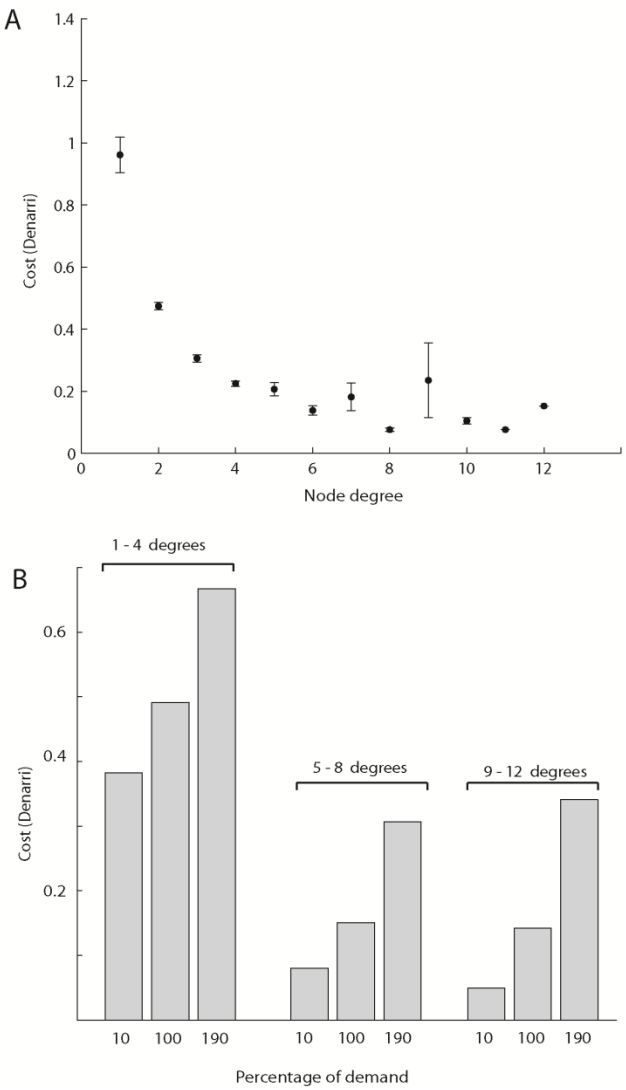

Figure S4.6 Cost to import VW in relation to node degree with VW of nodes and edge cost randomly redistributed. (A) Lower degree nodes generally have higher costs to import VW compared with high degree nodes irrespective of link cost or VW availability at the node. However certain highly connected nodes (hub nodes) have high import costs as they provide access to wider VW network for poorly connected nodes. As a result, demand at these nodes is actually the sum of demand from many nodes. Therefore nearby nodes are often depleted leading the need to import from further away with an associated increase in cost. This pattern is much stronger in the original network because a lot of hub nodes also have large populations with high demand **(B)** Costs increase incrementally across all node degrees for increases in demand when VW availability at nodes and edge costs are randomly distributed in the network.

Chapter 5

The resilience of Roman food supply to Holocene climate change

To be submitted

Abstract

We simulate the impact of the change in climate between the Roman Warm Period and Dark Ages Cold Period on the grain supply of the Roman Empire. We find that grain yields were likely higher on average during the Roman Warm Period owing to warmer growing season temperatures. However, coastal regions of the Central Mediterranean likely experienced low yields during the Roman Warm Period owing to relatively arid conditions in the region at the time. However, the Romans were highly resilient to lower yields in the Central Mediterranean because coastal cities of the Central Mediterranean were well connected to the grain trade-network.

5.1 Introduction

The resilience of societies to the impacts of climate change is a topic that has received increasing attention in recent years given the increased pressure placed on environmental resources arising from population growth and anthropogenic climate change (Rockström et al., 2009). However, current societies are not the first to be confronted with the pressures of climate change (de Menocal, 2001; Weiss et al., 1993). The Romans, one of the longest lasting ancient civilisations, were dependent on grain as their staple food source and were thus highly susceptible to climatic impacts on grain yields (Erdkamp, 2005). Dermody et al. (2014) demonstrated that the Roman use of irrigation and the redistribution of grain through trade greatly increased their resilience to interannual climate variability. Irrigation provided Romans with a far more reliable source of water for grain growth compared with precipitation, whilst the redistribution of grain through trade meant that regions with a deficit in grain could import from those with a surplus (Dermody et al., 2014; Erdkamp, 2005). However, given the length of their reign, the Romans were also confronted large amplitude and persistent climate change typical of Holocene climate anomalies (Bookman et al., 2004; Büntgen et al., 2011; Dermody et al., 2012; Jones et al., 2006; Martín-Puertas et al., 2009).

The Holocene was an epoch of warm and relatively stable climate beginning with the end of the last ice age 11,700 years ago in which human civilisation arose and flourished (Mayewski et al., 2004). Although, climate during the period was relatively stable compared with earlier inter-glacial periods, it was nonetheless characterised by anomalously warm and cool climate intervals lasting hundreds of years (Mayewski et al., 2004; Wanner et al., 2011, 2008). The height of the Roman civilisation corresponded with one such warm interval; known as the Roman Warm Period (RWP) (~250 BC – 450 AD) (Desprat et al., 2003). Climate reconstructions indicate that increased solar irradiance (Steinhilber et al., 2009) and warmer temperatures of the North Atlantic Ocean (Bond et al. 2001) at during the Late Republican and Early Imperial eras were associated with warming of the climate over the Mediterranean (Davis et al., 2003; Desprat et al., 2003; Ljungqvist, 2010). However, in the later Roman Period the North Atlantic cooled and solar irradiance reduced leading to a cooling of climate over Europe known as the Dark Ages Cold

Period (DCP) (~450 AD – 950 AD) (Desprat et al., 2003). Changes in the SST of the North Atlantic and solar irradiance variations not only influenced air temperatures but also had an impact on large scale circulation patterns over Europe associated with changes in the position and intensity of the Jetstream (Büntgen et al., 2011; Dermody et al., 2012; Martin-Puertas et al., 2012). Dermody et al. (2012) demonstrated that during the RWP climate in the Central Mediterranean was relatively dry whilst the West and South-eastern Mediterranean experienced relatively wet. They proposed that this pattern was linked with fluctuations in SST changes in the North Atlantic and solar irradiance variations (Bond et al. 2001; Martin-Puertas et al., 2012). The precipitation pattern in the Mediterranean reversed sometime between 250 – 500 yr BP as Europe moved into the DCP. With the switch to the DCP, the Central Mediterranean became relatively wet, whilst the West and South-eastern Mediterranean experienced aridification.

To understand the impact of these large amplitude and persistent shifts in climate on the Roman food supply we simulate grain yields under climate conditions consistent with the Roman Warm Period and Dark Ages Cold Period. Given the importance of trade to increasing resilience to climate variability, we also simulate the impact of these large amplitude climatic changes had on the grain trade during the Roman Period. It is envisaged that our approach of linking paleoclimate reconstructions to process-based models provides a more nuanced understanding of the impact of Holocene climate change on the Roman Empire (Cornell et al., 2010).

5.2 Methods

In order to understand the impact of Holocene climate change on grain yields in the Roman Empire, we analysed the yield response of winter wheat to climate conditions reflecting the Roman Warm Period and the Dark Ages Cold Period (Dermody et al., 2012). Grain yields were calculated based on:

$$\left(1 - \frac{Y_a}{Y_x}\right) = K_y \left(1 - \frac{ET_a}{ET_p}\right) \quad \text{(Eq. 5.1)}$$

where Y_x and Y_a are the maximum and actual yields, ET_p and ET_a are the potential and actual evapotranspiration, and K_y is the yield response factor of winter wheat, representing the effect of

a reduction in evapotranspiration on yield losses (FAO, 2012). The yield response factor was adapted to Roman yield levels based on yield estimates from Roman Egypt and Medieval Britain (Allen, 2008; Rickman, 1980). PC raster Global Water Balance Model (PCR GLOBWB) was used to calculate actual transpiration which was used to estimate yield according to eq. 5.1 (Doorenbos and A.H. Kassam, 1979; van Beek et al., 2011). PCR GLOBWB is a spatially explicit hydrological model at 5' horizontal resolution that calculates vertical water balance under different land cover types under prescribed meteorological conditions and routes the specific runoff to obtain discharge fields. (van Beek et al., 2011). Crop land cover was assigned in PCR GLOBWB based on reconstructions for 200 AD from the History Database of the Global Environment (HYDE) (Klein Goldewijk et al., 2011). Land with a potential for irrigation was assigned within HYDE cropland regions based on the MIRCA dataset of Portmann et al. (2008). Although MIRCA is based on current irrigated regions, the irrigated area is constrained by HYDE cropland reconstructions for 200AD. In addition, irrigation is constrained surface water availability and is only applied to regions within a 2m elevation of the riverbank. Natural land cover was assigned based on the Olson classification (Olson, 1994a, 1994b). A detailed description of our yield calculation methodology, including the crop calendar for irrigated and rain fed agriculture, can be found in Dermody et al. (2014).

Precipitation patterns matching reconstructions of RWP and DCP climate were extracted from current climate using NCEP/NCAR reanalysis data downscaled to 1 degree resolution for the period 1949 – 2000 by the Climate Research Unit (Ngo-Duc et al., 2005). The seesaw in precipitation patterns which characterised the RWP and DCP corresponds to the 2nd canonical correlation analysis pattern in Mediterranean precipitation during the reanalysis period associated with the East Atlantic West Russia Pattern (Barnston and Livezey, 1987; Dermody et al., 2012; Dünkeloh and Jacobeit, 2003; Xoplaki et al., 2004). This pattern is characterised by a warming (cooling) of the North Atlantic under precipitation patterns consistent with the RWP (DCP). Our RWP and DCP climates were thus based years with persistent positive (DCP, 1963) and negative (RWP, 1989) index values of the 2nd CCA pattern of Dünkeloh and Jacobeit (2003) (Fig. 5.1). It was decided to use reanalysis data to force the hydrological model rather than output from a regional climate model nested within GCM simulations for the RWP and DCP because it has

been demonstrated that RCMs perform poorly at capturing dominant precipitation patterns in the Mediterranean (Deidda et al., 2013; Hesselbjerg Christensen et al., 2010). However, although the climatic patterns are consistent with those reconstructed for these periods; the centennial timescale of this forcing is not captured. This should be kept in mind as centennial-scale persistence of a certain climatic pattern may have led to reduced discharge in certain river catchments owing to the impact on long term water storage in aquifers and high mountains (Immerzeel et al., 2010; Wada et al., 2010). Future transient simulations would benefit from applying paleo reanalysis forcing (Goosse et al., 2006) that the persistent feature of Holocene climate anomalies.

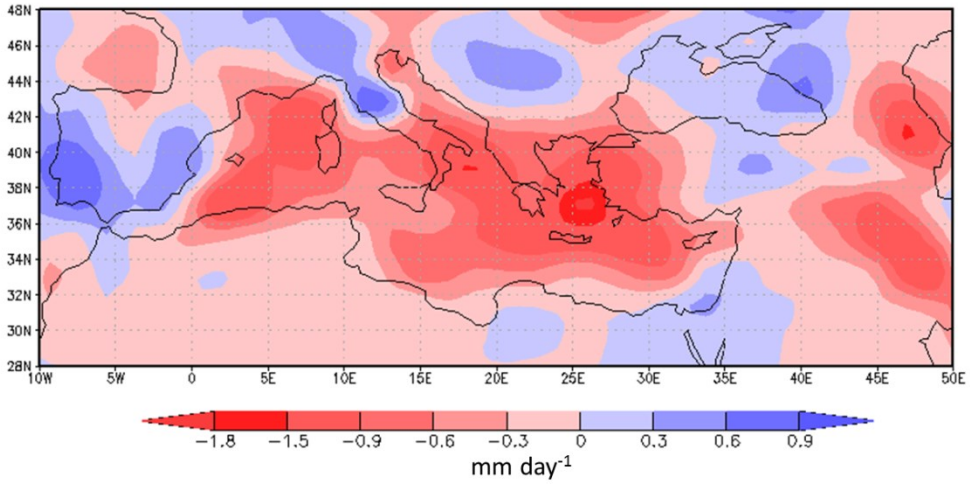

Figure 5.1 Prescribed precipitation anomaly RWP – DCP, derived from reanalysis data. A cooling of the surface temperatures in the North Atlantic from the Roman Warm Period to the Dark Ages Cold period was associated with a modification of the Jetstream over the Mediterranean. These changes resulted in a switch from dry conditions in the Central Mediterranean during the RWP to wet conditions during the DCP. The Western and South-eastern Mediterranean experienced an opposite shift with wetter conditions during the RWP and drier conditions during the DCP.

Grain demand was calculated based on HYDE gridded population estimates (Klein Goldewijk et al., 2011) and population estimates for the 20 most populous cities in the Empire (Chandler, 1987). Based on historical estimates, we prescribed a yearly consumption of 200kg of grain per person (Erdkamp, 2005; Goodchild, 2007). Grain surpluses and deficits were calculated for each

cell based on the annual yield minus the annual population demand. Grain surpluses and deficits differed between the RWP and DCP based on the yield response of grain to climate forcing in both scenarios. Population was kept constant between both scenarios as we wish to isolate the climate change impact on food supply. Grain surpluses and deficits were abstracted to our grain trade network, which is based on Orbis, the Stanford Geospatial Network of the Roman World (Scheidel, 2013). Orbis contains a database of 751 roman towns and cities that form the nodes within our network. A Theissen polygon operation was used to define agricultural regions around each city node. Based on the sum of cells within each region, regions were designated as having a surplus or deficit in grain. Cities in Orbis are linked by 1,371 edge segments that represent the cost to transport a kilogram of grain in *denarii* along Roman roads, rivers and over sea based on Diocletian's edict of Maximum Prices and physical cost distance calculations (Scheidel, 2013). Trade in Orbis was simulated along the minimum cost path. Thus we simulated the anomalies in the grain trade between the RWP and DCP.

5.3 Results

The grain yield anomaly between RWP – DCP is shown in Fig. 5.2. Yields were higher in the RWP scenario in most of the Mediterranean owing to warmer temperatures. However, coastal regions of the Central Mediterranean experienced lower yields during the RWP owing to decreased precipitation. The Nile experienced decreased discharge in our RWP forcing year owing to a negative precipitation anomaly over its upper catchment. That is not necessarily the case during the RWP. In total, yields were 11.14% higher in the RWP scenario compared with the DCP scenario (Table 5.1).

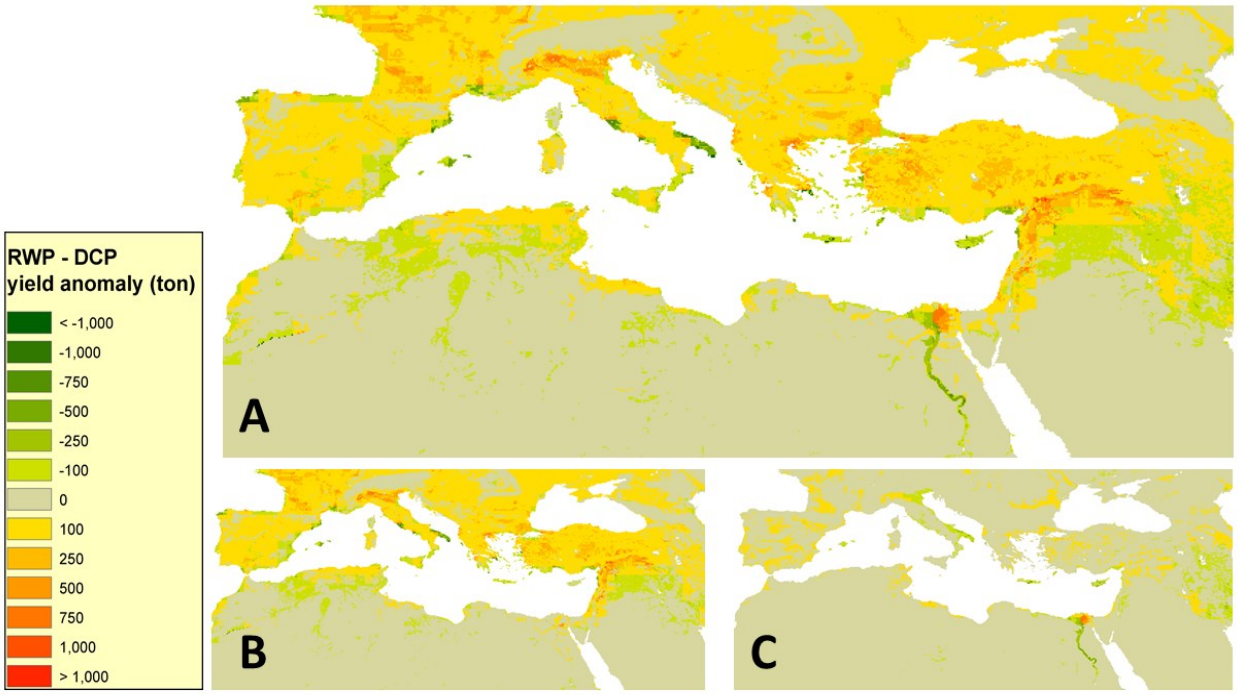

Figure 5.2 Grain yield anomaly (ton per 5'cell) between the Roman Warm Period - Dark Ages Cold Period climate scenarios (A). The yields rainfed **(B)** and irrigated **(C)** land are shown separately. Grain yields were likely higher in the majority of the Mediterranean during the RWP owing to an increase in temperature over the growing season during the RWP. Yields were decreased in coastal areas of the Central Mediterranean owing to a decreased precipitation during the RWP.

Table 5.1 Total annual grain yield during the Roman Warm Period and the Dark Ages Cold Period. Grain yields reduced by approximately 11% from the RWP to the DCP. Almost all the reduction was in rainfed agricultural land.

	Grain Yields (Tonnes yr^{-1})		
	Rainfed	**Irrigated**	**Total**
Roman Warm Period	3840400	1402000	5242400
Dark ages Cold Period	3293100	1396200	4689300
Anomaly	547300	5747	553040
Percentage anomaly	11.02	0.12	11.14

Table 5.2 Total annual demand for grain imports during the Roman Warm Period and the Dark Ages Cold Period. Import demands for grain were approximately 9% less during the RWP compared with the DCP owing to the increase in grain production under warm climatic conditions

Grain Trade (Tonnes yr^{-1})	
	Import Demand
Roman Warm Period	712,400
Dark ages Cold Period	780,910
Anomaly	-68,509
Percentage Anomaly	-9.20

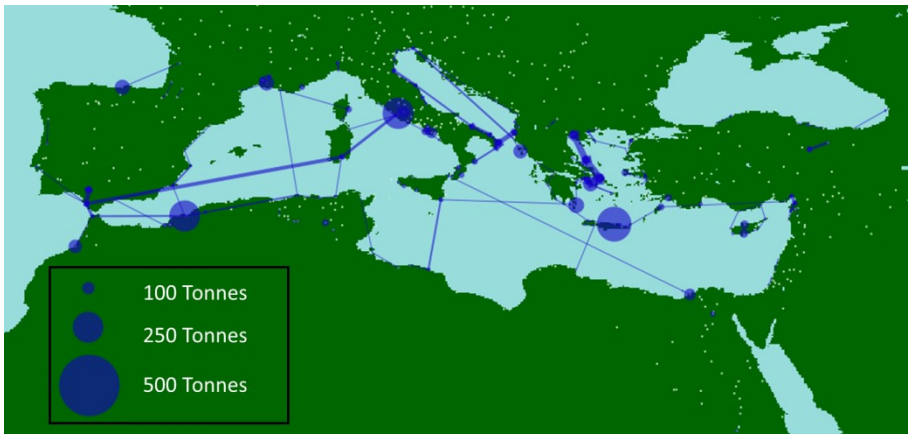

Figure 5.3 Grain import anomaly between Roman Warm Period – Dark Ages Cold Period in tonnes yr^{-1}. The blue nodes are city regions which experienced an increase in demand for grain imports during the RWP compared with the DCP. The size of the node corresponds to the relative demand increase, whilst the thickness of the links corresponds to the increase in imports along a trade route. Owing to the reduction in yields in coastal regions of the Central Mediterranean during the RWP an increase in grain imports was likely required. However, the increase in imports was low owing to the relatively high populations and small agricultural area of the low-lying, Central Mediterranean city regions. The total import demand was greater during the DCP (not shown) (Table 5.2).

Overall demand for grain imports was 9.2% less during the RWP compared with the DCP (Table 5.2) However, a number of city regions in the central Mediterranean exhibited an increase in grain demand during the RWP arising from a decrease grain production linked to a drier climate (Fig. 5.3).

5.4 Discussion

Our analysis indicates that warm climatic conditions during the Roman Warm Period were optimal for the growth of grain in most of the Mediterranean and shifted to poorer growing conditions during the cooler Dark Ages Cold Period (Fig. 5.2, Table 5.1). Grain is primarily a winter and spring season crop in the Mediterranean (Allen et al., 1998), which coincides with the cool, wet season in the region (Lionello, 2012). As a result, water is only limiting for the growth of grain in very dry regions (Fig. S5.1) (Ludwig and Asseng, 2006; van Ittersum et al., 2003). Increased winter temperatures arising from a warming of the North Atlantic during the RWP would therefore have brought about increased yields in most of the Mediterranean region, whilst cooler conditions during the DCP would have reduced yields (Dermody et al., 2014).

However, our simulations do indicate a reduction in grain yields in coastal regions of the Central Mediterranean during the RWP reflecting the reduction in rainfall between ~100 BC and 300 AD (Dermody et al., 2012). Most of the land area in the Mediterranean is typified by sharp increases in elevation moving inland, away from the sea (Lionello, 2012). As a result wet season temperatures tend to be cooler in higher elevation, inland regions compared with low lying coastal regions (Lionello, 2012). Given that grain yields are driven by evapotranspiration, cooler temperatures decrease yields where water is not limiting (Eq. 5.1). Therefore, in low lying coastal regions where growing season temperatures are on average warmer than inland regions, reductions in rainfall have a greater impact on yield than reductions in temperature. However, in cooler inland regions temperature is the main driver of yield variations (Fig. S5.1).

Dermody et al. (2014) demonstrated that the use of irrigation provided the Romans with increased resilience to climate variability because irrigated land produced highly stable year to year yields compared with rainfed agriculture. The results here indicate that irrigation also

provided resilience to long term and persistent climate change associated with Holocene climate anomalies. Our results indicate almost no change in productivity on irrigated land between RWP and DCP climate scenarios (Table 5.1). In irrigated regions such as Egypt and the Po Valley, a year round supply of surface water facilitated multi-cropping, which can take advantage of the summer season when temperatures for growth were optimal. Owing to warm summer growing seasons and the use of surface water, irrigated grain experienced almost no limits to growth (van Ittersum et al., 2003). In contrast, rainfed grain was dependent on warm and humid growing seasons for maximum productivity. With the switch to the DCP wet season temperature cooled leading to a reduction in grain yields (Davis et al., 2003; Desprat et al., 2003). However, as we have mentioned, our analysis does not include persistent climate forcing which would have impacted water storage in aquifers and high mountains and may have led to reduced discharge in rivers (Immerzeel et al., 2010; Wada et al., 2010).

Trade in food is also proposed to have allowed the Romans a certain amount of decoupling from the climate as regions with a deficit in one year could import from regions with a surplus (D'Odorico et al., 2010; Dermody et al., 2014; Erdkamp, 2005). Given the high connectivity of the Central Mediterranean and the relative ease of transport seafaring transport (Dermody et al., 2014; Limão and Venables, 2001; Scheidel, 2013), reduced yields in this region were likely easily offset by increased grain imports from neighbouring regions experiencing high grain yields during the RWP (Fig. 5.3). In fact, the yield anomaly in low-lying coastal regions of the Central Mediterranean between the RWP and the DCP was likely very low owing to the fact that they are relatively urbanised areas, with high population relative to the area of agriculturally productive land (Bowman and Wilson, 2011). For example, cities such as Rome and Athens massively overshot local agricultural carrying capacities and were thus dependent on imports irrespective of climate conditions (Erdkamp, 2005; Rickman, 1980). Therefore, climatic impacts in grain production in Central Mediterranean cities would have had little impact on total imports. These urban hubs were actually more susceptible to changes in yield in the regions they import from (Dermody et al., 2014).

Our simulations are based on reconstructions for 200AD, which coincided with the peak in population and urbanisation during the Roman Period (Scheidel, 2001). However, drier conditions in the Central Mediterranean likely began sometime in the Early Republican period (Dermody et al., 2012). In this period population density was much lower; whilst the Roman-controlled trade network of later periods had not yet emerged (Horden and Purcell, 2000). Thus it is likely that the early Romans were dependent on the local grain production for their food supply. As a result, changes in agricultural yields in coastal regions of the Central Mediterranean may have had more of an impact on local populations compared with later periods. It is plausible therefore that dry conditions in coastal regions of the Central Mediterranean may have been one incentive for expansion in this early period in Rome's history (Meijer, 1984).

5.5 Conclusions

Our analysis demonstrates that warm climatic conditions during the Late Republican and Early Imperial period in the Mediterranean were optimal for the growth of grain. Reductions in rainfall associated with centennial-scale changes in the position and intensity of Atlantic storm tracks likely didn't impact yields to a great extent owing to the sensitivity of grain growth to wet season temperature rather than precipitation in most of the Mediterranean. Only coastal regions of the Central Mediterranean exhibited a reduction in yields during the Roman Period. However, owing to the centrality of these cities within the grain trade network, they were highly resilient to reductions in yield. Our analysis demonstrates that by linking climate reconstructions to process-based models a nuanced picture of climate impacts can be detected.

Chapter 5 supplementary information

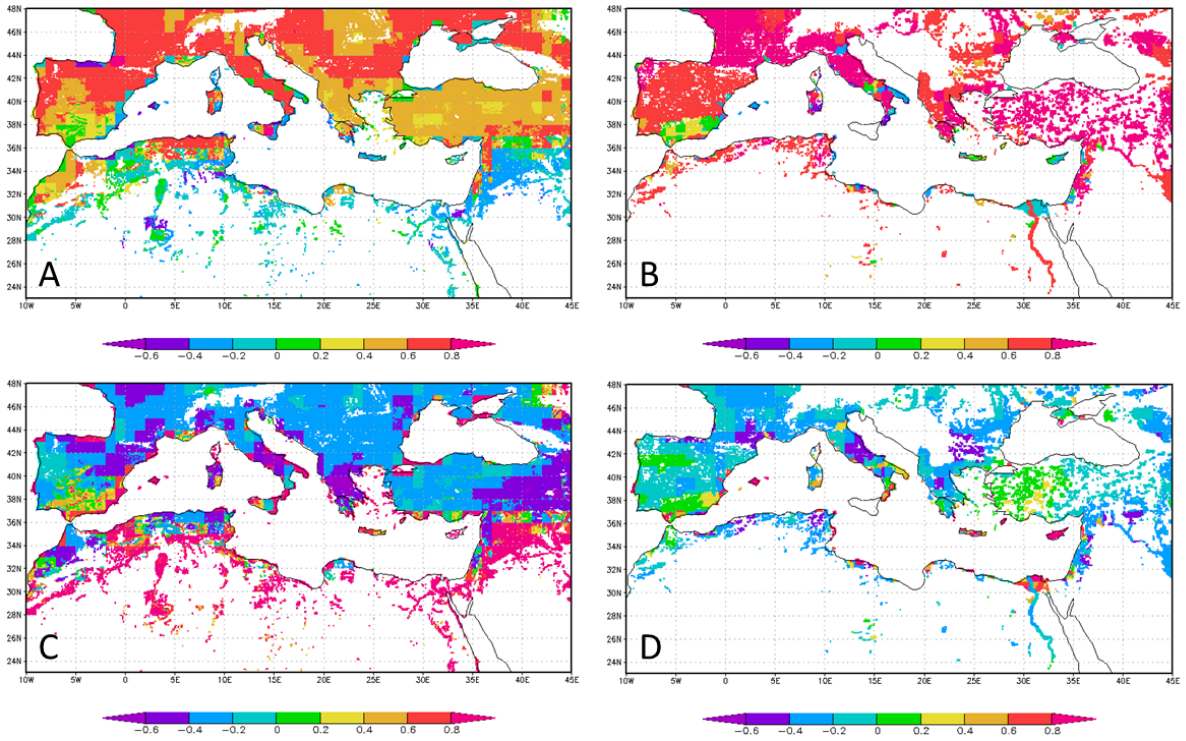

Fig. S5.1 Correlation between growing season temperature and precipitation with winter wheat yields. The correlation between temperature and yield on rainfed **(A)** and irrigated **(B)** land. The correlation between precipitation and yield on rainfed **(C)** and irrigated **(D)** land. White regions have no agricultural vegetation cover.

6 Synthesis and discussion

6.1 Research context

Improving predictions of future climate change requires improving our understanding of the climate system. However, many elements of the climate system operate on timescales longer than the period for which we have observational data (Mann et al., 1998). Thus, to understand the climate system it is necessary to extend our observations into the past, before the recent observational period (de Menocal, 2001). Using past observations we can begin to understand the full range of variability in the climate system and the mechanisms that bring about that variability.

Equally, our understanding of how human society is impacted by climate change was, until recently, largely restricted to the period for which we have reliable climate observations. However, as our knowledge of climate change since the birth of civilisation improves, we can begin to understand how different past societies were impacted and adapted to these changes. Given that some of the changes in climate during the Holocene were large and sudden, analysis of past societies can inform of how we may be able to adapt to the sudden and extreme changes predicted under anthropogenic climate change.

In this thesis I have endeavoured to close some of the knowledge gaps associated with these issues with the intention of understanding climate change and how we, as a globalised society, may adapt. Following is a synthesis and discussion of my findings. I conclude with recommendations for future research that will progress our understanding of the issues discussed further.

6.2 Summary of results

Research question 1: How are variations in solar irradiance communicated to the climate system?

By applying novel statistical analysis to a composite of climate reconstructions from the Tropical Pacific we found data-based evidence of solar forcing of the Tropical Pacific throughout the Holocene. Our analysis indicates that the coupled ocean-atmosphere system of the Tropical Pacific had an opposite response to solar forcing between the Early and Late Holocene. In the Early Holocene, the Tropical Pacific warmed (cooled) during solar maxima (minima), in a direct response to increased (decreased) radiation. In the Late Holocene the Tropical Pacific cooled (warmed) during solar maxima (minima). The reason for the switch in response was owing to orbital forced changes in the coupled ocean-atmosphere system of the Tropical Pacific, which strengthened solar forcing of the ocean dynamical thermostat. This meant that periods with increased (decreased) radiation were more likely to have La Niña (El Niño) conditions. At a longer timescale a dominance of La Niña conditions was associated with increased upwelling of cool waters from the deep ocean which cooled the ocean surface temperature. These results provide evidence that the Tropical Pacific played a role in amplifying and communicating variations in solar irradiance to the climate system during the Holocene.

Research question 2: How did the climate change during the Roman Period in the Mediterranean and what were the drivers of these changes?

By applying statistical analysis to a composite of climate reconstructions from the Mediterranean, we demonstrated that climate between 3000 and 1000 yr BP was typified by a millennial-scale seesaw in climatic humidity between West and South-eastern Mediterranean on one side and the Central Mediterranean on the other. This pattern is similar to precipitation anomalies associated with the East Atlantic/West Russia pattern in current climate. We found that changes in the position and intensity of the Jetstream indicated by our analysis correlate with millennial changes in North Atlantic sea surface temperature. Our model simulations indicate that it was unlikely that deforestation by the Romans caused regional scale aridification. In fact we find no evidence

of aridification during the Roman Period. Instead proxy records exhibit a wetting trend whilst an analysis of the distribution of archaeological sites in the Fertile Crescent indicate that human habitation distribution has been unaffected by climate change since ancient times.

Research question 3: How did the Roman water resource management strategy impact their resilience to climate variability?

We developed a virtual water network of the Roman world in order to understand Roman food production and redistribution in response to urbanisation and climate variability. Using this network we found that irrigation and virtual water trade increased Roman resilience to climate variability in the short term. However, urbanisation arising from virtual water trade likely pushed the Empire closer to its carrying capacity, led to an increase in import distance and cost, and reduced its resilience to climate variability in the long-term. In addition to improving our understanding of Roman water resource management, our cost-distance based analysis illuminated how increases in import costs arising from climatic and population pressures are likely to be distributed in the future global virtual water network.

Research question 4: What was the impact of Holocene climate change on Roman food supply?

We simulated the yield response of grain in the Mediterranean to reconstructed climate change between the Roman Warm Period and the Dark Ages Cold Period. We found that grain yields were likely higher on average during the Roman Warm Period owing to higher growing season temperatures. Yields were reduced in the coastal Central Mediterranean during the RWP owing to a reduction in precipitation in these regions. Reduced yields in the Central Mediterranean during the RWP likely increased Rome's reliance of grain imports from other parts of the Empire with driest conditions estimated to be 0 – 150 AD. However, the centrality of Rome within the grain trade network, likely made it highly resilient to reductions in yield in this period.

6.3 Holocene climate anomalies

There are a multitude of climate records that demonstrate correlations with solar irradiance variations during the Holocene (Asmerom et al., 2007; Fleitmann et al., 2003; Hodell et al., 2001; Martin-Puertas et al., 2012; Wang et al., 2005). However, finding direct evidence in data of a mechanism linking solar irradiance variations with changes in climate is complicated for a number of reasons. Firstly, model simulations indicate that at large spatial scales, solar irradiance variations exhibit a coherent response in the climate system, however at regional spatial scales internal dynamics of the climate often dominate the external forcing signal (Goosse and Renssen, 2007; Goosse et al., 2005). In addition, accurate dating of records is important for identifying solar forcing owing to the relatively short timescales associated with the well-known cycles in solar irradiance (Gray et al., 2010). In the absence of accurate dating anomalies in a reconstructed timeseries are often aligned among timeseries without an appreciation of the chronological errors among timeseries (Blaauw et al., 2010). This practice, known as wiggle matching, runs the risk of creating illusionary climatic events from unrelated anomalies in proxy time series (Blaauw et al., 2007). Dating is a particular problem with marine reconstructions owing to uncertainties related with the reservoir age of water through time. In most cases a constant reservoir age is assumed for the Holocene despite the fact that changes in currents may mix water of different ages (Reimer and Reimer, 2001; Sun et al., 2005). In the context of identifying how solar forcing impacts climate, this is particularly problematic as model simulations indicate that the ocean may play a critical role in amplifying and communicating solar irradiance variation to the atmosphere (Emile-Geay et al., 2007; Renssen et al., 2006).

In chapter 2 we confront these issues by analysing the impact of solar forcing on a number of SST reconstructions from the Tropical Pacific throughout the Holocene. We addressed the issue of regional signals arising from internal dynamics of the climate system by analysing records from throughout the Pacific that are under the influence of different but related oceanic currents. Additionally, we use stacked reconstructions of SST from the Indo Pacific Warm Pool which integrate changes across a number of records and are thus less sensitive to localised signals. Owing to chronological uncertainty of marine records, we focused our analysis at centennial

timescales relevant for 500 and 710 cycles in solar irradiance as well as the quasi-2200 year Hallstatt cycle (Steinhilber et al., 2012). To examine the relation between solar irradiance and SST in these records we applied change point analysis which provides an independent and quantitative method of calculating if a statistically significant correlation exists between two timeseries and whether a change in the sign of the correlation occurs.

Our analysis indicated that solar irradiance variations forced changes in the Tropical Pacific SST throughout the Holocene. This finding is important as it provides evidence that the Tropical Pacific plays a role in communicating solar irradiance variations to the atmosphere (Emile-Geay et al., 2007; Mann et al., 2005). Importantly, we demonstrate the response of the Pacific to solar forcing was opposite between the Holocene Climatic Optimum and the Late Holocene. That finding has important implications for the interpretation of Holocene climate anomalies in regions teleconnected with the Tropical Pacific. In studies that analyse correlations between a climate reconstructions and solar irradiance, a phase change in correlation is often interpreted as a lag correlation caused by internal dynamics in the climate system or dating error (Asmerom et al., 2007; Marchitto et al., 2010; Poore et al., 2004). However, our analysis indicates that in regions teleconnected with the Tropical Pacific, phase changes may actually be related to a change in how solar irradiance variations are communicated to the climate in that region. An added implication is that solar irradiance forcing of the Pacific may act constructively with other climate processes at certain times and destructively at others (Williams and Hanan, 2011).

As mentioned, at a regional scale, internal forcing can often dominate the influence of external forcing on the climate (Goosse et al., 2005). An understanding of these internal dynamics is important for improving predictions of the response of the climate system to global warming as internal processes often exhibit highly non-linear responses to external forcing (McManus et al., 2004). In chapter 3 we focused our analysis on the regional changes in climatic humidity in the Mediterranean during the Roman Period. In the extra-tropics, long-term changes in rainfall are an indicator of changes in the position of the winter storm tracks, particularly in the Mediterranean, which receives the majority of its precipitation in winter (Dünkeloh and Jacobeit, 2003; Xoplaki et al., 2004). The position and intensity of the annular storm tracks as they pass over Europe and the Mediterranean are dictated by a number of factors; however during the observational period

the majority of variation in the storm tracks is captured by a meridional pressure gradient between the mid-latitudes and sub polar region (Barnston and Livezey, 1987). From an analysis of precipitation reconstructions in Scotland and Morocco, Trouet et al. (2009) provided evidence of a persistent northward (southward) displacement of the storm tracks during the Medieval Climate Anomaly (Little Ice Age) consistent with meridional changes in sea level pressure (SLP). Trouet et al. (2009) proposed that La Niña-like warming of the Indo Pacific Warm Pool during the MCA solar maxima caused persistent NAO positive through atmospheric teleconnections with the North Atlantic (Hoerling et al., 2001; Hurrell et al., 2004; Li et al., 2006). Warming in the Eastern Pacific during the LIA had the opposite impact, stimulating persistent NAO-negative conditions at the time (Trouet et al., 2009). An analysis of a well dated, high resolution reconstruction of wind strength from a German lake provides evidence for an alternative forcing mechanism of persistent NAO-like conditions over Europe during solar minima in the Late Holocene (Martin-Puertas et al., 2012). Martin-Puertas et al. (2012) demonstrate that annual changes in wind strength during the solar minima at 2800 yr BP were correlated with solar irradiance variations, consistent with top-down forcing of atmospheric pressure gradients, a finding also supported by model simulations for the MCA (Shindell et al., 2001).

Our analysis in chapter 3 indicates a northward (southward) displacement of the storm tracks over Europe during solar maxima (minima) in the Roman period consistent with solar forcing. However, we find the principal mode of variability in precipitation in the Mediterranean was inconsistent with changes in meridional pressure gradients and precipitation associated with solar forcing. Rather our analysis indicates that climate in the Mediterranean was typified by a zonal seesaw in climatic humidity between the Central Mediterranean on one side and the Iberian Peninsula and South-western Mediterranean on the other during the Roman Period (Dermody et al., 2012). A paper published later in 2012 also demonstrated a seesaw in climatic humidity between Turkey and Spain during the Medieval Climate Anomaly and Little Ice Age consistent with EOF1 in our analysis (Roberts et al., 2012). These precipitation patterns in the Mediterranean during the Late Holocene were consistent with the second mode of variation in wet season precipitation in current climate which is related to pressure anomalies described by

the East Atlantic / West Russia pattern (Dermody et al., 2012; Dünkeloh and Jacobeit, 2003; Roberts et al., 2012; Xoplaki et al., 2004).

In current climate, wet (dry) conditions in the Central Mediterranean and dry (wet) conditions in Spain and Israel are correlated with a cooling (warming) of SST in the area of the North Atlantic where ice rafted debris were deposited during Holocene (Bond et al. 2001; Xoplaki et al., 2004). For the Roman Period we found that cool (warm) IRD events (intervals) were also correlated with wet (dry) conditions in the Central Mediterranean and dry (wet) conditions in the West and South-eastern Mediterranean. We concluded therefore that SST of the North Atlantic was likely the primary forcing mechanism of changes in climate in the Mediterranean during the Roman Period. It is simulated that the temperature of the North Atlantic impacts precipitation patterns in the Mediterranean by diabatic warming or cooling of the atmosphere, which impacts the location of the stationary Rossby waves in the Jetstream. The change in the location of stationary waves modifies the path of the storm tracks over the Mediterranean thus impacting wet season precipitation patterns (Wang et al., 2010). Therefore, climate over Europe was characterised by two principal modes of variation, one associated with meridional changes in the Jetstream and one associated with zonal changes in the Jetstream, which had a greater expression over the latitudinal Mediterranean. Roberts et al. (2012) propose that the centres of action of these two modes may not have been stable in time. This is certainly likely for the EA/WR pattern owing to the temperature change of the Atlantic over time and its impact on the location of stationary Rossby waves (Wang et al., 2010).

In summation, chapter 2 and 3 demonstrate the interplay between external solar irradiance variations and internal climate dynamics as forcing mechanisms of Holocene climate anomalies. The evidence we show for solar forcing of a thermostat response in the Tropical Pacific during the Late Holocene indicates that La Niña (El Niño) conditions were more likely during solar maxima (minima) (Newman et al., 2003). Therefore bottom-up solar forcing of the Tropical Pacific in the Late Holocene likely reinforced top-down solar forcing of meridional pressure gradients over the North Atlantic through atmospheric teleconnections (Emile-Geay et al., 2007; Goosse and Renssen, 2007; Mann et al., 2009; Martin-Puertas et al., 2012; Shindell et al., 2001). Solar forced changes in the storm tracks were superimposed on variations brought about by SST

change in the North Atlantic. The modification of the position of stationary Rossby waves through SST changes in the North Atlantic were likely the primary forcing of latitudinal climate variability in the Mediterranean.

6.4 Climate and society

Many studies infer a climatic cause for past detrimental societal events based on correlations between the two (Büntgen et al., 2011; de Menocal, 2001; Hodell et al., 2001; Zhang et al., 2008). Although interesting, such correlations don't improve our understanding of why the societies in question were vulnerable to climatic perturbations. In addition, it fosters a focus on catastrophe when actually much can be learned about climate adaptation by studying societies that had high resilience to climatic perturbations (McAnany and Yoffee, 2009). In this context the Romans are particularly interesting. Owing to the length of their reign, it appears that the Romans developed mechanisms that made them highly resilient to the variable climate of the Mediterranean (Lionello, 2012). However, the Western Roman Empire did fall more or less coincident with a shift from the Roman Warm Period to the Dark Ages Cold Period (Bruno et al., 2013; Büntgen et al., 2011), whereas the Eastern Empire continued for almost 1000 years in the guise of the Byzantine Empire (Gibbon, 1776). Thus, within this complex civilisation lies a potential wealth of information about what makes a society both resilient and vulnerable to climate change. To understand the resilience of the Romans to climate variability and climate change we focused our analysis on Roman grain production and redistribution which has been identified as central to their success and persistence as a civilisation (Erdkamp, 2005; Horden and Purcell, 2000; Rickman, 1980). In order to understand how climate impacted the Roman civilisation, we developed a Virtual Water network of the Roman World and simulated the impact of climate on Roman grain production and redistribution (Fig. 6.1).

Our analysis in chapter 4 indicates that Roman use of trade and irrigation provided them with a stable food supply despite the variable climate of the Mediterranean region. In terms of irrigation, rivers provided a much more stable water supply compared with rainfed agriculture. In essence, river discharge integrated precipitation temporally and spatially over in the upstream catchment area. As a result, very large catchments such as the Nile and Po rivers provided highly stable

water supplies. Trade enabled the Romans to take advantage of spatiotemporal variations in yields by redistributing grain from regions where it is in surplus to regions with a deficit.

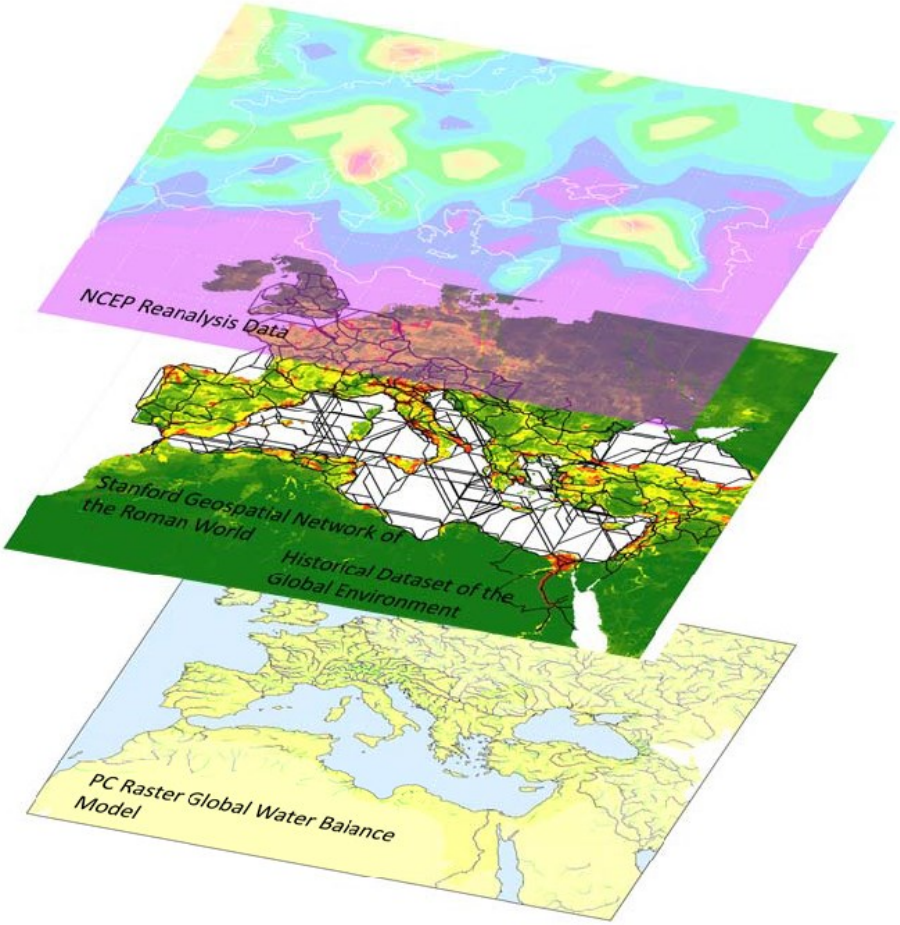

Figure 6.1 Virtual water network of the Roman World. Grain yields were calculated using the hydrological crop model PC Raster Global Water Balance (PCR GLOBWB) (Bierkens and van Beek, 2009; van Beek and Bierkens, 2009). PCR GLOBWB captures the heterogeneity in the hydrology of the Mediterranean region which has an important impact on the spatial heterogeneity of yields. In addition, PCR GLOBWB facilitates the calculation of crop irrigation demand based on the available surface water for irrigation. Roman agricultural land and population were assigned based on reconstructions from the History Database of the Global Environment (HYDE) (Klein Goldewijk et al., 2011). Grain yields were calculated based on NCEP daily climate forcing which allowed us to simulate the spatial and temporal heterogeneity of grain yields in response to climate. The redistribution of grain through trade was simulated using Orbis, the Stanford Geospatial Network of the Roman World as the network structure.

Therefore a stable supply of grain was ensured in well-connected regions of the trade network despite variability in climate (Erdkamp, 2005). However, trade also enabled populations to grow well beyond their local ecohydrological carrying capacities, thus promoting high levels of urbanisation in the Empire (Kessler and Temin, 2007). Population growth and urbanisation pushed the Empire closer to its carrying capacity as the most suitable and easily exploited land was increasingly used up to meet growing demand. In a network where trade costs covary with distance, increased competition for resources led to an increase in import distance and costs (Scheidel, 2001). Thus the stability of food supply at interannual timescales that trade and irrigation provided stimulated population growth and urbanisation and actually undermined Roman resilience to perturbations at longer timescales.

Chapter 4 was concerned with understanding the resilience of the system to interannual climate variability. However, Holocene climate anomalies were likely persistent over a number of centuries (Mayewski et al., 2004; Wanner et al., 2008). It is likely that the Roman food production and redistribution infrastructure developed to adapt to high frequency variability so the question is how adaptable it was to persistent changes at larger spatial scales? In chapter 5 we simulated the response of Roman water resource management climate conditions consistent with the Roman Warm Period (RWP) and Dark Ages Cold Period (DCP) Holocene climate anomalies. Our reconstruction of Mediterranean climate during these periods indicated a seesaw in climatic humidity between the Central Mediterranean on one side and the Iberian Peninsula and the South-eastern Mediterranean on the other. Temperature reconstructions indicate that climate was anomalously warm in the Mediterranean during the RWP and cold during the DCP (Davis et al., 2003; Desprat et al., 2003). We investigated the impact of these climate anomalies on grain growth and found that the warm temperatures during the RWP likely made conditions for the growth of grain optimal, whilst growing conditions deteriorated in the DCP. We found that the dry conditions in the Central Mediterranean likely only had a negative impact in low-lying coastal regions because temperature was the main limit to growth in higher elevation inland regions. However, the lower yields in coastal regions probably did not have a detrimental societal impact owing to the easy access coastal cities had to the grain trade network.

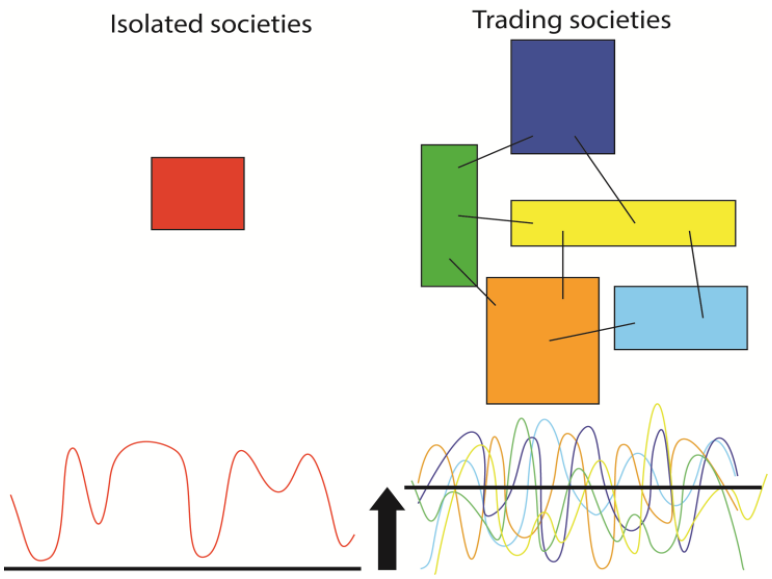

Figure 6.2 Conceptual figure illustrating the impact of trade on carrying capacity in a variable environment. Carrying capacities are variable over time owing to the impact of interannual climate variability on yields. In an isolated society populations must remain below the climate-forced carrying capacity to avoid famine. In societies with trade the carrying capacity becomes the average of the carrying capacity of the trading regions. Thus carrying capacity is increased without an increase in resource use in any of the trading societies. Carrying capacities are smoothed to illustrate the dampening effect of food storage.

Importantly, chapters 4 and 5 demonstrate that the impact of climate was extremely heterogeneous within the Empire. As mentioned, areas like the Po Valley and Nile Delta had stable yields compared with rainfed regions because irrigation offered them a certain amount of decoupling from the climate system. In the Eastern Empire grain yields exhibited less year to year variability compared with the West owing to higher average winter temperatures (Lionello, 2012) as well as the reduced influence of the winter storm tracks (Hurrell, 1995; Visbeck et al., 2001). Topographical variations also played an important role with grain yields limited by temperature at higher elevations whereas they were water limited at lower elevations and in more arid environments. It was the Romans ability to link these environmentally heterogeneous regions through trade that increased and stabilised their carrying capacity despite the variable climate of

the Mediterranean region (Fig. 6.2). In fact heterogeneity is proposed to provide resilience to perturbations in many natural systems (Lever et al., 2014; Thompson et al., 2009; Virah-Sawmy et al., 2009). The linked-heterogeneity of the Roman Empire undoubtedly contributed to their resilience to climate perturbations whereas other past societies in more homogenous environments collapsed (de Menocal, 2001; Diamond, 2005; Fraser, 2003; Virah-Sawmy et al., , 2009; Weiss et al., 1993).

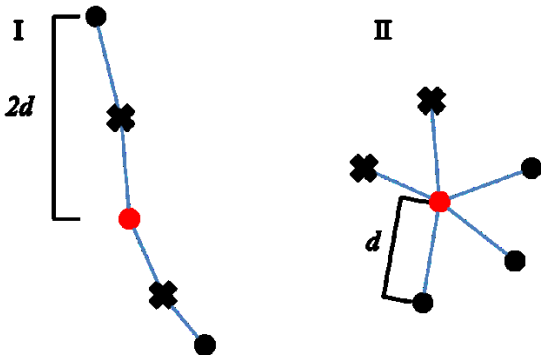

Figure 6.3 Relation between node degree and import distance. The 'x' symbolises regions where yield surpluses have been depleted. For the same demand increased node degree decreases import distance as the probability of neighbouring nodes being depleted is less.

Aside from environmental heterogeneity within the Empire, there was also heterogeneity in the Roman trade network itself. As with most real-world networks, the reconstructed Roman trade network exhibited a skewed distribution, with many nodes having few trade connections whilst a few had many (hub nodes) (Lewis, 2011; Suweis et al., 2011). Our analysis demonstrated that hub nodes had lower import costs on average compared with regions with a low number of trade connections irrespective of trade cost along trade links (Fig. 6.3). As with modern transport networks, coastal nodes had much lower import costs compared with inland nodes owing to the relative ease of moving bulk goods by ship (Braudel, 1995; Limão and Venables, 2001; Scheidel, 2013). For this reason, hub nodes in the Roman trade network were primarily located close to large water bodies (Scheidel, 2013; Sherbinin et al., 2007). Ultimately, our network analysis highlighted that trade works extremely well at ensuring stable food supplies under interannual climate variability. However, the short term resilience that trade provides is eroded in the long term because a stable food supply stimulates population growth and urbanisation and pushes a society towards a global carrying capacity.

6.5 Wider implications of research

6.5.1 Solar irradiance forcing

A vast body of research implicates greenhouse gas emissions as being by far the largest contributor to global warming trend since the beginning of the industrial era (Fig. 6.4) (IPCC, 2007; Mann et al., 1998). However, future trends in global warming will be superimposed on variations in solar irradiance. Our analysis demonstrates that although solar irradiance variations may only contribute a small percentage to global temperature (Solanki and Krivova, 2003), the mechanisms by which solar irradiance is magnified and communicated to the climate system may enable solar irradiance variations to tip oscillating elements of the climate system into one mode or another (Emile-Geay et al., 2007; Shindell et al., 2001).

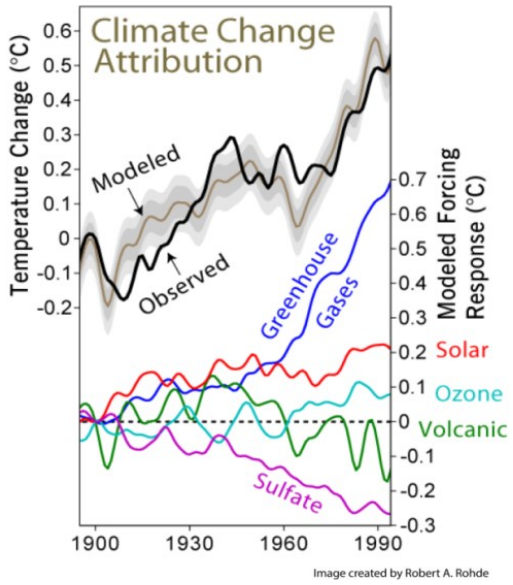

Figure 6.4 Modelled attribution of different forcings to global warming since the beginning of the 20th century. Greenhouse gas concentrations have a far bigger contribution to global warming compared with solar irradiance variations (IPCC, 2007). However, the impact of solar forcing is likely more relevant in the context of its ability to tip oscillating elements of the climate system into a certain phase rather than increasing the heat content of the atmosphere and oceans.

In a comprehensive review of literature relating to the impact of global warming on El Niño Southern Oscillation (ENSO), Collins et al. (2010) conclude that the weight of evidence indicates that global warming will increase the likelihood of El Niño events. El Niño is predicted to increase in frequency (Trenberth and Hoar, 1997) owing to a weakening of the trade winds, a reduction in upwelling and an associated reduction in the zonal SST gradient (Collins et al., 2010). Owing to increased energy in the climate system associated with global warming, the

intensity of ENSO is also predicted to increase (Timmermann et al., 1999). Our results indicate that solar forcing of the Tropical Pacific is strongest when the Tropical Pacific is in an oscillating mode because small increases in insolation at the equator during solar maxima can force a thermostat response (Emile-Geay et al., 2007; Mann et al., 2005). Therefore, solar irradiance forcing of the Tropical Pacific will likely be strengthened under global warming. If this is the case, the periodicity in the solar cycle may provide some predictability for ENSO and as a result climate change in regions teleconnected with the Tropical Pacific (Asmerom et al., 2013; Hoerling et al., 2001; Hurrell et al., 2004; Li et al., 2006).

6.5.2 The North Atlantic and climate change

Our analysis of climate change in the Mediterranean between 3000 and 1000 yr BP identifies two distinct modes of variability in climatic humidity (Dermody et al., 2012). The first is similar to the NAO in current climate and is associated with meridional shifts in the Jetstream linked to top-down (Martin-Puertas et al., 2012) and bottom-up (Trouet et al., 2009) solar forcing as well as changes in the SST of the North Atlantic (Peng et al., 2002; Rodwell et al., 1999). The second is similar to the EA/WR pattern in current climate and is typified by zonal shift in the locations of stationary Rossby waves related to heating of the atmosphere as it passes over the North Atlantic (Wang et al., 2010). Our finding is supported by similar findings for the MCA and LIA published later that same year (Roberts et al., 2012). Krichak et al. (2002) also isolated the NAO and EA/WR pattern as the two major modes of climate variability over Europe at decadal timescales in the period 1948 – 2002. These studies demonstrate the persistence and importance of these climatic modes at decadal and longer timescales throughout of the Late Holocene. Thus the relations we have identified contribute to providing some predictability for future climate. As mentioned the periodicity of solar irradiance variations allows us to use past solar irradiance timeseries to predict future solar irradiance changes. Since the North Atlantic Oscillation is more likely to move to a positive phase during future solar maxima (Boberg and Lundstedt, 2002) these predictions can help forecast the dominant future mode of the NAO. However, understanding how global warming trends will interact the dynamics of the North Atlantic is more uncertain owing to the complexity of factors influencing North Atlantic Ocean such as sea

ice cover (Kolstad et al., 2010), melting ice caps (Driesschaert et al., 2007) as well as internal dynamics of the overturning circulation (Dima and Lohmann, 2007). Therefore, although the persistence of the EA/WR pattern seems likely, the centre of action will be more difficult to predict owing to the latitudinal movement of stationary Rossby waves related to the SST of the North Atlantic. A better understanding of the dynamics of the overturning circulation in the Atlantic would improve climate predictions for the Mediterranean region.

6.5.3 Civilisation's resilience to climate change

It is clear that VW trade will play an important role in increasing civilizations' resilience to future climate change. Presently research on VW trade focuses on socioeconomic trade networks because socioeconomics dictate the quantity and direction of VW flows (Suweis et al., 2011). However, as we have discussed in chapter 4 predicting the future structure socioeconomic trade networks is difficult owing to the complex and temporally variable dynamics that contribute to trade network structure (Carr et al., 2012). For example, the wealth of certain regions change, wars begin and end, subsidies are created and broken down (Boersema et al., 2007). We have shown that trade costs have covaried with trade distance throughout history (Braudel, 1995; Limão and Venables, 2001). Given that distance among trade partners is a variable that remains fixed; a cost-distance based trade network structure is more predictable compared with socioeconomic trade network structure. Thus we propose that cost-distance based network structures can provide and additional avenue to understanding the future resilience of food production and redistribution under anthropogenic climate change. In this framework, climate model predictions based on multiple scenarios can be used as forcing for a global hydrological model to calculate future yield scenarios based on current land use and population. Virtual water redistribution is simulated based along a cost distance network defined using current infrastructure. Such an approach would enable researchers to diagnose vulnerability hotspots globally based on the environmental heterogeneity among potential import partners, location within the network, predicted climate variability etc. Once an understanding of the physical constraints is achieved, socioeconomic complexity can be added incrementally.

6.5.4 Networks and resilience

Our analysis has demonstrated that at short timescales trade networks increase resilience by enabling access to heterogeneous food supplies which provides a stability of supply. However, an increase in the stability of food supply increases carrying capacity without actually increasing resources (Fig. 6.2). Therefore population growth is stimulated whilst resource availability remains constant. Rather than reaching a local carrying capacity societies grow towards a global carrying capacity with reduced resource redundancy in case of perturbations (D'Odorico et al., 2010). It has also been demonstrated that once a perturbation occurs, the connectedness of the network can facilitate the rapid spread of that perturbation through the network (Holling, 2001; Lever et al., 2014). For instance, the Roman road network that facilitated trade and Roman military movement also facilitated the rapid movement of invading armies (Gibbon, 1776). These types of vulnerabilities should be explored for the future climate scenario. For example, will unsustainable depletion of the Central Plains Aquifer in the United States have a cascading effect in the global VW network (Torell et al., 1990; Wada et al., 2011)? It should also be explored how nodes within a network can become more self-reliant so that when perturbations occur within the network nodes are not completely reliant on the network for food supply (FAO, 2001; Karapinar and Tanaka, 2013). However, this will be a significant challenge given the current urbanizing trend globally (Chen, 2007).

6.6 Recommendations for future research

Continued research on the impact of solar irradiance forcing on the climate is important. It is clear that greenhouse gas emissions are the largest contribution to global warming with solar irradiance estimated to contribute a maximum of 30% warming (Scafetta and West, 2005). However, as we have shown, radiation from the sun interacts with the climate system in much more complex ways than simply warming the planet during solar maxima. Our analysis and other research indicate that amplification mechanisms within the climate system respond in predictable ways to solar irradiance variations. Global warming trends may modify how solar forcing is amplified within the climate system or increase the amplitude of climatic oscillations.

Nonetheless, a better understanding of the impact of solar forcing on climate will undoubtedly improve climate predictions.

Progress needs to be made on dating of paleo sediments, particularly marine sediments. If we want to understand the role of the ocean in the climate system from past data then an improvement in the dating of marine sediments is required. Marine reconstructions often have high dating uncertainties owing to variable sedimentation rates, reworking of sediments as well as uncertainties related with the reservoir age of water through time. In order to improve comparisons among marine records at short timescales relevant for much of the variability in solar irradiance it is necessary to address these areas of uncertainty in marine records.

A standardized and obligatory methodology should be set out for presenting paleoclimatic data. A global centralized database should be setup such as that hosted by the National Oceanic and Atmospheric Administration of the United States whereby age depth model data is provided to enable the reproduction of results. In essence every new piece of paleo data should contribute to filling a spatiotemporal gap in the paleoclimate map. Special journal issues could be used to incentivize scientists to submit pre-existing data to the project. This would enable scientists to make spatiotemporal comparisons among the wealth of pre-existing data transparently taking into account the resolution, chronological uncertainties etc.

Truly interdisciplinary, process-based approaches should be used to refine theories about the interaction between environmental and social systems. In the increasingly interdisciplinary discourse between the natural and social sciences studies are often weighted within one discipline leading to oversimplifications of the other (Cornell et al., 2010). For example, there are numerous paleoclimate studies that correlate climatic change with some societal event and qualitatively propose causality. Although interesting, this approach doesn't improve our understanding about why the two might be linked. Even where models are used they focus on either the natural or the human elements of the system in question. This negates an understanding of the feedbacks between these two interacting agents of change. With the ever increasing amounts of data on past environmental and societal changes as well as improvements

in our ability to model environmental and social systems new opportunities to refine theories are emerging (van der Leeuw et al., 2011). Where possible these quantitative, process-based methods should be exploited because they allow us to understand why the timing of past environmental and social changes might be correlated and refine our understanding of human and environmental systems.

Cost-distance based network analysis should be exploited to predict resilience to future climate change. The use of socioeconomic framework for understanding trade dynamics is essential as socioeconomic relations dictate trade. However, socioeconomic relations among countries are highly dynamic and extremely difficult to predict. Trade in bulk goods on the other hand exhibits a stable relation with distance over time (Braudel, 1995; Limão and Venables, 2001) and is therefore likely predictable in the future. A cost-distance based investigation of future virtual water trade based on current trade infrastructure will allow the identification of vulnerability hotspots around the globe to climate change. Therefore, vulnerable regions may be given incentives to improve their trade infrastructure or water resource management infrastructure to avoid the detrimental effects of climate change.

We need to extend past reconstructions in space as well as time. As we have demonstrated, much can be learned about past climate by relating timeseries across space. In doing so, we reveal the spatial pattern of change in addition to the timing and magnitude of change. We have also shown that capturing spatial heterogeneity in past landscapes is critical to understanding the impact of climate on past societies. However, much work is required to improve our knowledge past landscapes, particularly human-influenced landscapes. We require an interdisciplinary approach that strives to fill in the gaps between data points. A useful approach would be to correct modelled reconstructions such as those by Kaplan et al. (2009) and Klein Goldewijk et al. (2011) with archaeological and paleoecological data.

Mine the seam of information of human interactions with their environment contained within the Roman civilisation. We have only scratched the surface of the complexity of the

Roman interaction with their environment. For example, we only touched upon the issue of soil erosion and land degradation but it was an extremely serious issue during the Roman period and one they were acutely aware of as illustrated in this passage from Lucretius dating from 99 – 55 BC:

Our poor earth, worn out, exhausted, brings to birth no more great eons, titans, huge majestic beasts; only our own disgusting little days, midges and gnats… the same earth who nourishes them now once brought forth… vineyards and shining harvests, pastures, orchards and all this now our very utmost toil we hardly care for, we wear down our strength, whether in oxen or in men, we dull the edges of our ploughshares, and in return our fields turn mean and stingy, underfed. And so today the farmer shakes his head, more and more often sighing that his work, the labour of his hands, has come to naught. When he compares the present to the past, the past was better, infinitely so…. All things, little by little, waste away as times erosion crumbles them to doom.

Despite this pessimistic view, the Republic and then Empire went on to reach its zenith in the centuries after, illustrating that the impact of soil erosion on the Roman civilisation was not a simple one (Blaikie and Brookfield, 1987). As we have pointed out process-based models have the potential to illuminate a great deal about feedbacks between the Romans and their environment. In order to capture those feedbacks, socioeconomic processes should also be incorporated in such models. A modelling framework such as that presented in chapters 4 and 5, which couples models based on the physical environment with agent based modelling, is ideally suited to this purpose.

6.7 The fall of the Western Roman Empire

The question of what caused the decline and fall of the Western Roman Empire is one that has occupied scholars for centuries (Gibbon, 1776). Many and varied theories abound. For example, it is posited that the extent of the unstable Rhine and Danube borders in the West compared with the stable Eastern borders made the West particularly vulnerable to invasion (Elton and Elton, 2013), splits within Christianity are proposed to have drawn Imperial attention from other important matters of the Empire (Rives, 2007), failure to integrate Germanic tribes led to the establishment of highly independent territories within the Roman borders (Pitts, 1989) etc. Climate change has also been implicated as a contributing factor in the fall of the Western Roman Empire (Büntgen et al., 2011).

As we have shown in this thesis, the impact of climate change on a society is related to the magnitude of the change but also the resilience of the society to adapt to or absorb a climatic perturbation. The aforementioned factors as well as many others no doubt reduced the resilience of the Empire to perturbations. Indeed, the end of the Western Roman Empire was not so much a collapse as a crumble (Gibbon, 1776). In reality, the Empire never really recovered following the crisis of the third century (Lot, 1931). After this the centre of power moved East and the Empire was divided first into 4 parts and then into an Eastern and Western half. We proposed in chapter 4 that urbanisation, increased grain demand and increasing import distances and costs may have contributed to the crisis of the third century within the Empire. We also demonstrated that yields were likely more stable in the East compared with the West owing to warmer growing season temperature and a relatively widespread use of irrigation. Given that the trade network deteriorated following the third century crisis, stable yields likely became increasingly important owing to increased localisation of resources. Thus, from a food production perspective the Eastern Empire had likely more favourable conditions compared with the west. The change in climate from the Roman Warm Period to the Dark Ages Cold Period may have been the final kick the Western Empire required to initiate collapse (Scheffer, 2009). However, it is likely that a number of important socioeconomic factors had eroded its resilience to such perturbations in the preceding centuries (Blaikie and Brookfield, 1987; Gibbon, 1776; Vita-Finzi, 1969).

References

Allan, J. a., 1998. Virtual Water: A Strategic Resource Global Solutions to Regional Deficits. Ground Water 36, 545–546. doi:10.1111/j.1745-6584.1998.tb02825.x

Allen, R.C., 2008. The Nitrogen Hypothesis and the English Agricultural Revolution: A Biological Analysis. J. Econ. Hist. 68, 182–210. doi:10.1017/S0022050708000065

Allen, R.G., Pereira, L.S., Raes, D., Smith, M., 1998. Crop evapotranspiration-Guidelines for computing crop water requirements-FAO Irrigation and drainage paper 56. FAO Rome 300, 6541.

Alley, R.B., 2000. The Younger Dryas cold interval as viewed from central Greenland. Quat. Sci. Rev. 19, 213–226. doi:10.1016/S0277-3791(99)00062-1

Alpert, P., Mandel, M., 1986. Wind Variability. An Indicator for a Mesoclimatic Change in Israel. J. Appl. Meteorol. 25, 1568–1576. doi:10.1175/1520-0450(1986)025<1568:WVIFAM>2.0.CO;2

Anav, A., Ruti, P.M., Artale, V., Valentini, R., 2010. Modelling the effects of land-cover changes on surface climate in the Mediterranean region. Clim. Res. 41, 91–104. doi:10.3354/cr00841

Anderson, P.K., Cunningham, A.A., Patel, N.G., Morales, F.J., Epstein, P.R., Daszak, P., 2004. Emerging infectious diseases of plants: pathogen pollution, climate change and agrotechnology drivers. Trends Ecol. Evol. 19, 535–544.

Andrews, J.T., Domack, E.W., Cunningham, W.L., Leventer, A., Licht, K.J., Jull, A.J.T., DeMaster, D.J., Jennings, A.E., 1999. Problems and Possible Solutions Concerning Radiocarbon Dating of Surface Marine Sediments, Ross Sea, Antarctica. Quat. Res. 52, 206–216. doi:10.1006/qres.1999.2047

Arrow, K., Bolin, B., Costanza, R., Dasgupta, P., Folke, C., Holling, C.S., Jansson, B.-O., Levin, S., Mäler, K.-G., Perrings, C., Pimentel, D., 1995. Economic growth, carrying capacity, and the environment. Ecol. Econ. 15, 91–95. doi:10.1016/0921-8009(95)00059-3

Arz, H.W., Lamy, F., Pätzold, J., 2006. A pronounced dry event recorded around 4.2 ka in brine sediments from the northern Red Sea. Quat. Res. 66, 432–441. doi:10.1016/j.yqres.2006.05.006

Asmerom, Y., Polyak, V., Burns, S., Rassmussen, J., 2007. Solar Forcing of Holocene Climate: New Insights from a Speleothem Record, Southwestern United States. Geology 35, 1–4. doi:10.1130/G22865A.1

Asmerom, Y., Polyak, V.J., Rasmussen, J.B.T., Burns, S.J., Lachniet, M., 2013. Multidecadal to multicentury scale collapses of Northern Hemisphere monsoons over the past millennium. Proc. Natl. Acad. Sci. 110, 9651–9656. doi:10.1073/pnas.1214870110

Bakke, J., Lie, Ř., Dahl, S.O., Nesje, A., Bjune, A.E., 2008. Strength and spatial patterns of the Holocene wintertime westerlies in the NE Atlantic region. Glob. Planet. Change 60, 28–41.

Baldwin, M.P., Dunkerton, T.J., 1999. Propagation of the Arctic Oscillation from the stratosphere to the troposphere. J. Geophys. Res. 104, PP. 30,937–30,946. doi:199910.1029/1999JD900445

Barker, G., 1996. Farming the Desert: Synthesis. UNESCO Publishing Department of Antiquities.

Barnaby, W., 2009. Do nations go to war over water? Nature 458, 282–283. doi:10.1038/458282a

Barnston, A., Livezey, R., 1987. Classification, seasonality and persistence of low-frequency atmospheric circulation patterns. Mon. Weather Rev. 115, 1083–1126.

Beltrán Lloris, F., 2006. An Irrigation Decree from Roman Spain: The Lex Rivi Hiberiensis [WWW Document]. URL http://dialnet.unirioja.es/servlet/articulo?codigo=2721295 (accessed 11.22.10).

Berger, A., Loutre, M.F., 1991. Insolation values for the climate of the last 10 million years. Quat. Sci. Rev. 10, 297–317.

Berthelon, M., Freund, C., 2008. On the conservation of distance in international trade. J. Int. Econ. 75, 310–320. doi:10.1016/j.jinteco.2007.12.005

Bianchi, G.G., McCave, I.N., 1999. Holocene periodicity in North Atlantic climate and deep-ocean flow south of Iceland. Nature 397, 515–517. doi:10.1038/17362

Bierkens, M.F.P., van Beek, L.P.H., 2009. Seasonal Predictability of European Discharge: NAO and Hydrological Response Time. J. Hydrometeorol. 10, 953–968. doi:10.1175/2009JHM1034.1

Bjerknes, J., 1964. Atlantic Air-Sea Interaction. Adv. Geophys. 10, 1.

Blaauw, M., 2010. Methods and code for “classical” age-modelling of radiocarbon sequences. Quat. Geochronol. 5, 512–518. doi:10.1016/j.quageo.2010.01.002

Blaauw, M., Wohlfarth, B., Christen, J.A., Ampel, L., Veres, D., Hughen, K.A., Preusser, F., Svensson, A., 2010. Were last glacial climate events simultaneous between Greenland and France? A quantitative comparison using non-tuned chronologies. J. Quat. Sci. 25, 387–394. doi:10.1002/jqs.1330

Blaauw, M., Christen, J.A., Mauquoy, D., Plicht, J. van der, Bennett, K.D., 2007. Testing the timing of radiocarbon-dated events between proxy archives. The Holocene 17, 283–288. doi:10.1177/0959683607075857

Blaikie, P.M., Brookfield, H.C., 1987. Land degradation and society. Taylor & Francis.

Blázquez, J.M., 1992. The Latest Work on the Export of Baetican Olive Oil to Rome and the Army. Greece Rome Second Ser. 39, 173–188. doi:10.1017/S0017383500024153

Boberg, F., Lundstedt, H., 2002. Solar Wind Variations Related to Fluctuations of the North Atlantic Oscillation. Geophys. Res. Lett. 29, 13–1. doi:10.1029/2002GL014903

Boersema, J., Blowers, A., Martin, A., 2007. Biofuels and perverse subsidies: fuelling the wrong solutions? Environ. Sci. 4, 195–198. doi:10.1080/15693430701783457

Bogardi, J.J., Fekete, B.M., Vörösmarty, C.J., 2013. Planetary boundaries revisited: a view through the "water lens". Curr. Opin. Environ. Sustain., Aquatic and marine systems 5, 581–589. doi:10.1016/j.cosust.2013.10.006

Bonabeau, E., 2002. Agent-based modeling: Methods and techniques for simulating human systems. Proc. Natl. Acad. Sci. 99, 7280–7287. doi:10.1073/pnas.082080899

Bond, G., Kromer, B., Beer, J., Muscheler, R., Evans, M.N., Showers, W., Hoffmann, S., Lotti-Bond, R., Hajdas, I., Bonani, G., 2001. Persistent Solar Influence on North Atlantic Climate During the Holocene. Science 294, 2130–2136. doi:10.1126/science.1065680

Bond, G., Showers, W., Cheseby, M., Lotti, R., Almasi, P., deMenocal, P., Priore, P., Cullen, H., Hajdas, I., Bonani, G., 1997. A Pervasive Millennial-Scale Cycle in North Atlantic Holocene and Glacial Climates. Science 278, 1257–1266. doi:10.1126/science.278.5341.1257

Bookman, R., Enzel, Y., Agnon, A., Stein, M., 2004. Late Holocene lake levels of the Dead Sea. Geol. Soc. Am. Bull. 116, 555 –571. doi:10.1130/B25286.1

Booth, R.K., Jackson, S.T., Forman, S.L., Kutzbach, J.E., Bettis, E.A., Kreigs, J., Wright, D.K., 2005. A Severe Centennial-Scale Drought in Midcontinental North America 4200 Years Ago and Apparent Global Linkages. The Holocene 15, 321–328. doi:10.1191/0959683605hl825ft

Boserup, E., 1981. Population and technological change: A study of long-term trends. The University of Chicago Press

Bowman, A., Wilson, A., 2011. Settlement, Urbanization, and Population. Oxford University Press.

Box, G.E., Jenkins, G.M., 1976. Time Series Analysis: Forecasting and Control. Holden-Day Publishing.

Braconnot, P., Otto-Bliesner, B., Harrison, S., Joussaume, S., Peterchmitt, J.-Y., Abe-Ouchi, A., Crucifix, M., Driesschaert, E., Fichefet, T., Hewitt, C.D., Kageyama, M., Kitoh, A., Loutre, M.-F., Marti, O., Merkel, U., Ramstein, G., Valdes, P., Weber, L., Yu, Y., Zhao, Y., 2007. Results of PMIP2 coupled simulations of the Mid-Holocene and Last Glacial Maximum – Part 2: feedbacks with emphasis on the location of the ITCZ and mid- and high latitudes heat budget. Clim Past 3, 279–296.

Bransbourg, G., 2012. Rome and the Economic Integration of Empire [WWW Document]. URL http://www.academia.edu/1516398/Rome_and_the_Economic_Integration_of_Empire (accessed 2.28.14).

Braudel, F., 1995. A History of Civilizations. Penguin Books.

Brovkin, V., Claussen, M., Petoukhov, V., Ganopolski, A., 1998. On the stability of the atmosphere-vegetation system in the Sahara/Sahel region. J. Geophys. Res. 103, PP. 31,613–31,624. doi:199810.1029/1998JD200006

Brown, L.R., Kane, H., 1995. Full House: Reassessing the Earth's Population Carrying Capacity. Earthscan.

Bruno, L., Amorosi, A., Curina, R., Severi, P., Bitelli, R., 2013. Human–landscape interactions in the Bologna area (Northern Italy) during the mid–late Holocene, with focus on the Roman period. The Holocene 0959683613499054. doi:10.1177/0959683613499054

Büntgen, U., Tegel, W., Nicolussi, K., McCormick, M., Frank, D., Trouet, V., Kaplan, J.O., Herzig, F., Heussner, K.-U., Wanner, H., Luterbacher, J., Esper, J., 2011. 2500 Years of European Climate Variability and Human Susceptibility. Science. doi:10.1126/science.1197175

Butzer, K.W., Mateu, J.F., Butzer, E.K., Kraus, P., 1985. Irrigation agrosystems in eastern Spain: Roman or Islamic origins? Ann. Assoc. Am. Geogr. 75, 479–509.

Carr, J.A., D'Odorico, P., Laio, F., Ridolfi, L., 2012. On the temporal variability of the virtual water network. Geophys. Res. Lett. 39, n/a–n/a. doi:10.1029/2012GL051247

Casana, J., 2008. Mediterranean valleys revisited: Linking soil erosion, land use and climate variability in the Northern Levant. Geomorphology 101, 429–442. doi:10.1016/j.geomorph.2007.04.031

Chandler, T., 1987. Four Thousand Years of Urban Growth: An Historical Census. St. David's University Press.

Charney, J., Stone, P.H., Quirk, W.J., 1975. Drought in the Sahara: A Biogeophysical Feedback Mechanism. Science 187, 434–435. doi:10.1126/science.187.4175.434

Chen, J., 2007. Rapid urbanization in China: A real challenge to soil protection and food security. CATENA, Influences of rapid urbanization and industrialization on soil resource and its quality in China 69, 1–15. doi:10.1016/j.catena.2006.04.019

Chen, L., Zonneveld, K.A.F., Versteegh, G.J.M., 2011. Short term climate variability during "Roman Classical Period" in the eastern Mediterranean. Quat. Sci. Rev. 30, 3880–3891. doi:10.1016/j.quascirev.2011.09.024

Clement, A.C., Seager, R., Cane, M.A., 2000. Suppression of El Niño during the Mid-Holocene by changes in the Earth's orbit. Paleoceanography 15, 731–737. doi:10.1029/1999PA000466

Clement, A.C., Seager, R., Cane, M.A., 1999. Orbital controls on the El Niño/Southern Oscillation and the tropical climate. Paleoceanography 14, 441–456. doi:10.1029/1999PA900013

Clement, A.C., Seager, R., Cane, M.A., Zebiak, S.E., 1996. An ocean dynamical thermostat. J. Clim. 9, 2190–2196.

Cohen, J., Jones, J., 2011. Tropospheric precursors and stratospheric warmings. J. Clim. 24, 6562–6572.

Collins, M., An, S.-I., Cai, W., Ganachaud, A., Guilyardi, E., Jin, F.-F., Jochum, M., Lengaigne, M., Power, S., Timmermann, A., Vecchi, G., Wittenberg, A., 2010. The impact of global warming on the tropical Pacific Ocean and El Niño. Nat. Geosci. 3, 391–397. doi:10.1038/ngeo868

Columella, 70AD. LacusCurtius • Columella • de Re Rustica and de Arboribus [WWW Document]. URL http://penelope.uchicago.edu/Thayer/E/Roman/Texts/Columella/home.html (accessed 10.20.11).

Conroy, J.L., Overpeck, J.T., Cole, J.E., Shanahan, T.M., Steinitz-Kannan, M., 2008. Holocene changes in eastern tropical Pacific climate inferred from a Galápagos lake sediment record. Quat. Sci. Rev. 27, 1166–1180. doi:10.1016/j.quascirev.2008.02.015

Cook, E.R., D'Arrigo, R.D., Mann, M.E., 2002. A well-verified, multiproxy reconstruction of the winter North Atlantic Oscillation Index since ad 1400*. J. Clim. 15, 1754–1764.

Cornell, S., Costanza, R., Sörlin, S., van der Leeuw, S., 2010. Developing a systematic "science of the past" to create our future. Glob. Environ. Change 20, 426–427. doi:10.1016/j.gloenvcha.2010.01.005

Crucifix, M., Loutre, M.-F., Tulkens, P., Fichefet, T., Berger, A., 2002. Climate evolution during the Holocene: a study with an Earth system model of intermediate complexity. Clim. Dyn. 19, 43–60.

Cullen, H.M., deMenocal, P.B., 2000. North Atlantic influence on Tigris-Euphrates streamflow. Int. J. Climatol. 20, 853–863. doi:10.1002/1097-0088(20000630)20:8<853::AID-JOC497>3.0.CO;2-M

Cullen, H.M., deMenocal, P.B., Hemming, S., Hemming, G., Brown, F.H., Guilderson, T., Sirocko, F., 2000. Climate change and the collapse of the Akkadian empire: Evidence from the deep sea. Geology 28, 379–382. doi:10.1130/0091-7613(2000)28<379:CCATCO>2.0.CO;2

Curtis, F., 2009. Peak globalization: Climate change, oil depletion and global trade. Ecol. Econ. 69, 427–434. doi:10.1016/j.ecolecon.2009.08.020

Curtis, J.H., Brenner, M., Hodell, D.A., Balser, R.A., Islebe, G.A., Hooghiemstra, H., 1998. A multi-proxy study of Holocene environmental change in the Maya lowlands of Peten, Guatemala. J. Paleolimnol. 19, 139–159.

Dalin, C., Konar, M., Hanasaki, N., Rinaldo, A., and Rodriguez-Iturbe, I.: Evolution of the global virtual water trade network, 2012a P. Natl. Acad. Sci. USA, 109, 201203176, 5989–5994,5 doi:10.1073/pnas.1203176109.

Dalin, C., Suweis, S., Konar, M., Hanasaki, N., and Rodriguez-Iturbe, I.: Modeling past and future structure of the global virtual water trade network, 2012b Geophys. Res. Lett., 39, L24402, doi:10.1029/2012GL053871.

D'Odorico, P., Laio, F., Ridolfi, L., 2010. Does globalization of water reduce societal resilience to drought? Geophys. Res. Lett. 37, L13403. doi:10.1029/2010GL043167

Davis, B.A.S., Brewer, S., Stevenson, A.C., Guiot, J., 2003. The temperature of Europe during the Holocene reconstructed from pollen data. Quat. Sci. Rev. 22, 1701–1716. doi:10.1016/S0277-3791(03)00173-2

de Boer, H.J., Eppinga, M.B., Wassen, M.J., Dekker, S.C., 2012. A critical transition in leaf evolution facilitated the Cretaceous angiosperm revolution. Nat. Commun. 3, 1221. doi:10.1038/ncomms2217

de Fraiture, C., Cai, X., Amarasinghe, I., Rosegrant, M., Molden, D., 2004. Does international cereal trade save water? the impact of virtual water trade on global water use. International Water Management Institute.

de Ridder, K., Gallée, H., 1998. Land Surface–Induced Regional Climate Change in Southern Israel. J. Appl. Meteorol. 37, 1470–1485. doi:10.1175/1520-0450(1998)037<1470:LSIRCC>2.0.CO;2

Deidda, R., Marrocu, M., Caroletti, G., Pusceddu, G., Langousis, A., Lucarini, V., Puliga, M., Speranza, A., 2013. Regional climate models' performance in representing precipitation and temperature over selected Mediterranean areas. Hydrol Earth Syst Sci 17, 5041–5059. doi:10.5194/hess-17-5041-2013

Dekker, S.C., de Boer, H.J., Brovkin, V., Fraedrich, K., Wassen, M.J., Rietkerk, M., 2010. Biogeophysical feedbacks trigger shifts in the modelled vegetation-atmosphere system at multiple scales. Biogeosciences 7, 1237–1245.

de Menocal, P.B., 2001. Cultural Responses to Climate Change During the Late Holocene. Science 292, 667 –673. doi:10.1126/science.1059287

de Menocal, P., Ortiz, J., Guilderson, T., Sarnthein, M., 2000. Coherent High- and Low-Latitude Climate Variability During the Holocene Warm Period. Science 288, 2198–2202. doi:10.1126/science.288.5474.2198

Dermody, B.J., van Beek, R.P.H., Meeks, E., Klein Goldewijk, K., Scheidel, W., van der Velde, Y., Bierkens, M.F.P., Wassen, M.J., Dekker, S.C., 2014. A virtual water network of the Roman world. Hydrol Earth Syst Sci Discuss 11, 6561–6597. doi:10.5194/hessd-11-6561-2014

Dermody, B.J., de Boer, H.J., Bierkens, M.F.P., Weber, S.L., Wassen, M.J., Dekker, S.C., 2012. A seesaw in Mediterranean precipitation during the Roman Period linked to millennial-scale changes in the North Atlantic. Clim Past 8, 637–651. doi:10.5194/cp-8-637-2012

Desprat, S., Sánchez Goñi, M. F., Loutre, M. F., 2003. Revealing climatic variability of the last three millennia in northwestern Iberia using pollen influx data. Earth Planet. Sci. Lett. 213, 63–78. doi:10.1016/S0012-821X(03)00292-9

Diamond, J., 2005. Collapse: How Societies Choose to Fail Or Succeed. Penguin Group USA, New York, USA.

Dickson, R.R., Meincke, J., Malmberg, S.A., Lee, A.J., 1988. The great salinity anomaly in the northern North Atlantic 1968-1982. Prog. Oceanogr. 20, 103–151.

Dima, M., Lohmann, G., 2007. A Hemispheric Mechanism for the Atlantic Multidecadal Oscillation. J. Clim. 20, 2706–2719. doi:10.1175/JCLI4174.1

Dixon, J.E., Cann, J.R., Renfrew, C., 1968. Obsidian and the origins of trade. Sci. Am. 218, 38–46.

Dominguez-villar, D., Wang, X., Cheng, H., Martinchivelet, J., Edwards, R., 2008. A high-resolution late Holocene speleothem record from Kaite Cave, northern Spain: δ18O variability and possible causes. Quat. Int. 187, 40–51. doi:10.1016/j.quaint.2007.06.010

Donders, T.H., Wagner-Cremer, F., Visscher, H., 2008. Integration of proxy data and model scenarios for the mid-Holocene onset of modern ENSO variability. Quat. Sci. Rev. 27, 571–579. doi:10.1016/j.quascirev.2007.11.010

Donnelly Jr, J.S., 2012. The great Irish potato famine. The History Press.

Doorenbos, J., A.H. Kassam, 1979. Yield response to water (No. 33), FAO Irrigation and Drainage. Food and Agriculture Organization of the United Nations, Rome.

Driesschaert, E., Fichefet, T., Goosse, H., Huybrechts, P., Janssens, I., Mouchet, A., Munhoven, G., Brovkin, V., Weber, S.L., 2007. Modeling the influence of Greenland ice sheet melting on the Atlantic meridional overturning circulation during the next millennia. Geophys. Res. Lett. 34, L10707. doi:10.1029/2007GL029516

Dümenil Gates, L., Ließ, S., 2001. Impacts of deforestation and afforestation in the Mediterranean region as simulated by the MPI atmospheric GCM. Glob. Planet. Change 30, 309–328. doi:10.1016/S0921-8181(00)00091-6

Dünkeloh, A., Jacobeit, J., 2003. Circulation dynamics of Mediterranean precipitation variability 1948-98. Int. J. Climatol. 23, 1843–1866. doi:10.1002/joc.973

Dykoski, C.A., Edwards, R.L., Cheng, H., Yuan, D., Cai, Y., Zhang, M., Lin, Y., Qing, J., An, Z., Revenaugh, J., 2005. A high-resolution, absolute-dated Holocene and deglacial Asian monsoon record from Dongge Cave, China. Earth Planet. Sci. Lett. 233, 71–86.

Eastwood, W.J., Leng, M.J., Roberts, N., Davis, B., 2007. Holocene climate change in the eastern Mediterranean region: a comparison of stable isotope and pollen data from Lake Gölhisar, southwest Turkey. J. Quat. Sci. 22, 327–341. doi:10.1002/jqs.1062

Ehrlich, P.R., Ehrlich, A.H., 1990. The population explosion. Simon and Schuster New York.

Elton, A.P. of H.H., Elton, H., 2013. Frontiers of the Roman Empire. Routledge.

Emile-Geay, J., Cane, M., Seager, R., Kaplan, A., Almasi, P., others, 2007. El Niño as a mediator of the solar influence on climate. Paleoceanography 22, A3210.

Enzel, Y., Bookman (Ken Tor), R., Sharon, D., Gvirtzman, H., Dayan, U., Ziv, B., Stein, M., 2003. Late Holocene climates of the Near East deduced from Dead Sea level variations and modern regional winter rainfall. Quat. Res. 60, 263–273. doi:10.1016/j.yqres.2003.07.011

Erdkamp, P., 2005. The grain market in the Roman Empire: a social, political and economic study. Cambridge University Press.

Fader, M., Rost, S., Müller, C., Bondeau, A., Gerten, D., 2010. Virtual water content of temperate cereals and maize: Present and potential future patterns. J. Hydrol., Green-Blue Water Initiative (GBI) 384, 218–231. doi:10.1016/j.jhydrol.2009.12.011

Fairbanks, R.G., 1989. A 17, 000-year glacio-eustatic sea level record: influence of glacial melting rates on the Younger Dryas event and deep-ocean circulation. Nature 342, 637–642.

Fleitmann, D., Burns, S.J., Mudelsee, M., Neff, U., Kramers, J., Mangini, A., Matter, A., 2003. Holocene Forcing of the Indian Monsoon Recorded in a Stalagmite from Southern Oman. Science 300, 1737 –1739. doi:10.1126/science.1083130

Food and Agriculture Organization of the United Nations, 2009. Irrigation in the Middle East region in figures (Survey No. 34), FAO Water Reports. Food and Agriculture Organisation of the United Nations, Rome.

Food and Agriculture Organization of the United Nations, 2001. Analysis of the medium-term effects of Hurricane Mitch on food security in Central America. Food and Agriculture Organization of the United Nations, Rome.

Foss, C., 1997. Syria in Transition, A. D. 550-750: An Archaeological Approach. Dumbart. Oaks Pap. 51, 189–269.

Fox, H.S.A., 1986. The Alleged Transformation from Two-field to Three-field Systems in Medieval England1. Econ. Hist. Rev. 39, 526–548. doi:10.1111/j.1468-0289.1986.tb01255.x

Fraedrich, K., Jansen, H., Kirk, E., Luksch, U., Lunkeit, F., 2005a. The Planet Simulator: Towards a user friendly model. Meteorol. Z. 14, 299–304. doi:10.1127/0941-2948/2005/0043

Fraedrich, K., Jansen, H., Kirk, E., Lunkeit, F., 2005b. The Planet Simulator: Green planet and desert world. Meteorol. Z. 14, 305–314. doi:10.1127/0941-2948/2005/0044

Fraser, E.D., 2003. Social vulnerability and ecological fragility: building bridges between social and natural sciences using the Irish Potato Famine as a case study. Conserv. Ecol. 7, 9.

Frier, B., 1982. Roman Life Expectancy: Ulpian's Evidence. Harv. Stud. Class. Philol. 86, 213–251. doi:10.2307/311195

Frogley, M.R., Griffiths, H.I., Heaton, T.H.E., 2001. Historical Biogeography and Late Quaternary Environmental Change of Lake Pamvotis, Ioannina (North-Western Greece): Evidence from Ostracods. J. Biogeogr. 28, 745–756.

Gaillard, M.-J., Sugita, S., Mazier, F., Kaplan, J.O., Trondman, A.-K., Broström, A., Hickler, T., Kjellström, E., Kuneš, P., Lemmen, C., Olofsson, J., Smith, B., Strandberg, G., 2010. Holocene land-cover reconstructions for studies on land cover-climate feedbacks. Clim. Past Discuss. 6, 307–346. doi:10.5194/cpd-6-307-2010

Garnsey, P., 1988. Famine and food supply in the Graeco-Roman world: responses to risk and crisis. Cambridge University Press.

Garnsey, P., Saller, R., 1987. The Roman Empire: Economy, Society and Culture. Berkeley and Los Angeles.

Geels, F.W., 2002. Technological transitions as evolutionary reconfiguration processes: a multi-level perspective and a case-study. Res. Policy, Nelson + Winter + 20 31, 1257–1274. doi:10.1016/S0048-7333(02)00062-8

Gibbon, E., 1776. The History of the Decline and Fall of the Roman Empire. W. Strahan and T. Cadell.

Gill, R.B., 2001. The Great Maya Droughts: Water, Life, and Death. University of New Mexico Press.

Godfray, H.C.J., Beddington, J.R., Crute, I.R., Haddad, L., Lawrence, D., Muir, J.F., Pretty, J., Robinson, S., Thomas, S.M., Toulmin, C., 2010. Food Security: The Challenge of Feeding 9 Billion People. Science 327, 812–818. doi:10.1126/science.1185383

Göktürk, O.M., Fleitmann, D., Badertscher, S., Cheng, H., Edwards, R.L., Leuenberger, M., Fankhauser, A., Tüysüz, O., Kramers, J., 2011. Climate on the southern Black Sea coast during the Holocene: implications from the Sofular Cave record. Quat. Sci. Rev. 30, 2433–2445. doi:10.1016/j.quascirev.2011.05.007

Goodchild, H., 2007. Modelling Roman agricultural production in the Middle Tiber Valley, Central Italy. University of Birmingham Doctoral Thesis.

Goosse, H., Renssen, H., 2007. Regional Response of the Climate System to Solar Forcing: The Role of the Ocean, in: Calisesi, Y., Bonnet, R.-M., Gray, L., Langen, J., Lockwood, M. (Eds.), Solar Variability and Planetary Climates, Space Sciences Series of ISSI. Springer New York, pp. 227–235.

Goosse, H., Renssen, H., Timmermann, A., Bradley, R.S., Mann, M.E., 2006. Using paleoclimate proxy-data to select optimal realisations in an ensemble of simulations of the climate of the past millennium. Clim. Dyn. 27, 165–184. doi:10.1007/s00382-006-0128-6

Goosse, H., Renssen, H., Timmermann, A., Bradley, R.S., 2005. Internal and forced climate variability during the last millennium: a model-data comparison using ensemble simulations. Quat. Sci. Rev. 24, 1345–1360. doi:10.1016/j.quascirev.2004.12.009

Gray, L.J., Beer, J., Geller, M., Haigh, J.D., Lockwood, M., Matthes, K., Cubasch, U., Fleitmann, D., Harrison, G., Hood, L., Luterbacher, J., Meehl, G.A., Shindell, D., Geel, B. van, White, W., 2010. Solar Influences on Climate. Rev. Geophys. 48, RG4001. doi:10.1029/2009RG000282

Grinsted, A., Moore, J.C., Jevrejeva, S., 2004. Application of the cross wavelet transform and wavelet coherence to geophysical time series. Nonlin Process. Geophys 11, 561–566. doi:10.5194/npg-11-561-2004

Hagemann, S., 1999. Derivation of Global GCM Boundary Conditions from 1 Km Land Use Satellite Data. Max-Planck-Institut für Meteorologie.

Haigh, J.D., 1996. The Impact of Solar Variability on Climate. Science 272, 981–984. doi:10.1126/science.272.5264.981

Halley, E., 1705. A Synopsis of the Astronomy of Comets. John Senex London.

Hanasaki, N., Inuzuka, T., Kanae, S., Oki, T., 2010. An estimation of global virtual water flow and sources of water withdrawal for major crops and livestock products using a global hydrological model. J. Hydrol. 384, 232–244. doi:10.1016/j.jhydrol.2009.09.028

Hannachi, A., 2004. A primer for EOF analysis of climate data. University of Reading Press.

Haug, G.H., Hughen, K.A., Sigman, D.M., Peterson, L.C., Röhl, U., 2001. Southward Migration of the Intertropical Convergence Zone Through the Holocene. Science 293, 1304–1308. doi:10.1126/science.1059725

Heck, P., Lüthi, D., Wernli, H., Schär, C., 2001. Climate impacts of European-scale anthropogenic vegetation changes: A sensitivity study using a regional climate model. J. Geophys. Res. 106, PP. 7817–7835. doi:200110.1029/2000JD900673

Helbaek, H., 1960. Ecological Effects of Irrigation in Ancient Mesopotamia. Iraq 22, 186–196. doi:10.2307/4199684

Hesselbjerg Christensen, J., Kjellström, E., Giorgi, F., Lenderink, G., Rummukainen, M., 2010. Weight assignment in regional climate models. Clim. Res. 44, 179–194.

Hodell, D.A., Brenner, M., Curtis, J.H., Guilderson, T., 2001. Solar Forcing of Drought Frequency in the Maya Lowlands. Science 292, 1367–1370. doi:10.1126/science.1057759

Hodell, D.A., Curtis, J.H., Brenner, M., 1995. Possible role of climate in the collapse of Classic Maya civilization. Publ. Online 01 June 1995 Doi101038375391a0 375, 391–394. doi:10.1038/375391a0

Hoekstra, A.Y., Chapagain, A.K., 2011. Globalization of water: Sharing the planet's freshwater resources. John Wiley & Sons.

Hoerling, M.P., Hurrell, J.W., Xu, T., 2001. Tropical Origins for Recent North Atlantic Climate Change. Science 292, 90–92. doi:10.1126/science.1058582

Holling, C.S., 2001. Understanding the Complexity of Economic, Ecological, and Social Systems. Ecosystems 4, 390–405. doi:10.1007/s10021-001-0101-5

Holling, C.S., 1986. The Resilience of Terrestrial Ecosystems: Local Surprise and Global Change, in: Sustainable Development of the Biosphere. Cambridge University Press.

Holzhauser, H., Magny, M., Zumbuühl, H.J., 2005. Glacier and lake-level variations in west-central Europe over the last 3500 years. The Holocene 15, 789 –801. doi:10.1191/0959683605hl853ra

Horden, P., Purcell, N., 2000. The corrupting sea: a study of Mediterranean history. Wiley-Blackwell.

Houston, G., 1988. Ports in Perspective: Some Comparative Materials on Roman Merchant Ships and Ports. Am. J. Archaeol. 92, 553–564.

Huang, C.C., Pang, J., Zha, X., Su, H., Jia, Y., 2011. Extraordinary floods related to the climatic event at 4200 a BP on the Qishuihe River, middle reaches of the Yellow River, China. Quat. Sci. Rev. 30, 460–468. doi:10.1016/j.quascirev.2010.12.007

Hummels, D., 2007. Transportation Costs and International Trade in the Second Era of Globalization. J. Econ. Perspect. 21, 131–154. doi:10.1257/jep.21.3.131

Huntington, E., 1911. Palestine and its transformation. Houghton Mifflin company.

Hurrell, J.W., Hoerling, M.P., Phillips, A.S., Xu, T., 2004. Twentieth century North Atlantic climate change. Part I: assessing determinism. Clim. Dyn. 23, 371–389. doi:10.1007/s00382-004-0432-y

Hurrell, J.W., 1995. Decadal Trends in the North Atlantic Oscillation: Regional Temperatures and Precipitation. Science 269, 676–679. doi:10.1126/science.269.5224.676

Immerzeel, W.W., Beek, L.P.H. van, Bierkens, M.F.P., 2010. Climate Change Will Affect the Asian Water Towers. Science 328, 1382–1385. doi:10.1126/science.1183188

Intergovernmental Panel on Climate Change, 2007. IPCC Fourth Assessment Report. Phys. Sci. Basis.

Issar, A.S., Yakir, D., 1997. Isotopes from Wood Buried in the Roman Siege Ramp of Masada: The Roman Period's Colder Climate. Biblic. Archaeol. 60, 101. doi:10.2307/3210599

James, S.R., Dennell, R.W., Gilbert, A.S., Lewis, H.T., Gowlett, J.A.J., Lynch, T.F., McGrew, W.C., Peters, C.R., Pope, G.G., Stahl, A.B., James, S.R., 1989. Hominid Use of Fire in the Lower and Middle Pleistocene: A Review of the Evidence [and Comments and Replies]. Curr. Anthropol. 30, 1–26.

Jones, M.D., Roberts, C.N., Leng, M.J., Türkeş, M., 2006. A high-resolution late Holocene lake isotope record from Turkey and links to North Atlantic and monsoon climate. Geology 34, 361. doi:10.1130/G22407.1

Kaplan, J., Krumhardt, K., Zimmermann, N., 2009. The prehistoric and preindustrial deforestation of Europe. Quat. Sci. Rev.

Karapinar, B., Tanaka, T., 2013. How to Improve World Food Supply Stability Under Future Uncertainty: Potential Role of WTO Regulation on Export Restrictions in Rice (135th Seminar, August 28-30, 2013, Belgrade, Serbia No. 160387). European Association of Agricultural Economists.

Karcher, M., Gerdes, R., Kauker, F., Köberle, C., Yashayaev, I., 2005. Arctic Ocean change heralds North Atlantic freshening. Geophys. Res. Lett. 32, 1–5.

Keating, B.., Carberry, P.., Hammer, G.., Probert, M.., Robertson, M.., Holzworth, D., Huth, N.., Hargreaves, J.N.., Meinke, H., Hochman, Z., McLean, G., Verburg, K., Snow, V., Dimes, J.., Silburn, M., Wang, E., Brown, S., Bristow, K.., Asseng, S., Chapman, S., McCown, R.., Freebairn, D.., Smith, C.., 2003. An overview of APSIM, a model designed for farming systems simulation. Eur. J. Agron. 18, 267–288. doi:10.1016/S1161-0301(02)00108-9

Keeling, C.D., 1960. The Concentration and Isotopic Abundances of Carbon Dioxide in the Atmosphere. Tellus 12, 200–203. doi:10.1111/j.2153-3490.1960.tb01300.x

Kennett, D.J., Kennett, J.P., 2006. Early State Formation in Southern Mesopotamia: Sea Levels, Shorelines, and Climate Change. J. Isl. Coast. Archaeol. 1, 67–99. doi:10.1080/15564890600586283

Kessler, D., Temin, P., 2007. The organization of the grain trade in the early Roman Empire. Econ. Hist. Rev. 60, 313–332. doi:10.1111/j.1468-0289.2006.00360.x

Khider, D., Jackson, C. s., Stott, L. d., 2014. Assessing millennial-scale variability during the Holocene: A perspective from the western tropical Pacific. Paleoceanography 29, 2013PA002534. doi:10.1002/2013PA002534

Klein Goldewijk,.K., Verburg, P.H., 2013. Uncertainties in global-scale reconstructions of historical land use: an illustration using the HYDE data set. Landsc. Ecol. 28, 861–877. doi:10.1007/s10980-013-9877-x

Klein Goldewijk, K., Beusen, A., van Drecht, G., de Vos, M., 2011. The HYDE 3.1 spatially explicit database of human-induced global land-use change over the past 12,000 years. Glob. Ecol. Biogeogr. 20, 73–86. doi:10.1111/j.1466-8238.2010.00587.x

Knudsen, M.F., Seidenkrantz, M.-S., Jacobsen, B.H., Kuijpers, A., 2011. Tracking the Atlantic Multidecadal Oscillation through the last 8,000 years. Nat. Commun. 2, 178. doi:10.1038/ncomms1186

Kolstad, E.W., Breiteig, T., Scaife, A.A., 2010. The association between stratospheric weak polar vortex events and cold air outbreaks in the Northern Hemisphere. Q. J. R. Meteorol. Soc. 136, 886–893. doi:10.1002/qj.620

Konar, M., Hussein, Z., Hanasaki, N., Mauzerall, D. L., and Rodriguez-Iturbe, I.: Virtual water trade flows and savings under climate change, Hydrol. Earth Syst. Sci., 17, 3219-3234, doi:10.5194/hess-17-3219-2013, 2013.

Konar, M., Dalin, C., Suweis, S., Hanasaki, N., Rinaldo, A., Rodriguez-Iturbe, I., 2011. Water for food: The global virtual water trade network. Water Resour. Res. 47, 5. doi:10.1029/2010WR010307

Koutavas, A., Joanides, S., 2012. El Niño–Southern Oscillation extrema in the Holocene and Last Glacial Maximum. Paleoceanography 27, doi:10.1029/2012PA002378

Koutavas, A., deMenocal, P.B., Olive, G.C., Lynch-Stieglitz, J., 2006. Mid-Holocene El Niño–Southern Oscillation (ENSO) attenuation revealed by individual foraminifera in eastern tropical Pacific sediments. Geology 34, 993–996. doi:10.1130/G22810A.1

Krebs, U., Timmermann, A., 2007. Tropical air-sea interactions accelerate the recovery of the Atlantic meridional overturning circulation after a major shutdown. J. Clim. 20, 4940–4956.

Krichak, S.O., Kishcha, P., Alpert, P., 2002. Decadal trends of main Eurasian oscillations and the Eastern Mediterranean precipitation. Theor. Appl. Climatol. 72, 209–220. doi:10.1007/s007040200021

Lamb, H.H., 1965. The early medieval warm epoch and its sequel. Palaeogeogr. Palaeoclimatol. Palaeoecol. 1, 13–37. doi:10.1016/0031-0182(65)90004-0

Larsen, C.S., 2006. The agricultural revolution as environmental catastrophe: Implications for health and lifestyle in the Holocene. Quat. Int., Impact of rapid environmental changes on humans and ecosystems Impact of rapid environmental changes on humans and ecosystems 150, 12–20. doi:10.1016/j.quaint.2006.01.004

Leemans, R., 1992. Global Holdridge Life Zone Classifications. (Digital Raster Data on a 0.5-degree Cartesian Orthonormal Geodetic (lat/long) 360x720 grid), Global Ecosystems Database. NOAA National Geophysical Data Center, Boulder, CA.

Leemans, R., 1990. Global data sets collected and compiled by the Biosphere Project. Presented at the IIASA-Laxenburg, Austria.

Leontidou, L., 1990. The Mediterranean City in Transition: Social Change and Urban Development. Cambridge University Press.

Lever, J.J., van Nes, E.H., Scheffer, M., Bascompte, J., 2014. The sudden collapse of pollinator communities. Ecol. Lett. 17, 350–359. doi:10.1111/ele.12236

Levi, C., Labeyrie, L., Bassinot, F., Guichard, F., Cortijo, E., Waelbroeck, C., Caillon, N., Duprat, J., de Garidel-Thoron, T., Elderfield, H., 2007. Low-latitude hydrological cycle and rapid climate changes during the last deglaciation. Geochem. Geophys. Geosystems 8, Q05N12.

Lewis, T.G., 2011. Network Science: Theory and Applications. John Wiley & Sons.

Li, S., Hoerling, M.P., Peng, S., Weickmann, K.M., 2006. The Annular Response to Tropical Pacific SST Forcing. J. Clim. 19, 1802–1819. doi:10.1175/JCLI3668.1

Limão, N., Venables, A.J., 2001. Infrastructure, Geographical Disadvantage, Transport Costs, and Trade. World Bank Econ. Rev. 15, 451–479. doi:10.1093/wber/15.3.451

Linsley, B.K., Rosenthal, Y., Oppo, D.W., 2010. Holocene evolution of the Indonesian throughflow and the western Pacific warm pool. Nat. Geosci. 3, 578–583. doi:10.1038/ngeo920

Lionello, P., ed. 2012. The Climate of the Mediterranean Region, Elsevier

Lionello, P., Malanotte-Rizzoli, P., Boscolo, R. eds., 2006. Mediterranean Climate Variability. Elsevier.

Liu, J., Savenije, H.H.G., 2008. Food consumption patterns and their effect on water requirement in China. Hydrol Earth Syst Sci 12, 887–898. doi:10.5194/hess-12-887-2008

Ljungqvist, F.C., 2010. A new reconstruction of temperature variability in the extra-tropical northern hemisphere during the last two millennia. Geogr. Ann. Ser. Phys. Geogr. 92, 339–351. doi:10.1111/j.1468-0459.2010.00399.x

Lorenz, S.J., Kim, J.-H., Rimbu, N., Schneider, R.R., Lohmann, G., 2006. Orbitally driven insolation forcing on Holocene climate trends: Evidence from alkenone data and climate modeling. Paleoceanography 21, PA1002. doi:10.1029/2005PA001152

Lot, F., 1931. The End of the Ancient World and the Beginnings of the Middle Ages. K. Paul, Trench, Trubner & Company, Limited.

Ludwig, F., Asseng, S., 2006. Climate change impacts on wheat production in a Mediterranean environment in Western Australia. Agric. Syst. 90, 159–179. doi:10.1016/j.agsy.2005.12.002

Magny, M., de Beaulieu, J.-L., Drescher-Schneider, R., Vannière, B., Walter-Simonnet, A.-V., Miras, Y., Millet, L., Bossuet, G., Peyron, O., Brugiapaglia, E., Leroux, A., 2007. Holocene climate changes in the central Mediterranean as recorded by lake-level fluctuations at Lake Accesa (Tuscany, Italy). Quat. Sci. Rev. 26, 1736–1758. doi:10.1016/j.quascirev.2007.04.014

Maisels, C.K., 1993. The emergence of civilization: From hunting and gathering to agriculture, cities, and the state in the Near East. Psychology Press.

Mann, M.E., Bradley, R.S., Hughes, M.K., 1998. Global-scale temperature patterns and climate forcing over the past six centuries. Nature 392, 779–787. doi:10.1038/33859

Mann, M.E., Cane, M.A., Zebiak, S.E., Clement, A., 2005. Volcanic and Solar Forcing of the Tropical Pacific over the Past 1000 Years. J. Clim. 18, 447–456. doi:10.1175/JCLI-3276.1

Mann, M.E., Zhang, Z., Rutherford, S., Bradley, R.S., Hughes, M.K., Shindell, D., Ammann, C., Faluvegi, G., Ni, F., 2009. Global Signatures and Dynamical Origins of the Little Ice Age and Medieval Climate Anomaly. Science 326, 1256–1260. doi:10.1126/science.1177303

Mantua, N.J., Hare, S.R., Zhang, Y., Wallace, J.M., Francis, R.C., 1997. A Pacific Interdecadal Climate Oscillation with Impacts on Salmon Production. Bull. Am. Meteorol. Soc. 78, 1069–1079. doi:10.1175/1520-0477(1997)078<1069:APICOW>2.0.CO;2

Marchitto, T.M., Muscheler, R., Ortiz, J.D., Carriquiry, J.D., Geen, A. van, 2010. Dynamical Response of the Tropical Pacific Ocean to Solar Forcing During the Early Holocene. Science 330, 1378–1381. doi:10.1126/science.1194887

Marquer, L., Pomel, S., Abichou, A., Schulz, E., Kaniewski, D., Van Campo, E., 2008. Late Holocene high resolution palaeoclimatic reconstruction inferred from Sebkha Mhabeul, southeast Tunisia. Quat. Res. 70, 240–250. doi:16/j.yqres.2008.06.002

Martin-Puertas, C., Matthes, K., Brauer, A., Muscheler, R., Hansen, F., Petrick, C., Aldahan, A., Possnert, G., Geel, B. van, 2012. Regional atmospheric circulation shifts induced by a grand solar minimum. Nat. Geosci. doi:10.1038/ngeo1460

Martín-Puertas, C., Jiménez-Espejo, F., Martínez-Ruiz, F., Nieto-Moreno, V., Rodrigo, M., Mata, M.P., Valero-Garcés, B.L., 2010. Late Holocene climate variability in the southwestern Mediterranean region: An integrated marine and terrestrial geochemical approach. Clim. Past 6, 807–816.

Martín-Puertas, C., Valero-Garcés, B.L., Brauer, A., Mata, M.P., Delgado-Huertas, A., Dulski, P., 2009. The Iberian-Roman Humid Period (2600-1600 cal yr BP) in the Zoñar Lake varve record (Andalucía, southern Spain). Quat. Res. 71, 108–120. doi:10.1016/j.yqres.2008.10.004

Mayewski, P.A., Rohling, E.E., Curt Stager, J., Karlén, W., Maasch, K.A., David Meeker, L., Meyerson, E.A., Gasse, F., van Kreveld, S., Holmgren, K., Lee-Thorp, J., Rosqvist, G., Rack, F., Staubwasser, M., Schneider, R.R., Steig, E.J., 2004. Holocene climate variability. Quat. Res. 62, 243–255. doi:10.1016/j.yqres.2004.07.001

Mazier, F., Kuneš, P., Sugita, S., Trondman, A.-K., Broström, A., Gaillard, M.-J., 2010. Pollen-inferred quantitative reconstructions of Holocene land-cover in NW Europe for the evaluation of past climate-vegetation feedbacks -Evaluation of the REVEALS-based reconstruction using the Czech Republic database. EGU General Assembly

Mazoyer, M., Roudart, L., 2006. A History of World Agriculture: From the Neolithic Age to the Current Crisis. Earthscan.

McAnany, P.A., Yoffee, N., 2009. Questioning collapse: human resilience, ecological vulnerability, and the aftermath of empire. Cambridge University Press.

McDermott, F., Mattey, D.P., Hawkesworth, C., 2001. Centennial-Scale Holocene Climate Variability Revealed by a High-Resolution Speleothem δ18O Record from SW Ireland. Science 294, 1328–1331. doi:10.1126/science.1063678

McManus, J.F., Francois, R., Gherardi, J.-M., Keigwin, L.D., Brown-Leger, S., 2004. Collapse and rapid resumption of Atlantic meridional circulation linked to deglacial climate changes. Nature 428, 834–837. doi:10.1038/nature02494

Meehl, G.A., Arblaster, J.M., Matthes, K., Sassi, F., Loon, H. van, 2009. Amplifying the Pacific Climate System Response to a Small 11-Year Solar Cycle Forcing. Science 325, 1114–1118. doi:10.1126/science.1172872

Meehl, G.A., Arblaster, J.M., Branstator, G., van Loon, H., 2008. A coupled air-sea response mechanism to solar forcing in the Pacific region. J. Clim. 21, 2883–2897.

Meeks, E., 2013. Modeling Transportation in the Roman World: Implications for World Systems. Leonardo 46, 278–278. doi:10.1162/LEON_a_00574

Meijer, F.J., 1984. Cato's African Figs. Mnemosyne, Fourth Series 37, 117–124.

Messerlin, P., 2011. Climate, Trade and Water: A "Grand Coalition"? World Econ. 34, 1883–1910. doi:10.1111/j.1467-9701.2011.01419.x

Meyer, P.S., Ausubel, J.H., 1999. Carrying Capacity: A Model with Logistically Varying Limits. Technol. Forecast. Soc. Change 61, 209–214. doi:10.1016/S0040-1625(99)00022-0

Migowski, C., Stein, M., Prasad, S., Negendank, J.F.W., Agnon, A., 2006. Holocene climate variability and cultural evolution in the Near East from the Dead Sea sedimentary record. Quat. Res. 66, 421–431. doi:10.1016/j.yqres.2006.06.010

Montecino, V., Lange, C.B., 2009. The Humboldt Current System: Ecosystem components and processes, fisheries, and sediment studies. Prog. Oceanogr., Eastern Boundary Upwelling Ecosystems: Integrative and Comparative Approaches :Integrative and comparative approaches, 2-8 June 2008, Las Palmas, Gran Canaria, Spain Eastern Boundary Upwelling Ecosystems Symposium 83, 65–79. doi:10.1016/j.pocean.2009.07.041

Montgomery, D.R., 2008. Dirt: The Erosion of Civilizations. University of California Press.

Moy, C.M., Seltzer, G.O., Rodbell, D.T., Anderson, D.M., 2002. Variability of El Nino/Southern Oscillation activity at millennial timescales during the Holocene epoch. Nature 420, 162–165.

Namias, J., 1950. The index cycle and its role in the general circulation. J. Atmospheric Sci. 7, 130–139.

Nesje, A., Lie, Ø., Dahl, S.O., 2000. Is the North Atlantic Oscillation reflected in Scandinavian glacier mass balance records? J. Quat. Sci. 15, 587–601. doi:10.1002/1099-1417(200009)15:6<587::AID-JQS533>3.0.CO;2-2

Newman, M., Compo, G.P., Alexander, M.A., 2003. ENSO-Forced Variability of the Pacific Decadal Oscillation. J. Clim. 16, 3853–3857. doi:10.1175/1520-0442(2003)016<3853:EVOTPD>2.0.CO;2

Newton, A., Thunell, R., Stott, L., 2006. Climate and hydrographic variability in the Indo-Pacific Warm Pool during the last millennium. Geophys. Res. Lett. 33, L19710.

Ngo-Duc, T., Polcher, J., Laval, K., 2005. A 53-year forcing data set for land surface models. J. Geophys. Res. Atmospheres 110, D06116. doi:10.1029/2004JD005434

Olson, J.S., 1994a. Global ecosystem framework-definitions (Internal Report). USGS EROS Data Center, Sioux Falls, SD.

Olson, J.S., 1994b. Global ecosystem framework-translation strategy (Internal Report). USGS EROS Data Center, Sioux Falls, SD.

Oppo, D.W., Rosenthal, Y., Linsley, B.K., 2009. 2,000-year-long temperature and hydrology reconstructions from the Indo-Pacific warm pool. Nature 460, 1113–1116. doi:10.1038/nature08233

Orland, I., Bar-matthews, M., Kita, N., Ayalon, A., Matthews, A., Valley, J., 2009. Climate deterioration in the Eastern Mediterranean as revealed by ion microprobe analysis of a speleothem that grew from 2.2 to 0.9 ka in Soreq Cave, Israel. Quat. Res. 71, 27–35. doi:10.1016/j.yqres.2008.08.005

Ortloff, C.R., 2005. The Water Supply and Distribution System of the Nabataean City of Petra (Jordan), 300 BC– AD 300. Camb. Archaeol. J. 15, 93–109. doi:10.1017/S0959774305000053

Parker, A.J., 1992. Ancient shipwrecks of the Mediterranean and Roman Provinces. Oxford: Tempus Reparatum.

Pedersen, O., 2010. Ancient near east sites on google earth [WWW Document]. URL http://www.anst.uu.se/olofpede/Links.htm (accessed 10.20.10).

Peel, M.C., Finlayson, B.L., McMahon, T.A., 2007. Updated world map of the Köppen-Geiger climate classification. Hydrol Earth Syst Sci 11, 1633–1644.

Peng, S., Robinson, W.A., Li, S., 2002. North Atlantic SST Forcing of the NAO and Relationships with Intrinsic Hemispheric Variability. Geophys. Res. Lett. 29, 4 PP. doi:200210.1029/2001GL014043

Perry, R.A., 1986. Desertification processes and impacts in irrigated regions. Clim. Change 9, 43–47. doi:10.1007/BF00140523

Pierrehumbert, R.T., 2000. Climate change and the tropical Pacific: The sleeping dragon wakes. Proc. Natl. Acad. Sci. 97, 1355–1358. doi:10.1073/pnas.97.4.1355

Pierrehumbert, R.T., 1995. Thermostats, radiator fins, and the local runaway greenhouse. J. Atmospheric Sci. 52, 1784–1806.

Pitts, L.F., 1989. Relations between Rome and the German “Kings” on the Middle Danube in the First to Fourth Centuries A.D. J. Roman Stud. 79, 45–58. doi:10.2307/301180

Polyakov, I.V., Johnson, M.A., 2000. Arctic decadal and interdecadal variability. Geophys. Res. Lett. 27, 4097–4100.

Poore, R.Z., Pavich, M.J., Grissino-Mayer, H.D., 2005. Record of the North American southwest monsoon from Gulf of Mexico sediment cores. Geology 33, 209–212. doi:10.1130/G21040.1

Poore, R.Z., Quinn, T.M., Verardo, S., 2004. Century-scale movement of the Atlantic Intertropical Convergence Zone linked to solar variability. Geophys Res Lett 31, L12214.

Portmann, F.T., 2008. Global estimation of monthly irrigated and rainfed crop areas on a 5 arc-minute grid.

Possehl, G.L., 1997. Climate and the Eclipse of the Ancient Cities of the Indus, in: Dalfes, H.N., Kukla, G., Weiss, H. (Eds.), Third Millennium BC Climate Change and Old World Collapse, NATO ASI Series. Springer Berlin Heidelberg, pp. 193–243.

Qiu, B., 2003. Kuroshio Extension Variability and Forcing of the Pacific Decadal Oscillations: Responses and Potential Feedback. J. Phys. Oceanogr. 33, 2465–2482. doi:10.1175/2459.1

Reale, O., Dirmeyer, P., 2000. Modeling the effects of vegetation on Mediterranean climate during the Roman Classical Period: Part I: Climate history and model sensitivity. Glob. Planet. Change 25, 163–184. doi:10.1016/S0921-8181(00)00002-3

Reale, O., Shukla, J., 2000. Modeling the effects of vegetation on Mediterranean climate during the Roman Classical Period: Part II. Model simulation. Glob. Planet. Change 25, 185–214. doi:10.1016/S0921-8181(00)00003-5

Rees, D.W.E., Wackernagel, M., 1996. Ecological Footprints and Appropriated Carrying Capacity: Measuring the Natural Capital Requirements of the Human Economy. Focus 6, 45–60.

Reimer, P.J., Reimer, R.W., 2001. A marine reservoir correction database and on-line interface. Radiocarbon 43, 461–464.

Rein, B., Lückge, A., Reinhardt, L., Sirocko, F., Wolf, A., Dullo, W.-C., 2005. El Niño variability off Peru during the last 20,000 years. Paleoceanography 20, PA4003. doi:10.1029/2004PA001099

Renssen, H., Goosse, H., Muscheler, R., 2006. Coupled climate model simulation of Holocene cooling events: oceanic feedback amplifies solar forcing. Clim Past 2, 79–90. doi:10.5194/cp-2-79-2006

Reynolds, R.W., Rayner, N.A., Smith, T.M., Stokes, D.C., Wang, W., 2002. An improved in situ and satellite SST analysis for climate. J. Clim. 15, 1609–1625.

Rickman, G.E., 1980. The Grain Trade under the Roman Empire. Mem. Am. Acad. Rome 36, 261–275. doi:10.2307/4238709

Rimbu, N., Lohmann, G., Kim, J.-H., Arz, H.W., Schneider, R., 2003. Arctic/North Atlantic Oscillation signature in Holocene sea surface temperature trends as obtained from alkenone data. Geophys. Res. Lett. 30, 1280–1283. doi:200310.1029/2002GL016570

Rives, J.B., 2007. Religion in the Roman empire. Blackwell Pub.

Roberts, N., Moreno, A., Valero-Garcés, B.L., Corella, J.P., Jones, M., Allcock, S., Woodbridge, J., Morellón, M., Luterbacher, J., Xoplaki, E., Türkeş, M., 2012. Palaeolimnological evidence for an east–west climate see-saw in the Mediterranean since AD 900. Glob. Planet. Change 84–85, 23–34. doi:10.1016/j.gloplacha.2011.11.002

Roberts, N., Reed, J.M., Leng, M.J., Kuzucuoğlu, C., Fontugne, M., Bertaux, J., Woldring, H., Bottema, S., Black, S., Hunt, E., Karabiyikoğlu, M., 2001. The tempo of Holocene climatic change in the eastern Mediterranean region: new high-resolution crater-lake sediment data from central Turkey. The Holocene 11, 721 –736. doi:10.1191/09596830195744

Rockström, J., Steffen, W., Noone, K., Persson, Å., Chapin, F.S., Lambin, E.F., Lenton, T.M., Scheffer, M., Folke, C., Schellnhuber, H.J., Nykvist, B., de Wit, C.A., Hughes, T., van der Leeuw, S., Rodhe, H., Sörlin, S., Snyder, P.K., Costanza, R., Svedin, U., Falkenmark, M., Karlberg, L., Corell, R.W., Fabry, V.J., Hansen, J., Walker, B., Liverman, D., Richardson, K., Crutzen, P., Foley, J.A., 2009. A safe operating space for humanity. Nature 461, 472–475. doi:10.1038/461472a

Rodwell, M.J., Rowell, D.P., Folland, C.K., 1999. Oceanic forcing of the wintertime North Atlantic Oscillation and European climate. Nature 398, 320–323. doi:10.1038/18648

Rose, J.I., 2010. New Light on Human Prehistory in the Arabo-Persian Gulf Oasis. Curr. Anthropol. 51, 849–883. doi:10.1086/657397

Rosenthal, Y., Oppo, D.W., Linsley, B.K., 2003. The amplitude and phasing of climate change during the last deglaciation in the Sulu Sea, western equatorial Pacific. Geophys. Res. Lett. 30, 1428. doi:10.1029/2002GL016612

Santley, R.S., Killion, T.W., Lycett, M.T., 1986. On the Maya Collapse. J. Anthropol. Res. 42, 123–159.

Scafetta, N., West, B.J., 2005. Estimated solar contribution to the global surface warming using the ACRIM TSI satellite composite. Geophys. Res. Lett. 32, L18713. doi:10.1029/2005GL023849

Scheffer, M., 2009. Critical transitions in nature and society. Princeton University Press.

Scheidel, W., 2013. The Shape of the Roman World (SSRN Scholarly Paper No. ID 2242325). Social Science Research Network, Rochester, NY.

Scheidel, W., 2010. Approaching the Roman economy, Stanford University Press.

Scheidel, W., 2001. Debating Roman Demography. BRILL.

Schmidhuber, J., Tubiello, F.N., 2007. Global food security under climate change. Proc. Natl. Acad. Sci. 104, 19703–19708. doi:10.1073/pnas.0701976104

Seager, R., Zebiak, S.E., Cane, M.A., 1988. A model of the tropical Pacific sea surface temperature climatology. J. Geophys. Res. Oceans 93, 1265–1280. doi:10.1029/JC093iC02p01265

Sherbinin, A.D., Schiller, A., Pulsipher, A., 2007. The vulnerability of global cities to climate hazards. Environ. Urban. 19, 39–64. doi:10.1177/0956247807076725

Shi, J., Liu, J., Pinter, L., 2014. Recent evolution of China's virtual water trade: analysis of selected crops and considerations for policy. Hydrol Earth Syst Sci 18, 1349–1357. doi:10.5194/hess-18-1349-2014

Shiklomanov, I.A., 2000. Appraisal and Assessment of World Water Resources. Water Int. 25, 11–32. doi:10.1080/02508060008686794

Shindell, D.T., Schmidt, G.A., Mann, M.E., Rind, D., Waple, A., 2001. Solar Forcing of Regional Climate Change During the Maunder Minimum. Science 294, 2149 –2152. doi:10.1126/science.1064363

Shindell, D.T., Miller, R.L., Schmidt, G.A., Pandolfo, L., 1999. Simulation of recent northern winter climate trends by greenhouse-gas forcing. Nature 399, 452–455.

Shindell, D.T, Rind, D., Balachandran, N., Lean, J., Lonergan, P., 1999. Solar Cycle Variability, Ozone, and Climate. Science 284, 305–308. doi:10.1126/science.284.5412.305

Sivapalan, M., Savenije, H.H.G., Blöschl, G., 2012. Socio-hydrology: A new science of people and water. Hydrol. Process. 26, 1270–1276. doi:10.1002/hyp.8426

Solanki, S.K., Krivova, N.A., 2003. Can solar variability explain global warming since 1970? J. Geophys. Res. Space Phys. 108, 1200. doi:10.1029/2002JA009753

Staubwasser, M., 2003. Climate change at the 4.2 ka BP termination of the Indus valley civilization and Holocene south Asian monsoon variability. Geophys. Res. Lett. 30, 1425–1428. doi:10.1029/2002GL016822

Stein, A., 1941. The Ancient Trade Route Past Hatra and Its Roman Posts. J. R. Asiat. Soc. G. B. Irel. 299–316.

Steinhilber, F., Abreu, J.A., Beer, J., Brunner, I., Christl, M., Fischer, H., Heikkilä, U., Kubik, P.W., Mann, M., McCracken, K.G., Miller, H., Miyahara, H., Oerter, H., Wilhelms, F., 2012. 9,400 Years of Cosmic Radiation and Solar Activity from Ice Cores and Tree Rings. Proc. Natl. Acad. Sci. 109, 5967–5971. doi:10.1073/pnas.1118965109

Steinhilber, F., Beer, J., Fröhlich, C., 2009. Total solar irradiance during the Holocene. Geophys Res Lett 36.

Steinke, S., Kienast, M., Groeneveld, J., Lin, L.-C., Chen, M.-T., Rendle-Bühring, R., 2008. Proxy dependence of the temporal pattern of deglacial warming in the tropical South China Sea: toward resolving seasonality. Quat. Sci. Rev. 27, 688–700. doi:10.1016/j.quascirev.2007.12.003

Stewart, O.C., 1951. Burning and Natural Vegetation in the United States. Geogr. Rev. 41, 317. doi:10.2307/211026

Stott, L., Timmermann, A., Thunell, R., 2007. Southern Hemisphere and Deep-Sea Warming Led Deglacial Atmospheric CO2 Rise and Tropical Warming. Science 318, 435–438. doi:10.1126/science.1143791

Stott, L., Cannariato, K., Thunell, R., Haug, G.H., Koutavas, A., Lund, S., 2004. Decline of surface temperature and salinity in the western tropical Pacific Ocean in the Holocene epoch. Nature 431, 56–59. doi:10.1038/nature02903

Stuiver, M., Grootes, P.M., Braziunas, T.F., 1995. The GISP2 δ18O climate record of the past 16,500 years and the role of the sun, ocean, and volcanoes. Quat. Res. 44, 341–354.

Sun, D.Z., Liu, Z. 1996. Dynamic Ocean-Atmosphere Coupling: A Thermostat for the Tropics. Science 272, 1148–1150.

Sun, Y., Oppo, D.W., Xiang, R., Liu, W., Gao, S., 2005. Last deglaciation in the Okinawa Trough: Subtropical northwest Pacific link to Northern Hemisphere and tropical climate. Paleoceanography 20, PA4005. doi:10.1029/2004PA001061

Suweis, S., Konar, M., Dalin, C., Hanasaki, N., Rinaldo, A., Rodriguez-Iturbe, I., 2011. Structure and controls of the global virtual water trade network. Geophys. Res. Lett. 38, L10403. doi:10.1029/2011GL046837

Suweis, S., Rinaldo, A., Maritan, A., D'Odorico, P., 2013. Water-controlled wealth of nations. Proc. Natl. Acad. Sci. 110, 4230–4233. doi:10.1073/pnas.1222452110

Tateishi, R., Bayer, M., Ghar, A., Al-Bilbisi, H., 2008. A New Global Land Cover Map (GLCNMO). United States Geological Survey.

Taylor, W. A.., 2000 Change-point analysis: a powerful new tool for detecting changes, Available from: http://www.variation.com/cpa/tech/changepoint.html (Accessed 30 January 2013)

Temin, P., 2012. The Roman Market Economy. Princeton University Press.

Thompson, D.W.J., Wallace, J.M., 1998. The Arctic oscillation signature in the wintertime geopotential height and temperature fields. Geophys. Res. Lett. 25, 1297. doi:10.1029/98GL00950

Thompson, I., Mackey, B., McNulty, S., Mosseler, A., 2009. Forest resilience, biodiversity, and climate change, in: A Synthesis of the Biodiversity/resilience/stability Relationship in Forest Ecosystems. Secretariat of the Convention on Biological Diversity, Montreal. Technical Series.

Thornalley, D.J.R., Elderfield, H., McCave, I.N., 2009. Holocene oscillations in temperature and salinity of the surface subpolar North Atlantic. Nature 457, 711–714. doi:10.1038/nature07717

Tierney, J.E., Oppo, D.W., Rosenthal, Y., Russell, J.M., Linsley, B.K., 2010. Coordinated hydrological regimes in the Indo-Pacific region during the past two millennia. Paleoceanography 25, PA1102.

Timmermann, A., Okumura, Y., An, S.I., Clement, A., Dong, B., Guilyardi, E., Hu, A., Jungclaus, J., Renold, M., Stocker, T., others, 2007. The influence of a weakening of the Atlantic meridional overturning circulation on ENSO. J. Clim. 20, 4899–4919.

Timmermann, A., Oberhuber, J., Bacher, A., Esch, M., Latif, M., Roeckner, E., 1999. Increased El Niño frequency in a climate model forced by future greenhouse warming. Nature 398, 694–697. doi:10.1038/19505

Torell, L.A., Libbin, J.D., Miller, M.D., 1990. The Market Value of Water in the Ogallala Aquifer. Land Econ. 66, 163. doi:10.2307/3146366

Trenberth, K.E., Hoar, T.J., 1997. El Niño and climate change. Geophys. Res. Lett. 24, 3057–3060. doi:10.1029/97GL03092

Trouet, V., Esper, J., Graham, N.E., Baker, A., Scourse, J.D., Frank, D.C., 2009. Persistent Positive North Atlantic Oscillation Mode Dominated the Medieval Climate Anomaly. Science 324, 78 –80. doi:10.1126/science.1166349

Tyndall, J., 1861. The Bakerian Lecture: On the Absorption and Radiation of Heat by Gases and Vapours, and on the Physical Connexion of Radiation, Absorption, and Conduction. Royal Society of London.

United Nations, 2012. World Urbanization Prospects. United Nations, Department of Economic and Social Affairs, Population Division, New York.

van Beek, L.P.H., Wada, Y., Bierkens, M.F.P., 2011. Global monthly water stress: 1. Water balance and water availability. Water Resour. Res. 47, 7. doi:10.1029/2010WR009791

van Beek, L.P.H., Bierkens, M.F.P., 2009. The Global Hydrological Model PCR-GLOBWB: Conceptualization, Parameterization and Verification. Utrecht University.

van der Leeuw, S., Costanza, R., Aulenbach, S., Brewer, S., Burek, M., Cornell, S., Crumley, C., Dearing, J.A., Downy, C., Graumlich, L.J., Heckbert, S., Hegmon, M., Hibbard, K., Jackson, S.T., Kubiszewski, I., Sinclair, P., Sörlin, S., Steffen, W., 2011. Toward an Integrated History to Guide the Future. Ecol. Soc. 16. doi:10.5751/ES-04341-160402

van der Leeuw, S, 1998. The Archaeomedes project: understanding the natural and anthropogenic causes of land degradation and desertification in the Mediterranean basin : research results. Office for Official Publications of the European Communities.

van Ittersum, M.K., Howden, S.M., Asseng, S., 2003. Sensitivity of productivity and deep drainage of wheat cropping systems in a Mediterranean environment to changes in CO2, temperature and precipitation. Agric. Ecosyst. Environ. 97, 255–273. doi:10.1016/S0167-8809(03)00114-2

van Zeist, W., Woldring, H., 1978. A Postglacial pollen diagram from Lake Van in East Anatolia. Rev. Palaeobot. Palynol. 26, 249–276.

Virah-Sawmy, M., Gillson, L., Willis, K.J., 2009. How does spatial heterogeneity influence resilience to climatic changes? Ecological dynamics in southeast Madagascar. Ecol. Monogr. 79, 557–574. doi:10.1890/08-1210.1

Visbeck, M.H., Hurrell, J.W., Polvani, L., Cullen, H.M., 2001. The North Atlantic Oscillation: past, present, and future. Proc. Natl. Acad. Sci. U. S. A. 98, 12876.

Visser, K., Thunell, R., Stott, L., 2003. Magnitude and timing of temperature change in the Indo-Pacific warm pool during deglaciation. Nature 421, 152–155. doi:10.1038/nature01297

Vita-Finzi, C., 1969. The Mediterranean valleys: geological changes in historical times. Cambridge U.P.

Wada, Y., van Beek, L.P.H., Viviroli, D., Dürr, H.H., Weingartner, R., Bierkens, M.F.P., 2011. Global monthly water stress: 2. Water demand and severity of water stress. Water Resour. Res. 47, 7. doi:10.1029/2010WR009792

Wada, Y., Beek, L.P.H. van, Kempen, C.M. van, Reckman, J.W.T.M., Vasak, S., Bierkens, M.F.P., 2010. Global depletion of groundwater resources. Geophys. Res. Lett. 37, 5 PP. doi:201010.1029/2010GL044571

Wallace, J., 2000. On the Arctic and Antarctic oscillations, in: Proceedings of the 23rd Annual Climate. Diagnostics and Prediction Workshop, NOAA, NWS, Department of Commerce, Florida, USA.

Wang, C., 2007. Variability of the Caribbean low-level jet and its relations to climate. Clim. Dyn. 29, 411–422.

Wang, T., Surge, D., Mithen, S., 2012. Seasonal temperature variability of the Neoglacial (3300–2500 BP) and Roman Warm Period (2500–1600 BP) reconstructed from oxygen isotope ratios of limpet shells (Patella vulgata), Northwest Scotland. Palaeogeogr. Palaeoclimatol. Palaeoecol. 317–318, 104–113. doi:10.1016/j.palaeo.2011.12.016

Wang, X., Wang, C., Zhou, W., Wang, D., Song, J., 2010. Teleconnected influence of North Atlantic sea surface temperature on the El Niño onset. Clim. Dyn. 37, 663–676. doi:10.1007/s00382-010-0833-z

Wang, Y., Cheng, H., Edwards, R.L., He, Y., Kong, X., An, Z., Wu, J., Kelly, M.J., Dykoski, C.A., Li, X., 2005. The Holocene Asian Monsoon: Links to Solar Changes and North Atlantic Climate. Science 308, 854–857. doi:10.1126/science.1106296

Wanner, H., Solomina, O., Grosjean, M., Ritz, S.P., Jetel, M., 2011. Structure and origin of Holocene cold events. Quat. Sci. Rev. 30, 3109–3123. doi:10.1016/j.quascirev.2011.07.010

Wanner, H., Beer, J., Bütikofer, J., Crowley, T.J., Cubasch, U., Flückiger, J., Goosse, H., Grosjean, M., Joos, F., Kaplan, J.O., Küttel, M., Müller, S.A., Prentice, I.C., Solomina, O., Stocker, T.F., Tarasov, P., Wagner, M., Widmann, M., 2008. Mid- to Late Holocene climate change: an overview. Quat. Sci. Rev. 27, 1791–1828. doi:10.1016/j.quascirev.2008.06.013

Weber, S.L., Crowley, T.J., der Schrier, G., 2004. Solar irradiance forcing of centennial climate variability during the Holocene. Clim. Dyn. 22, 539–553.

Webster, D.L., 2002. The Fall of the Ancient Maya: Solving the Mystery of the Maya Collapse. Thames & Hudson Press.

Weiss, H., Courty, M.-A., Wetterstrom, W., Guichard, F., Senior, L., Meadow, R., Curnow, A., 1993. The Genesis and Collapse of Third Millennium North Mesopotamian Civilization. Science 261, 995–1004. doi:10.1126/science.261.5124.995

Weiss, B., 1982. The decline of Late Bronze Age civilization as a possible response to climatic change. Clim. Change 4, 173–198. doi:10.1007/BF02423389

White, K.D., 1970. Fallowing, Crop Rotation, and Crop Yields in Roman Times. Agric. Hist. 44, 281–290.

Wick, L., Lemcke, G., Sturm, M., 2003. Evidence of Lateglacial and Holocene climatic change and human impact in eastern Anatolia: high-resolution pollen, charcoal, isotopic and geochemical records from the laminated sediments of Lake Van, Turkey. The Holocene 13, 665 –675. doi:10.1191/0959683603hl653rp

Wilensky, U., 1999. Netlogo, 1999. Cent. Connect. Learn. Comput.-Based Model. Northwest. Univ. Evanst. IL.

Williams, C.A., Hanan, N.P., 2011. ENSO and IOD teleconnections for African ecosystems: evidence of destructive interference between climate oscillations. Biogeosciences 8, 27–40. doi:10.5194/bg-8-27-2011

Wilson, A.I., 1997. Water Management and Usage in Roman North Africa: A Social and Technological Study. University of Oxford.

Woolf, G., 1992. Imperialism, empire and the integration of the Roman economy. World Archaeol. 23, 283–293. doi:10.1080/00438243.1992.9980180

Wunsch, C., 2002. What Is the Thermohaline Circulation? Science 298, 1179–1181. doi:10.1126/science.1079329

Xoplaki, E., Gonzalez-Rouco, J.F., Luterbacher, J., Wanner, H., 2004. Wet season Mediterranean precipitation variability: influence of large-scale dynamics and trends. Clim. Dyn. 23, 63–78.

Xu, J., Holbourn, A., Kuhnt, W., Jian, Z., Kawamura, H., 2008. Changes in the thermocline structure of the Indonesian outflow during Terminations I and II. Earth Planet. Sci. Lett. 273, 152–162. doi:10.1016/j.epsl.2008.06.029

Yan, H., Sun, L., Oppo, D.W., Wang, Y., Liu, Z., Xie, Z., Liu, X., Cheng, W., 2011a. South China Sea hydrological changes and Pacific Walker Circulation variations over the last millennium. Nat. Commun. 2, 293. doi:10.1038/ncomms1297

Yan, H., Sun, L., Wang, Y., Huang, W., Qiu, S., Yang, C., 2011b. A record of the Southern Oscillation Index for the past 2,000 years from precipitation proxies. Nat. Geosci. 4, 611–614. doi:10.1038/ngeo1231

Yang, H., Zehnder, A., 2001. China's regional water scarcity and implications for grain supply and trade. Environ. Plan. A 33, 79–96.

Yasuda, Y., Kitagawa, H., Nakagawa, T., 2000. The earliest record of major anthropogenic deforestation in the Ghab Valley, northwest Syria: a palynological study. Quat. Int. 73-74, 127–136. doi:10.1016/S1040-6182(00)00069-0

Yatagai, A., Xie, P., Alpert, P., 2008. Development of a daily gridded precipitation data set for the Middle East. Adv. Geosci., 12, 165–170. doi:10.5194/adgeo-12-165-2008

Young, O.R., Berkhout, F., Gallopin, G.C., Janssen, M.A., Ostrom, E., Van Der Leeuw, S., 2006. The globalization of socio-ecological systems: An agenda for scientific research. Glob. Environ. Change 16, 304–316. doi:10.1016/j.gloenvcha.2006.03.004

Zanchetta, G., Drysdale, R.N., Hellstrom, J.C., Fallick, A.E., Isola, I., Gagan, M.K., Pareschi, M.T., 2007. Enhanced rainfall in the Western Mediterranean during deposition of sapropel S1: stalagmite evidence from Corchia cave (Central Italy). Quat. Sci. Rev. 26, 279–286. doi:10.1016/j.quascirev.2006.12.003

Zebiak, S.E., Cane, M.A., 1987. A Model EI Nino-Southern Oscillation. Mon. Weather Rev. 115, 2262–2278.

Zhang, H., Oweis, T., 1999. Water–yield relations and optimal irrigation scheduling of wheat in the Mediterranean region. Agric. Water Manag. 38, 195–211. doi:10.1016/S0378-3774(98)00069-9

Zhang, P., Cheng, H., Edwards, R.L., Chen, F., Wang, Y., Yang, X., Liu, J., Tan, M., Wang, X., Liu, J., An, C., Dai, Z., Zhou, J., Zhang, D., Jia, J., Jin, L., Johnson, K.R., 2008. A Test of Climate, Sun, and Culture Relationships from an 1810-Year Chinese Cave Record. Science 322, 940–942. doi:10.1126/science.1163965

Ziv, B., Dayan, U., Kushnir, Y., Roth, C., Enzel, Y., 2006. Regional and global atmospheric patterns governing rainfall in the southern Levant. Int. J. Climatol. 26, 55–73. doi:10.1002/joc.1238

Zwart, S.J., Bastiaanssen, W.G.M., de Fraiture, C., Molden, D.J., 2010. A global benchmark map of water productivity for rainfed and irrigated wheat. Agric. Water Manag. 97, 1617–1627. doi:10.1016/j.agwat.2010.05.018

Summary

A great deal of humanity's success as a species has been our capacity to adapt to diverse and variable environmental conditions. That adaptive capacity extends to an ability to manipulate the environment so that conditions are better suited for the survival of our species. For example, the earliest civilisations constructed irrigation infrastructure that transformed the arid regions of Southern Mesopotamia into a remarkably productive agricultural area. Since then, humanity's ability to engineer our surroundings has rapidly progressed to a point where we now modify the environment at a global scale. An unforeseen outcome of our efforts to engineer the environment has been a warming of the climate owing to the burning of fossil fuels. It is unclear the impact that global warming will have but the weight of evidence indicates that extreme climatic events will become more common. More worrying still, is the prospect that we will be confronted with large-scale and persistent climate change on a magnitude greater than human civilisation has ever experienced. It is thus highly uncertain how vulnerable we are to global warming and whether the adaptive capacity of our species extends sufficiently to cope with the changes that may await us.

In order to diagnose our vulnerability it is vital to have reasonable estimates of how climate will change in the future. That requires improving our understanding of the climate system so that we can develop better predictive models. One avenue of research that has proved incredibly fruitful for understanding the climate system is the study of past climate. We can learn much from looking into the past because many of the processes important for climate change operate on timescales much longer than the period for which we have observations. Through the study of past climate we can gain an understanding of the full range of climate variability and the processes that contribute to that variability.

Equally, our understanding of how humans adapt to climate change has mainly been informed by events during recent centuries. However, with improved paleo dating techniques we can now compare societal changes with climatic changes right back to the beginning of human civilisation. From this analysis it appears that certain past civilisations, such as the Amorite people of present-day Northern Syria, were wiped out by changes in climate whilst others persisted through often large climate perturbations. Therefore, by looking to the past we can learn

a great deal about what makes certain societies vulnerable to climate change and others more resilient. In this thesis we follow this line of enquiry to uncover how climate has changed during the Holocene and the impact that these changes had on past societies. It is envisaged that these investigations will contribute to improving our understanding of the climate system and inform how society may adapt to future climate change.

We begin by focusing on the most important component of the climate system: the sun. Over time, radiation emitted by the sun varies by very small amounts relative to the total average radiation. However, these small variations have been linked with climate change throughout the Holocene geological epoch (11,700 years ago until present day). In terms of the energy emitted, the variability in solar irradiance is too small to directly cause climate changes of the magnitude we see in past climate records. Thus it is proposed that certain elements of the climate system respond to these variations in such a way as to amplify their climatic impact. Simulations using general circulation models indicate that the coupled ocean-atmosphere system of the Tropical Pacific may be one such amplifier. It is suggested that a positive feedback within the coupled ocean-atmosphere system of the Tropical Pacific reinforces the impact of small changes in radiation. Increases or decreases in radiation are simulated to tip the system into a La Niña (a build-up of warm surface wasters in the Western Tropical Pacific) or El Niño (advection of warm surface waters towards the Eastern Tropical Pacific) state respectively. During the Holocene the El Niño Southern Oscillation (ENSO) is proposed to have intensified owing to changes in the angle at which the Earth orbits around the sun. Simulations indicate that these orbital changes may have strengthened solar forcing of the ENSO in recent millennia.

In chapter 2 we set out to find evidence in data whether ENSO serves as a magnifier of solar irradiance variations. To do so we analyse changes in the surface temperature of the Pacific Ocean during the Holocene. We focus our analysis in regions where changes in the ocean surface temperature are closely linked with changes in ENSO. In order to confront the problems associated with dating uncertainty among a composite of marine reconstructions, we devised a statistical method that facilitates comparison among reconstructions whilst taking into account dating uncertainty of each record. Our results indicated that small variations in solar radiation did

impact the temperature of the Tropical Pacific Ocean. However, the response of the Tropical Pacific to solar forcing was opposite between the Holocene Climate Optimum (6,000 – 9,000 years ago) and the Late Holocene (the last 4,000 years). During the Holocene Climate Optimum the surface temperature of the Tropical Pacific Ocean warmed when solar radiation increased and cooled when radiation decreased. In the Late Holocene the response of the Tropical Pacific to solar forcing was opposite with cooling during solar maxima and warming during solar minima. The reason for the switch in response was owing to the strengthening of the influence of solar forcing in the Late Holocene. The stronger response of the Tropical Pacific to solar forcing in the Late Holocene led to a dominance of La Niña conditions under increased radiation. At a longer timescale a dominance of La Niña conditions is associated with increased upwelling of cool waters from the deep ocean and a cooling of the ocean surface temperature. Given that the Tropical Pacific is the largest source of heat and moisture for the atmosphere, these changes had potentially global climate implications during the Holocene.

Having gained insight into changes in climate at a global scale, in chapter 3 we focused on regional changes in precipitation in the Mediterranean between 3,000 and 1,000 years ago. Precipitation changes in the Mediterranean are particularly interesting to study in this period because it coincides with the emergence of the Roman civilisation in the region. In addition, rainfall patterns in the Mediterranean are linked with the position and intensity of the winter Jetstream. Thus by reconstructing past precipitation patterns we can infer how the Northern Hemisphere polar Jet changed during the period of analysis.

We reconstructed the regional change in precipitation by compositing paleoecological-based reconstructions of precipitation from around the Mediterranean. Our analysis indicated that between 3,000 and 1,000 years ago the pattern of precipitation in the Mediterranean seesawed between dry conditions in the Central Mediterranean and wet conditions in the Western and South-eastern Mediterranean coinciding with the Roman Warm Period (~250 BC – 450 AD) to the opposite during the Dark Ages Cold Period (~450 AD – 950 AD). The timing of this seesawing indicated that it was caused by changes in the position and intensity of the Jetstream related to warming and cooling of the surface temperature of the North Atlantic Ocean. Previous studies based on climate simulations had proposed that large-scale deforestation by the Romans

had caused climate to become drier in the Mediterranean owing to a reduction in evaporative recycling. We confronted this hypothesis with paleoecological and archaeological data. Paleoecological data indicated a wetting trend during the 2,000 year period of analysis. Archaeological data indicated that the location of the Fertile Crescent ecotone, which is determined by rainfall rates, has remained more or less stable in the past 3,000 years. Thus we concluded that Roman deforestation did not cause regional-scale climatic aridification in the Mediterranean.

In the second half of the thesis we stay in the Mediterranean region but switch focus to understanding the impact that past climate changes had on the Roman civilisation. The Roman civilisation is particularly interesting to study in this regard as there are many parallels between their civilisation and our own. For example, the Romans were confronted with managing their environmental resources in the face of rapid population growth and urbanisation. Given the length of their reign they also had to adapt to a greater amplitude of climate variability than most post-industrial civilisations have so far experienced. In chapter 4 we set out to understand how the Romans ensured reliable food supply to their cities under the highly variable climate of the Mediterranean region. We examined this in the context of virtual water trade. Virtual water is a way of quantifying the water used in the production of goods and services and tracking how those water resources are redistributed through trade. By redistributing water resources, regions can buffer against climate variability because they can import when they experience deficit and export when they have a surplus. To understand Roman virtual water trade we developed a Virtual Water Network of the Roman World. Using the hydrological model PC Raster Global Water Balance (PCR GLOBWB), we simulated the impact of climate variability on grain yields. We simulated trade using the Stanford Geospatial Network of the Roman World (Orbis) which is a reconstruction of transport costs in the Roman Empire at 200 AD based on Diocletian's edict on maximum prices: an effort by Emperor Diocletian to reverse rampant inflation within the Empire.

Surprisingly we found that the Mediterranean was temperature-limited rather than water-limited for the growth of grain. This was because grain was primarily grown in winter and spring when the region received the majority of its rainfall but when temperatures were relatively cool. Our

analysis also illustrated that the reliability of yields varied a great deal throughout the Mediterranean. Irrigated regions exhibited the most reliable yields because rivers provided a reliable source of water whilst growth could take place in summer when temperatures were warm and stable. For rainfed agriculture, the Eastern part of the Empire exhibited more stable yields compared with the West owing to warmer average winter temperatures. Stable yields were extremely important for the Romans because cities on one side of the Mediterranean generally had no information on prospective yields until trade ships arrived in port. Therefore provinces such as Egypt became particularly important as cities could be more or less assured of reliable grain supplies from such regions.

Our analysis highlighted that a city's location within the trade network was critical for ensuring reliable and cost effective access to grain supplies. Those cities that were well connected could import grain from a variety of regions without incurring a dramatic increase in import cost whereas poorly connected regions were more likely to import from further away. In general, virtual water trade worked extremely well at increasing Roman resilience to interannual climate variability. However, a stable supply of food also promoted population growth and urbanisation. Thus in the long term the resilience to climate variability provided by trade may have been eroded as the Empire approached the limits of its water resources.

In chapter 5 we assessed how Roman water resource management infrastructure responded to large-scale and persistent climate change typical of Holocene climate anomalies. We examined the change in yield and virtual water trade between the Roman Warm Period and Dark Ages Cold Period based on reconstructions of precipitation from chapter 3 and temperature reconstructions from other authors. Our climate reconstructions indicated that during the Roman Warm Period the Central Mediterranean had relatively low rainfall. However, when we simulated grain growth for the Roman Warm Period we found that the dry conditions in the Central Roman Empire likely had little negative impact on grain yields. As we established in chapter 4, temperature was the main limit to grain growth in the Mediterranean so drier conditions were outweighed by the warmer climate during the Roman Warm Period. Even in regions where yields were reduced, the high connectivity of coastal Central Mediterranean cities meant that the societal impact was minimal owing to the ability to offset low yields with imports from other parts of the Empire.

The shift to cooler temperatures ~450AD reduced grain yields throughout the Mediterranean. Given that the trade network deteriorated following the third century crisis, stable yields likely became increasingly important owing to increased localisation of resources. The Eastern Empire was likely more resilient to the changing climate because warmer average winter temperatures and a greater use of irrigation meant that yields were more stable compared with the West. However, this was likely just one contributing factor to the fall of the Western Empire whose resilience had been eroded in previous centuries owing to a number of socioeconomic developments.

It was envisaged that the results presented in this thesis would contribute to our understanding of the climate system as well as the impact of climate change on current and future society. To that end, we have demonstrated that variations in solar irradiance appear to impact ENSO in a predictable way. Given that the variations in solar irradiance exhibit periodic behaviour; this understanding may contribute to improving predictions of whether La Niña or El Niño events are more likely to occur in the future. For the Mediterranean we have demonstrated that the principal mode of variability in precipitation between 3,000 and 1,000 years ago appears to be linked to changes in the surface temperature of the North Atlantic Ocean. In fact the same precipitation pattern has been identified for the last 3,000 years at decadal and longer timescales. Therefore in order to improve decadal-scale climate predictions in the densely populated Mediterranean region, our analysis highlights that researchers should focus on understanding the dynamics of the North Atlantic Ocean.

In terms of the impact of climate change on humanity, we have demonstrated that the way a society to responds to climatic perturbations is at least as important as the magnitude of the climatic perturbation. For instance, Roman water resource management infrastructure increased their resilience to climate variability in the short term but by promoting population growth and urbanisation, resilience was eroded in the long term. That finding reinforces the message that the current globalisation of resources and associated population and urbanisation trends are pushing global society closer to the boundary of our global water resources and reducing our resilience to climate change. Just like the Romans, our current water resource management infrastructure was

designed to cope with interannual climate variability and to facilitate exponential growth. However, if we want to avoid going the way of the Western Roman Empire we need to focus on adapting the global water resource management infrastructure so that it promotes sustainable growth whilst being resilient to large-amplitude and persistent climate changes.

Samenvatting

Een belangrijke reden voor het succes van de mensheid is haar aanpassingsvermogen. In tegenstelling tot veel andere soorten kan de mens zich relatief makkelijk aanpassen aan uiteenlopende en veranderende milieuomstandigheden. Sinds het begin van onze beschaving hebben we daarnaast ook het vermogen ontwikkeld om onze omgeving aan te passen aan onze behoeften. Bijvoorbeeld in Zuid-Mesopotamië zijn door irrigatie droge gebieden met lage productiviteit veranderd in hoog productieve landbouwgebieden. In de loop van de tijd heeft de mens zijn omgeving dusdanig aangepast dat zelfs het milieu op wereldschaal is veranderd. Door menselijk handelen is de uitstoot van broeikasgassen in de atmosfeer verhoogd. Een verdere toename van deze uitstoot zal, volgens de huidige wetenschappelijke inzichten, het klimaat verder opwarmen waarbij ook meer extreme weersomstandigheden zullen voorkomen. De verwachting is dat de toekomstige klimaatveranderingen groter zullen zijn dan de mens ooit heeft meegemaakt. Of ons aanpassingsvermogen groot genoeg is om met deze veranderingen om te gaan is uiterst onzeker.

Om te begrijpen hoe kwetsbaar de menselijke beschaving is voor toekomstige klimaatveranderingen moeten de klimaatvoorspellingen verbeteren. Het maken van betrouwbare voorspellingen is niet eenvoudig vanwege de complexiteit van het klimaatsysteem. Veel processen die van belang zijn voor klimaatverandering werken over een langere tijdspanne dan de meetperiode. Daarom is het zeer nuttig om naar het verleden te kijken om het heden te kunnen begrijpen en de toekomst te kunnen voorspellen. We krijgen bijvoorbeeld meer inzicht in het klimaat als we processen die klimaatschommelingen in het verleden hebben veroorzaakt beter begrijpen. Ook ons begrip van hoe mensen zich aanpassen aan het klimaat was tot voor kort beperkt tot gebeurtenissen in de afgelopen eeuwen. Door verbeterde dateringstechnieken kunnen we nu maatschappelijke veranderingen vergelijken met klimaatveranderingen die teruggaan naar het begin van de menselijke beschaving. Uit deze analyse blijkt dat bepaalde beschavingen uit het verleden zijn weggevaagd door klimaatveranderingen, zoals bijvoorbeeld de Amorieten uit Syrië, terwijl anderen zijn blijven bestaan. Het verleden heeft ons dus veel geleerd over de kwetsbaarheid van beschavingen voor klimaatverandering. In dit proefschrift volgen we deze lijn

van onderzoek. Eerst willen we begrijpen hoe het klimaat is veranderd sinds het begin van de beschaving. Vervolgens bekijken we wat de gevolgen van deze veranderingen zijn op de Romeinse beschaving. Ons uiteindelijke doel is om het klimaatsysteem beter te begrijpen en ook hoe de mens zich kan aanpassen aan toekomstige klimaatveranderingen.

In dit proefschrift beginnen we met het bestuderen van het belangrijkste onderdeel van het klimaatsysteem: de zon. De straling vanuit de zon is niet constant, maar laat kleine verschillen zien. Deze kleine verschillen worden gezien als de oorzaak van klimaatverandering gedurende het Holoceen dat loopt van 11.700 jaar geleden tot nu. De variabiliteit van de zonne-energie is te klein om direct een klimaatverandering te veroorzaken. Daarom is vaak verondersteld dat bepaalde onderdelen van het klimaatsysteem zodanig reageren op deze variabiliteit dat ze indirect het klimaat beïnvloeden door zichzelf versterkende processen, zogenaamde positieve terugkoppelingen. Klimaatmodelsimulaties geven aan dat het gekoppelde oceaan-atmosfeersysteem van de tropische Stille Oceaan een dergelijke versterker kan zijn. Een kleine toe- of afname van de zonnestraling kan ervoor zorgen dat het klimaatsysteem verandert van La Niña (waarbij warm water wordt opgebouwd in het westelijk deel van de tropische Stille Oceaan) naar El Niño (waar dit warme water juist opgebouwd wordt in het oostelijk deel van de tropische Stille Oceaan) of omgekeerd. Hiernaast laten modelsimulaties zien dat in de afgelopen 10.000 jaar het El Niño Zuidelijke Oscillatiesysteem (ENSO) sterker geworden is doordat de hoek is veranderd waaronder de aarde rond de zon beweegt.

Hoewel modellen hebben laten zien dat ENSO kan dienen als versterkend mechanisme is dit nog nooit aangetoond in data. In hoofdstuk 2 van dit proefschrift laten we zien welk bewijs daarvoor te vinden is in bestaande mariene reconstructies. We richten ons op die gebieden waar de oppervlaktetemperatuur van de oceaan nauw verbonden is met de veranderingen in ENSO. De data bestaan uit samengestelde mariene reconstructies die grote onzekerheden vertonen. Daarom hebben we een nieuwe statistische methode ontwikkeld die rekening houdt met de onzekerheid van de individuele reconstructies in de samengestelde dataset. Onze resultaten geven aan dat kleine variaties in zonnestraling een invloed hebben gehad op de temperatuur in de tropische Stille Oceaan. Interessant is dat de tropische Stille Oceaan in het Vroeg en Midden Holoceen

(6000 - 9000 jaar geleden) tegenovergesteld reageerde op een kleine variatie van zonnestraling ten opzichte van het Laat Holoceen (de laatste 4000 jaar). Tijdens het Vroeg en Midden Holoceen werd de oppervlaktetemperatuur van de tropische Stille Oceaan opgewarmd wanneer de zonnestraling hoger was en gekoeld wanneer de straling lager was. In het laat Holoceen was deze reactie van de tropische Stille Oceaan juist tegenovergesteld: een koeling tijdens zon-maxima en opwarming tijdens zon-minima. Dit omslagpunt is een gevolg van de intensivering van ENSO in het Late Holoceen die veroorzaakt wordt door een dominantie van La Niña tijdens de zon-maxima. Bij een langdurige dominantie van La Niña zal er meer koel water opwellen uit de diepere lagen van de oceaan waardoor het zeeoppervlak afkoelt. Doordat de tropische Stille Oceaan wereldwijd de grootste bron van warmte en vocht is voor de atmosfeer, zullen veranderingen in de tropische Stille Oceaan wereldwijde implicaties hebben gehad op het klimaat. Dit hoofdstuk onderstreept dat de gemodelleerde positieve terugkoppeling in het gekoppelde oceaan-atmosfeersysteem versterkt wordt door zonnestraling. De tegenovergestelde reactie tussen het Vroeg en Laat Holoceen die we identificeerden vanuit de data zal verder moeten worden getest in modellen.

In hoofdstuk 3 gebruiken we informatie over mondiale klimaatveranderingen om te begrijpen hoe neerslagpatronen in het Middellandse Zeegebied tussen 3.000 en 1.000 jaar geleden veranderd zijn. Veranderingen in neerslag gedurende deze periode zijn bijzonder interessant omdat dit samenvalt met de opkomst van de Romeinse beschaving. De huidige regenpatronen in het Middellandse Zeegebied zijn afhankelijk van de positie en intensiteit van de winterstraalstroom. Door neerslagpatronen uit het verleden te reconstrueren kunnen we afleiden hoe de polaire straalstroom in het noordelijk halfrond veranderd is.

De regionale neerslagveranderingen in het Middellandse Zeegebied zijn met paleo-ecologische gegevens gereconstrueerd. Uit onze analyse blijkt dat tussen 3.000 en 1.000 jaar geleden het neerslagpatroon in het Middellandse Zeegebied wisselt. Tijdens droge omstandigheden in het centrale deel is het west- en zuidoostelijke deel nat (de Romeinse Warme Periode, van 250BC tot 450AD) en andersom, nat in het centrale deel en droog in het westen en het oosten in de periode 450AD tot 950AD. Het moment waarop het systeem omslaat werd veroorzaakt door

veranderingen in de straalstroom waarbij het oppervlaktewater van de Noord-Atlantische Oceaan dan wel opwarmde of afkoelde.

Hoofdstuk 3 werpt ook nog licht op een andere vraag die wetenschappers al lang bezig houdt. Tijdens de Romeinse overheersing zijn namelijk grote gebieden ontbost en er wordt veel gespeculeerd over de vraag of klimaatverandering heeft bijgedragen aan de ineenstorting van het Romeinse rijk en of wellicht de grootschalige ontbossing daar debet aan is, dus met andere woorden, of grootschalige landgebruiksveranderingen via terugkoppelingen op het klimaat de ondergang inluidde. Met modelstudies is eerder aangetoond dat het Middellandse Zeegebied droger is geworden doordat een afname van bos een vermindering geeft van de verdamping en daardoor een vertraging van de hydrologische cyclus. We hebben deze hypothese vergeleken met paleo-ecologische en archeologische gegevens. De paleo-ecologische gegevens laten een vernattingstrend zien gedurende deze periode. Uit archeologische gegevens blijkt bovendien dat de locatie van de Vruchtbare Sikkel (dit is de regio Israël, Libanon, Syrië, Zuid-Turkije, Irak) nagenoeg onveranderd is gebleven gedurende de laatste 3000 jaar. Uit deze gegevens mogen we dus afleiden dat de ontbossing door de Romeinen geen regionale verdroging in het Middellandse Zeegebied heeft veroorzaakt.

In de tweede helft van het proefschrift blijven we in het Middellandse Zeegebied, waarbij we nu verder proberen te begrijpen wat de gevolgen zijn van de klimaatveranderingen op de Romeinse beschaving. De Romeinse beschaving is interessant omdat er veel parallellen zijn tussen deze en onze huidige beschaving. Zo moesten de Romeinen hun natuurlijke hulpbronnen goed beheren tijdens een periode van snelle bevolkingsgroei en verstedelijking. Gezien de lange duur van hun heerschappij moesten de Romeinen zich bovendien aanpassen aan grotere klimaatsveranderingen dan de meeste postindustriële beschavingen.

In hoofdstuk 4 onderzoeken we hoe de Romeinen een betrouwbare voedselvoorziening voor hun steden konden garanderen onder het sterk wisselende klimaat van het Middellandse Zeegebied. We onderzochten dit door middel van de handel in virtueel water. Het concept ‘Virtueel water’ is een manier om het waterverbruik voor de productie van goederen en diensten te kwantificeren. Door uit te rekenen hoeveel water er nodig is voor de productie van voedingsgewassen en te

bepalen hoe de handelsstromen van deze producten loopt, wordt er bij wijze van spreken virtueel water verhandeld, hetgeen ook duidelijk maakt hoe watervoorraden worden herverdeeld. Door een herverdeling van water kunnen regio's zich ook wapenen tegen klimaatschommelingen, omdat ze virtueel water kunnen importeren tijdens tekorten en virtueel water kunnen exporteren tijdens overschotten. Met een virtueel waternetwerk proberen we dus de Romeinse virtuele waterhandel te begrijpen. Het hydrologische model PC Raster Global Water Balance (PCR GLOBWB) hebben we gebruikt om de graanproductie te simuleren onder verschillende klimaten. Het handelsnetwerk is gebaseerd op het Stanford Geospatial Network of the Roman World (Orbis). In dit netwerk is een reconstructie van de transportkosten in het Romeinse Rijk omstreeks 200 AD gemaakt op basis van het Diocletianus edictum. In dit edict werd de maximumprijs voor goederen en diensten vastgesteld ter voorkoming van inflatie.

Tot onze verbazing vonden wij dat de productie van graan in het Middellandse Zeegebied niet gelimiteerd werd door een gebrek aan water, maar afhing van de temperatuur. Dit komt omdat het meeste graan geteeld werd in de winter wanneer de regenval het hoogste is en de temperaturen relatief koel. Uit onze analyse komt ook naar voren dat de betrouwbaarheid van de graanopbrengsten verschillend is voor een groot deel van het Middellandse Zeegebied. Geïrrigeerde regio's, zoals bijvoorbeeld de Nijldelta of de Povlakte, hebben duidelijk de meest betrouwbare opbrengst. Dit komt omdat de rivieren een betrouwbare bron voor irrigatiewater zijn, waardoor graan in de zomer kon groeien met hoge en stabielere temperaturen. Voor regio's waar geen irrigatie plaatsvond en de landbouw puur afhankelijk is van regen, blijkt dat het oostelijk deel van het Rijk een stabielere opbrengst heeft dan het westen. De belangrijkste reden hiervoor is dat de gemiddelde wintertemperatuur in het oostelijk Middellandse Zeegebied hoger is dan in het westen, hetgeen gunstig is voor de productie van graan. Onze analyse laat ook zien dat de locatie van een stad binnen het handelsnetwerk van cruciaal belang is om een betrouwbare en kosteneffectieve toegang tot waterbronnen te waarborgen. Steden die goed verbonden zijn in het waternetwerk kunnen graan uit verschillende regio's importeren, zonder dat de importkosten drastisch toenemen. Slecht aangesloten regio's moeten juist water importeren vanuit verder gelegen gebieden. Virtuele waterhandel in het zeer heterogene Middellandse Zeegebied heeft daardoor zeer goed gewerkt om een stabiele aanvoer van graan naar de steden te waarborgen. Op

korte termijn steeg hierdoor de Romeinse veerkracht tegen klimaatschommelingen. Maar een stabieler aanbod van voedsel heeft ook geleid tot bevolkingsgroei en verstedelijking. Op de langere termijn is de veerkracht tegen klimaatschommelingen daardoor juist afgenomen, zeker toen het Rijk aanliep tegen de grenzen van zijn watervoorraden.

In hoofdstuk 5 onderzochten we hoe de Romeinse waterinfrastructuur gereageerd heeft op grootschalige en aanhoudende klimaatveranderingen die typerend zijn voor het Holoceen. We hebben daarbij gekeken naar de verandering in de opbrengst en de virtuele waterhandel tussen de Romeinse Warme Periode (ca. 250 BC – 450 AD) en de koude Vroege Middeleeuwen (ca. 450 AD – 950 AD) op basis van reconstructies van de neerslag uit hoofdstuk 3 en de temperatuurreconstructies van andere auteurs. Onze klimaatreconstructies geven aan dat er tijdens de Romeinse Warme Periode in het centrale Middellandse Zeegebied relatief weinig neerslag viel. Echter, wanneer we de graangroei simuleerden voor de Romeinse Warme Periode vonden we dat deze droge omstandigheden in het Centraal-Romeinse Rijk waarschijnlijk weinig invloed hadden op de graanopbrengst. Zoals we al in hoofdstuk 4 analyseerden, is de temperatuur de belangrijkste beperkende factor voor de groei van graan in het Middellandse Zeegebied. In de Romeinse Warme Periode werden dus de ongunstigere drogere omstandigheden gecompenseerd door het warmere klimaat. Zelfs in gebieden waar de rendementen verminderden, beperkte de hoge connectiviteit van het centrale Middellandse Zeegebied de maatschappelijke impact, dankzij de mogelijkheid om lage opbrengsten te compenseren met relatief goedkope invoer uit andere delen van het Rijk. De verschuiving naar koelere temperaturen rond 450AD verminderde de graanopbrengst in het hele Middellandse Zeegebied. Gezien het geleidelijke verval van het Romeinse handelsnetwerk dat omstreeks de 3_e eeuw begon, evenals een aantal andere factoren die het Rijk destabiliseerden (zoals inflatie, de opkomst van verschillende geloven en het bewaken van de grens bij de Rijn en de Donau), is het aannemelijk dat de verschuiving in het klimaat heeft bijgedragen aan de val van het westelijke Romeinse rijk. De langere levensduur van het Oost-Romeinse rijk kan daarentegen voor een deel gerelateerd worden aan warmere gemiddelde temperaturen in de winter en een groter gebruik van irrigatie in het oostelijke Middellandse Zeegebied, hetgeen bijdroeg aan een grotere veerkracht van deze regio.

De resultaten van dit proefschrift dragen bij aan ons begrip van het klimaatsysteem en de gevolgen van klimaatverandering op de maatschappij. Wat kunnen we hier nu uit leren voor het begrijpen van het heden en is de gegenereerde kennis ook relevant voor onze toekomst? We hebben aangetoond dat variaties in de zonnestraling een voorspelbare invloed hebben op ENSO. Gegeven het feit dat de variaties in zonnestraling periodiek gedrag vertonen kan dit inzicht bijdragen aan het verbeteren van voorspellingen over bijvoorbeeld de vraag of de kans op La Niña en El Niño groter is in de toekomst. Voor het Middellandse Zeegebied hebben we aangetoond dat de belangrijkste variatie in neerslag tussen 3.000 en 1.000 jaar geleden verband lijkt te houden met veranderingen in de oppervlaktetemperatuur van de Noord-Atlantische Oceaan. Dit wordt ook bevestigd door studies van klimaatverandering over de laatste 1000 jaar. Daarom is het nodig dat onderzoekers zich richten op het begrijpen van de dynamiek van de Noord-Atlantische Oceaan als we het klimaat op een tijdschaal van decennia willen voorspellen voor het dichtbevolkte Middellandse Zeegebied.

Voor wat betreft de gevolgen van klimaatverandering op de mensheid, hebben we laten zien dat de wijze waarop een samenleving reageert op klimatologische verstoringen minstens zo belangrijk is als de omvang van de klimatologische verstoring. De hoog ontwikkelde Romeinse waterinfrastructuur en de daarop gebaseerde virtuele waterhandel maakten het Romeinse Rijk behoorlijk robuust voor klimaatschommelingen. Klimaatadaptatie is dus zeer belangrijk. Er is hiernaast nog een les te leren. De Romeinse waterbeheerinfrastructuur verhoogde aanvankelijk de weerbaarheid tegen klimaatschommelingen, maar doordat dit verdere bevolkingsgroei en verstedelijking stimuleerde, werd de veerkracht op de lange termijn uitgehold. Deze vaststelling onderstreept de boodschap dat de huidige globalisering van de economie en handel en de bijbehorende bevolkingsgroei en verstedelijkingstrends, de mondiale samenleving dichter tegen de grens van onze mondiale beschikbare watervoorraad aanduwen en onze bestendigheid tegen klimaatverandering verminderen. Net als bij de Romeinen, is onze huidige waterbeheerinfrastructuur ontworpen om ons te wapenen tegen hoog-frequente variatie van het klimaat. Als we willen voorkomen dat we de weg inslaan die het West-Romeinse Rijk is ingeslagen, zullen we ons moeten concentreren op het aanpassen van de wereldwijde

waterbeheerinfrastructuur, zodat duurzame groei mogelijk wordt gemaakt en waarbij meebewogen kan worden met relatief grote amplitudes en aanhoudende klimaatveranderingen.

Acknowledgements

First of all I would like to thank my daily supervisor Stefan. A PhD student could not wish for a better supervisor. Stefan always had time for me and was always encouraging particularly through the uncertain times I faced. He gave me the confidence to follow my own ideas and be creative. I am daily astounded at how he can switch between so many diverse research topics alongside a heavy teaching load and maintain such a high standard. I would not have completed this without his dedicated supervision.

Thanks to Marc who has been a source of creative thinking and enthusiasm throughout my PhD project. Marc has the impressive quality of generating the same creative thinking and enthusiasm in every meeting I've had with him. Despite being extremely busy Marc has always found time to provide invaluable feedback on every piece of material I've sent him.

Next I would like to thank Martin. One of the first meetings I had with my thesis supervisor's involved Stefan and Marc enthusiastically discussing different potential research directions for the project. I was a bit lost but didn't have the confidence to say so. At this point Martin interrupted and said that he had no idea what they were talking about and he was pretty sure that Brian didn't either! Throughout my PhD Martin has been able to see above the details and maintain a clear overview of what was best for me and the project. He has been invaluable in providing excellent feedback and guiding the research direction of the project.

Thanks to Nanne who provided a different perspective at the critical early phase of my PhD. Sometimes scientists with a physics background can intimidate us natural scientists but Nanne's kind and generous nature gave me confidence to delve into the discipline of paleoclimate modelling. Despite what must have been terribly difficult times personally, she maintained her bright disposition and was always available to provide me with invaluable advice.

Thanks to Hugo who helped me a hell of a lot in the early stages of my PhD with setting up models and such as well as integrating into the department generally. It has been inspiring to work alongside him. Thanks to Mara and Angie who have been a huge support to me over the years in Utrecht and are just generally a wonderful source of positive energy in my life. I don't

know who is going to feed me whenever I leave! Thanks to Ype who has been an absolute joy to work with. It's been great fun working out various problems together. Thanks to Rens. Our common interest in the Romans has made it a very enjoyable and stimulating collaboration thus far. Thanks to Maarten and Inge who along with Martin I learned a lot from in my role as teaching assistant on the course Environmental Impact Assessment. Thanks to everyone at the Royal Netherlands Meteorological Institute, particularly Sybren and Bart for thought provoking and challenging feedback. Thank you to my other collaborators: Kees, Elijah, Walter and Timme.

Thanks to my other office mates Ineke and Myrna. I've not been the tidiest of people to share an office with but that doesn't seem to have bothered you too much. It seems you realised that it is easier to embrace the mess rather than try to fight it!

Thanks to everyone on the 11th floor. Every single morning in the last 5 years I've looked forward to coming into work. That's a pretty amazing thing and it's due to every person in the department that has bought into the atmosphere of support, fun and respect that exists in our group.

Thanks to my friends from back home. I've spent the majority of the last decade outside of Ireland. A big part of being able to be away for so long is knowing that when I go home, I can meet up with mates and our conversation picks up as if we just saw each other the day before. I cannot overstate the importance of that to me.

Thanks to all the great friends I've made here in Utrecht. I wouldn't have been able to finish this PhD without you either. Being surrounded by such wonderful people from all over the world has made my life extremely vibrant the last 5 years and helped me through the rough times one faces when being away from home. Thanks to all at Boksvereniging Joop Verbon. Any of the stresses or frustrations of my work could be quickly lifted by a punch in the face from one of you. Thanks to Romain who, along with my time spent in China, brought sustainability issues to the front of my mind. Thanks to everyone I studied with and learned from at DIT and Trinity. Thanks to my paranymphs Bertil and Stephen. You have been a big part of the happy times I've had in the last 5 years.

Finally, and most importantly, thank you to my family. My mam and dad always highlighted the importance of knowledge and learning, even though it took me a bit of maturing before I took those ideals on board! They have always done what was best for me and my sisters. An example of that was their decision to move from Dublin city to the countryside of Wicklow because they thought it would be a better environment for us to grow up. I'm sure that decision led to me developing an interest in nature and the environment. Thanks to Orla who was the first in our family to attain a PhD and who along with Paul gave me great advice when I decided to apply for one. Thanks to Aisling who has been a great support in recent years. It's very hard being away from home but by being a supportive presence at home, Aisling has made me worry a little less. Thanks to Luke. Having grown up with two sisters it's great to finally have a nephew who I can have the craic with! Lorcan, you can't read this, but I look forward to much fun with you in the coming years too.

Curriculum vitae

I was born on the 2nd of June 1982. I grew up in County Wicklow, Ireland where I also attended primary school. In 2001 I graduated from Cross and Passion secondary school in Kilcullen and began a 4 year B.Sc. in Geomatics at Dublin Institute of Technology. My studies in Geomatics focused on developing the skills to gather, store, process, and deliver spatial information. My degree thesis was entitled 'An investigation into the performance of predictive GIS archaeological models in an Irish context' and was supervised by Eamonn Donnelly and Alain Chenaux. I graduated from Geomatics in 2005 with a 1st class honours degree. From 2005 to 2007 I worked as a GIS analyst at UPC in Dublin. I left UPC in early 2007 and moved to China where I became an English teacher at Jiangshan Middle school. From September 2007 to June 2008 I worked as an English teacher at Zhejiang University of Technology. In 2008 I returned to Ireland to begin a 1 year M.Sc. course in Environmental Sciences at Trinity College Dublin. Here I learned the range of practical skills required to become an environmental consultant. In addition, I completed a desk study focusing on the social and ecological impact of transboundary protected areas in Sub-Saharan Africa under the supervision of Ken Irvine. My M.Sc. thesis was entitled 'The evolutionary pathway to obligate scavenging in Gyps vultures' and was supervised by Andrew Jackson. We later published my thesis as an article in the journal PlosOne along with Colby Tanner. I graduated in 2009 with a Masters of distinction in Environmental Sciences. After graduating, I moved to the Netherlands where I began a PhD at the Environmental Sciences department of Utrecht University under the supervision of Stefan Dekker, Martin Wassen, Marc Bierkens and Nanne Weber. Here, I carried out research and teaching relating to the field of environmental sciences. I completed my PhD in 2014. The details of my PhD research can be read in this thesis.

Publications

Dermody, B.J., van Beek, R.P.H., Meeks, E., Klein Goldewijk, K., Scheidel, W., van der Velde, Y., Bierkens, M.F.P., Wassen, M.J., Dekker, S.C., 2014. A virtual water network of the Roman world. Hydrol. Earth Syst. Sci. Discuss. 11, 6561–6597. doi:10.5194/hessd-11-6561-2014

Dermody, B.J., de Boer, H.J., Bierkens, M.F.P., Weber, S.L., Wassen, M.J., Dekker, S.C., 2012. A seesaw in Mediterranean precipitation during the Roman Period linked to millennial-scale changes in the North Atlantic. Clim. Past 8, 637–651. doi:10.5194/cp-8-637-2012

Dermody, B.J., Tanner, C.J., Jackson, A.L., 2011. The evolutionary pathway to obligate scavenging in gyps vultures. PLoS ONE 6(9): e24635. doi:10.1371/journal.pone.0024635